BEACH GEOMORPHOLOGY AND KEMP'S RIDLEY (*LEPIDOCHELYS KEMPII*) NEST SITE SELECTION ALONG PADRE ISLAND, TX, USA

A Thesis

by

MICHELLE F. CULVER

BS, Baylor University, 2016

Submitted in Partial Fulfillment of the Requirements for the Degree of

MASTER OF SCIENCE

in

COASTAL AND MARINE SYSTEM SCIENCE

Texas A&M University-Corpus Christi
Corpus Christi, Texas

May 2018

May 2018

BEACH GEOMORPHOLOGY AND KEMP'S RIDLEY (*LEPIDOCHELYS KEMPII*) NEST SITE SELECTION ALONG PADRE ISLAND, TX, USA

A Thesis

by

MICHELLE F. CULVER

This thesis meets the standards for scope and quality of
Texas A&M University-Corpus Christi and is hereby approved.

James C. Gibeaut, PhD
Chair

Michael J. Starek, PhD
Committee Member

Philippe Tissot, PhD
Committee Member

Donna J. Shaver, PhD
Committee Member

May 2018

ABSTRACT

The Kemp's ridley sea turtle (*Lepidochelys kempii)* is the most endangered sea turtle species in the world, largely due to historic take of eggs at the primary nesting beach in Mexico, loss of juveniles and adults incidental to fisheries operations, and the limited geographic range of its nesting habitat. In the USA, the majority of nesting occurs along Padre Island in Texas. There has been limited research regarding the connection between beach geomorphology and Kemp's ridley nesting patterns, but studies concerning other sea turtle species suggest that certain beach geomorphology variables, such as beach slope and width, influence nest site selection. This research addresses the literature gap by quantifying the terrestrial habitat variability of the Kemp's ridley and investigating the connection between beach geomorphology characteristics and Kemp's ridley nesting preferences on Padre Island, Texas, USA.

Beach geomorphology characteristics, such as beach slope and dune peak height, were extracted from airborne topographic lidar data collected annually along the Texas coast from 2009 through 2012. The coordinates of observed Kemp's ridley nests from corresponding years were integrated with the geomorphic data, which was then statistically analyzed using generalized linear models and random forest models. These models were successful in predicting Kemp's ridley nest presence. The top generalized linear models explained 40-46% of nest presence variability with a relatively low prediction error. The final random forest model was superior in performance in comparison to the generalized linear models, with a true positive rate above 85%. Nest elevation, distance from shoreline, maximum dune slope, and average beach slope were the significant variables in the top two generalized linear models and the relatively most important variables in the random forest model, with elevation and distance from shoreline being the most influential in each.

Kemp's ridleys nested at a median elevation of 1.04 m above mean sea level and a median distance from shoreline of 12.79 m, which corresponds to the area directly below the potential vegetation line, which is defined as the lowest elevation where dune plants may persist. Kemp's ridleys also exhibited a preference for a limited range of the study area and avoided nesting on beaches with extreme values for maximum dune slope, average beach slope, and beach width. This study provides new information regarding Kemp's ridley terrestrial habitat and nesting preferences that have many applications for species conservation and management.

DEDICATION

I would like to dedicate this work to my parents, Ronald Wayne and Tracey Culver. Your endless support and encouragement allowed me to follow my dreams, and for that I will be forever grateful.

ACKNOWLEDGEMENTS

First, I would like to thank my advisor and committee chair, Dr. James Gibeaut, for receiving me as both a researcher and student and for guiding me through this journey. Thank you for encouraging me to pursue projects and classes for which I am passionate and for sharing your knowledge and experiences with me. Your mentorship and trust empowered me to overcome the challenges of this pursuit and helped shaped me into a better researcher. Next, I would like to acknowledge my committee members Dr. Donna Shaver, Dr. Philippe Tissot, and Dr. Michael Starek for their guidance, support, and insight. Thank you for your genuine interest in my research and for your time and priceless advice. Your expertise helped improve my work tremendously.

I would also like to thank the Harte Research Institute for Gulf of Mexico Studies for funding my research and providing me with countless opportunities to learn and grow as a leader and professional. Many thanks to Gail Sutton and Dr. Larry McKinney for their mentorship. Additionally, I would like to express my gratitude to the staff at Save the Manatee Club, especially Dr. Katie Tripp and Anne Harvey-Holbrook, for continually inspiring me with your passion, work ethic, and pure brilliance and motivating me to pursue an advanced degree.

Great thanks to my family, friends, and coworkers who offered me support and guidance. A special thanks to my mom for inspiring me with her strength and perseverance and for her infinite support. I would also like to acknowledge Diana Del Angel for being my rock during this process; thanks for answering all of my minute questions and calming my needless anxieties.

TABLE OF CONTENTS

LIST OF FIGURES

FIGURES PAGE

LIST OF TABLES

TABLES PAGE

INTRODUCTION

Purpose and Objectives

The main goal of this project is to assess the relationship between beach geomorphology and Kemp's ridley (*Lepidochelys kempii*) nest site selection on Padre Island National Seashore on North Padre Island and South Padre Island, Texas, USA. A secondary goal of this research is to determine the influence of environmental conditions on Kemp's ridley nest presence. This study intends to fulfill the following objectives:

1. Identify the terrestrial habitat variability of the Kemp's ridley sea turtle on the beaches of North and South Padre Islands, Texas;
2. Quantify the influence of beach geomorphology characteristics on Kemp's ridley nest site selection;
3. Assess the impact of daily average environmental conditions, such as wind speed and direction, on Kemp's ridley daily nest abundance.

This study will generate a better understanding of Kemp's ridley nesting preferences and beach habitat, which will allow for greater insight into habitat vulnerability. The results of this study have many applications for the conservation and management of the species, including protecting and recreating identified beach characteristics associated with nesting preferences, informing nest location and monitoring efforts, and assisting with a critical habitat designation.

Background: Kemp's Ridley Sea Turtle

The Kemp's ridley (*Lepidochelys kempii*), also known as the Atlantic ridley, is the world's most endangered sea turtle species. Even with recent conservation efforts, their future is still largely uncertain (Plotkin, 2007). Kemp's ridley nesting sites are primarily located on

beaches in the western Gulf of Mexico. The largest nesting site of the Kemp's ridley is the beach at Rancho Nuevo, Mexico (NMFS & USFWS, 2015; Shaver *et al.*, 2005). In the United States, nesting occurs primarily on Padre Island, a barrier island in Texas (NMFS & USFWS, 2015). Previous studies have described sea turtle nesting habitat, but there has been little to no research regarding the connection between beach geomorphology and Kemp's ridley nesting site selection (Plotkin, 2007).

Listing Status and Population Trends

Internationally, the Kemp's ridley is considered the most endangered sea turtle (Plotkin, 2007; USFWS, 1999). The Kemp's ridley sea turtle was listed as endangered throughout its range on December 2, 1970 (NMFS *et al.*, 2010; USFWS, 1999). On July 1, 1975, the Kemp's ridley was listed on Appendix I by the Convention on International Trade in Endangered Species of Wild Fauna and Flora (CITES), which prohibited all commercial international trade. Furthermore, the International Union for the Conservation of Nature lists the Kemp's ridley as Critically Endangered (NMFS *et al.*, 2010; USFWS, 1999). In 1996, the Kemp's ridley was classified as critically endangered by the IUCN Red List of Threatened Species, where it remains today (IUCN, 1996). Even with recent conservation efforts, the Kemp's ridley continues to face a number of threats, including: habitat loss and destruction, cold-stunning, climate change, ingestion of and entrapment in marine debris, pollution, boat collisions, poaching, and incidental capture (National Research Council *et al.*, 1990; NMFS & USFWS, 2015; USFWS, 1999).

Historic information demonstrates that the Kemp's ridley population was copious in the mid-20th century (Bevan *et al.*, 2016). Tens of thousands of ridleys nested around Rancho Nuevo, Mexico during the late 1940s, indicative a very large adult population (NMFS & USFWS, 2015). During this time, an estimate of over 40,000 female Kemp's ridleys would nest

in one day, as shown in the 1947 "Herrera" film (Bevan *et al.*, 2016) (Figure 1). This would equate to over 120,000 nests for the 1947 season (Bevan *et al.*, 2016).

Figure 1: Snapshot of 1947 film footage taken by Andres Herrera showing thousands of Kemp's ridleys nesting at Rancho Nuevo, Mexico. (Herrera, 1947).

Between the late 1940s and mid-1980s, the Kemp's ridley experienced a significant population decline (Figure 2). In 1985, a record low of 702 nests was recorded at Rancho Nuevo; at the time, it was estimated that there were less than 250 nesting females (NMFS & USFWS, 2015; Shaver *et al.*, 2005). The Kemp's ridley population slowly began to recover in the 1990s, with the number of nests at Rancho Nuevo increasing to 1,430 in 1995, 6,947 in 2005, and 15,459 in 2009 (NMFWS & USFWS, 2015). Between 2002 and 2009, 771 nests were documented on the Texas coast, greatly surpassing a total of 81 nests recorded in Texas from 1948-2001 (NMFS *et al.*, 2010) (Figure 3). In both Mexico and Texas, there was a noticeable drop in the number of observed nests in 2010 due to a large mortality event, but this was followed by a higher count of nests in 2011 and 2012 (Gallaway *et al.*, 2016b; Shaver *et al.*, 2016b). In 2013 and 2014, there was a decline in the number of observed nests once again (NMFS & USFWS, 2015). It is possible that the decline in 2013 was caused by a recent change in the ability of Kemp's ridley to attain a body condition required for remigration and reproduction due to a combination of reduced food supply and an increasing population in the northern Gulf of Mexico (Gallaway *et al.*, 2016b).

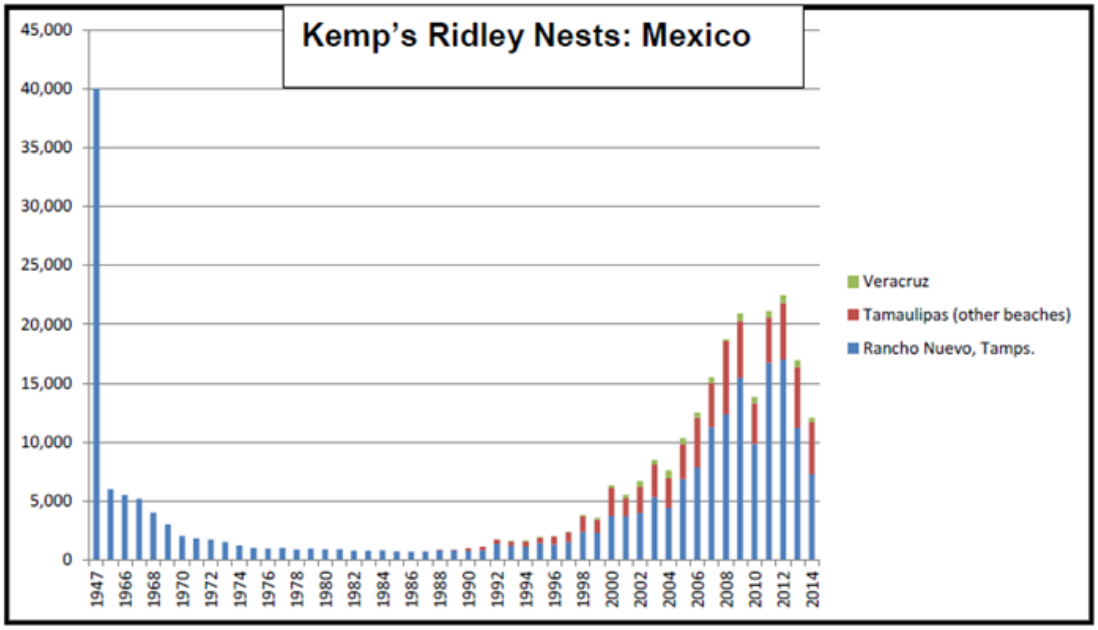

Figure 2: Total number of Kemp's ridley nests recorded at Rancho Nuevo, Mexico and other beaches from 1947-2014. Rancho Nuevo was the only location surveyed before 1988. (NMFWS & USFWS 2015).

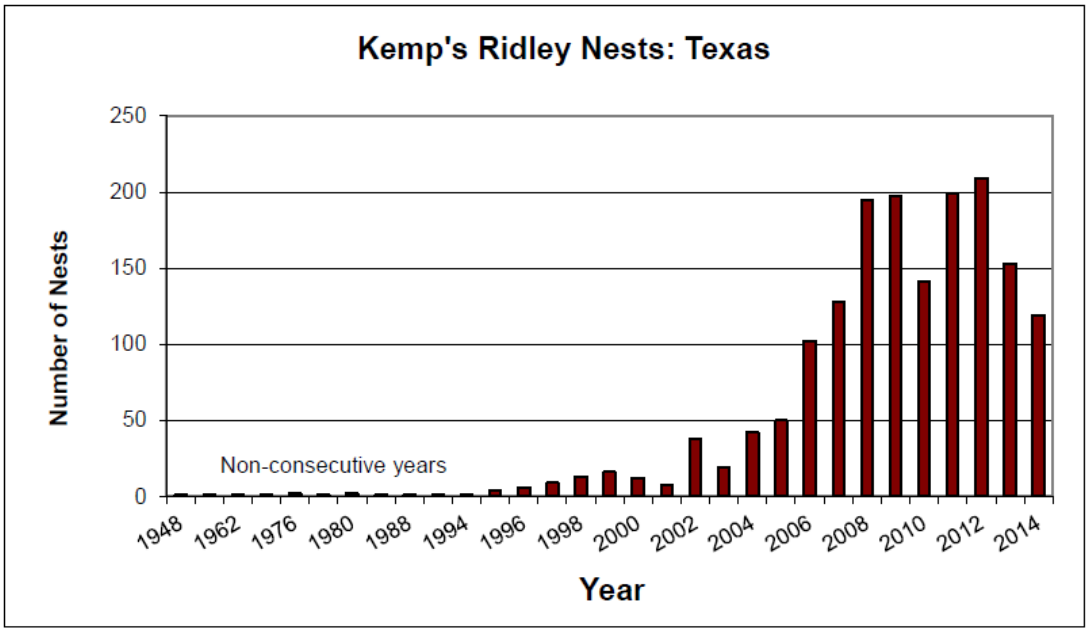

Figure 3: Total number of Kemp's ridley nests recorded at Padre Island National Seashore, Texas from 1948-2014. (NMFWS & USFWS 2015).

According to a recent stock assessment by Gallaway *et al.* (2016a), the estimated female population for age 2 and older in 2012 was approximately 188,713. If females compose 76% of the population (based on a sex ratio of 0.76), the estimated total population of age 2 and older

Kemp's ridley sea turtles in 2012 was 248,307 (Gallaway *et al.*, 2016a; NMFS& USFWS, 2015). The stock assessment report concluded that the total population, including hatchlings younger than 2 years old, might have surpassed 1 million turtles in 2012 (Gallaway *et al.*, 2016a). However, 2012 was the highest year for recorded nests since the beginning of monitoring. The number of nests recorded in 2014 was almost half the amount in 2012, resulting in a much lower current population estimate (NMFS & USFWS, 2015). Monitoring the nesting turtles in the entirety of Texas is logistically challenging due to the long stretch of beach coupled with the small nesting population, so it is possible that the Kemp's ridley nesting population in Texas is larger than indicated by current nesting data (Frey *et al.*, 2014).

For the Kemp's ridley sea turtle to be considered for downlisting from Endangered to Threatened, there must be at least 10,000 nesting females in a single season distributed at the primary nesting beaches (NMFS & USFWS, 2015). According to the cumulative number of nests and an average of 2.5 clutches/female/season, approximately 4,395 females nested at the primary nesting beaches in 2014 (NMFS & USFWS, 2015).

Species Description

Samuel Garman originally identified the Kemp's ridley in 1880 (NMFS *et al.*, 2010). The sea turtle was named after Richard Kemp, a fisherman who submitted the specimen from Key West, Florida (NMFS & USFWS, 2015). While the Kemp's ridley is a close relative of the olive ridley, it is a genetically distinct species (NMFS & USFWS, 2015). It is estimated that the Kemp's ridley diverged from the olive ridley between 2.5 to 5 million years ago (NMFS & USFWS, 2015; USFWS, 1999).

The Kemp's ridley and its congener, the olive ridley, are the smallest of all sea turtles with the Kemp's ridley being slightly larger and heavier than the olive ridley. Adults typically

weigh between 32-49 kg, and the length of the straight carapace is typically 60-65 cm with the shell being almost as wide as it is long (NMFS *et al.*, 2010; USFWS, 1999). Hatchlings weigh approximately 15-20 g, measure 42-48 mm in carapace length, and measure 32-44 mm in width (NMFS *et al.*, 2010). The eggs range from 34-45 mm in diameter and 24-40g in weight (NMFS *et al.*, 2010; National Research Council *et al.*, 1990). Coloration changes significantly as a hatchling develops into an adult. Hatchlings typically have a grey-black dorsum and plastron, which changes to a grey-black dorsum with a yellow-white plastron as a juvenile. A lighter grey-olive carapace with a white or yellowish plastron are characteristic of adults (NMFS *et al.*, 2010). The adult carapace usually has five pairs of costal scutes and five vertebral scutes, and adults generally have a large head and powerful jaws (National Research Council *et al.*, 1990).

Unlike other sea turtles, ridleys often aggregate to nest, emerging from the sea to nest in a somewhat synchronized manner referred to as an "arribada" (National Research Council *et al.*, 1990; Shaver *et al.*, 2005). Nesting in aggregations may have several advantages, such as locating mates, increasing the likelihood of survival of the young, and preserving genetic diversity in the population (NMFS & USFWS, 2015; Plotkin, 2007). There is an average of about 25 days between arribadas, but overall the timing is largely unpredictable (NMFS & USFWS, 2015). Some studies suggest that there may be cues that initiate an arribada, including strong onshore wind, lunar and tidal cycles, olfactory signals, or social facilitation (Shaver & Rubio, 2008). Jimenez-Quiroz *et al.* (2005) found a coherence between nesting cycles and temperature and wind fluctuations, implying that these environmental variables could serve as stimuli. Shaver *et al.* (2017) discerned that Kemp's ridleys prefer to nest on windy days and may be prompted to nest by increases in wind speed and surf. It is possible that these conditions are

preferable because the sand is cooler and the risk of predation is reduced, as any signs of nesting would be quickly erased (Shaver *et al.*, 2017).

Another distinct characteristic of Kemp's ridley reproduction is that this species prefers to nest during the day while other species primarily nest at night (National Research Council *et al.*, 1990; Shaver *et al.*, 2016b). Nesting turtles are usually only on the beach for 30 to 60 minutes, and there are 95 to 112 eggs per clutch on average, which incubate 42-62 days before hatching (NMFS & USFWS, 2015; Shaver *et al.*, 2016b). Females may lay one to four clutches per season, but the average number of clutches laid per female is highly debated and may vary between nesting sites (Frey *et al.*, 2014).

Terrestrial Habitat

The range of the Kemp's ridley sea turtle encompasses the Gulf of Mexico and extends into the northwestern Atlantic Ocean (Putman *et al.*, 2013) (Figure 4). Most nesting occurs on beaches along the west-central Gulf of Mexico, with the greatest nesting numbers near Rancho Nuevo, Tamaulipas, Mexico (Caillouet *et al.*, 2015; Shaver & Caillouet, 2015; Shaver & Rubio, 2008). The Mexican government began protecting the nests in 1966 because the population was rapidly declining (Caillouet *et al.*, 2015; Shaver & Caillouet, 2015). By 1977, extinction of the species was imminent, so a bi-national, multi-agency imprinting and head-start project was implemented to increase Kemp's ridley nesting at Padre Island National Seashore (PAIS), known as the PAIS Restoration Program (Shaver & Caillouet, 2015; Shaver & Rubio, 2008). The overall goal of this project was to create a secondary nesting colony in a location that was both protected and within the native range of the species (Shaver & Rubio, 2008). Due to these and other efforts, both Rancho Nuevo in Mexico and Padre Island National Seashore in the United States serve as main nesting sites for the Kemp's ridley sea turtle today (Caillouet *et al.*, 2015)

(Figure 4). Nesting also occurs in Veracruz, Mexico and occasionally in Florida, Alabama, South Carolina, and North Carolina in the United States (NMFS & USFWS, 2015).

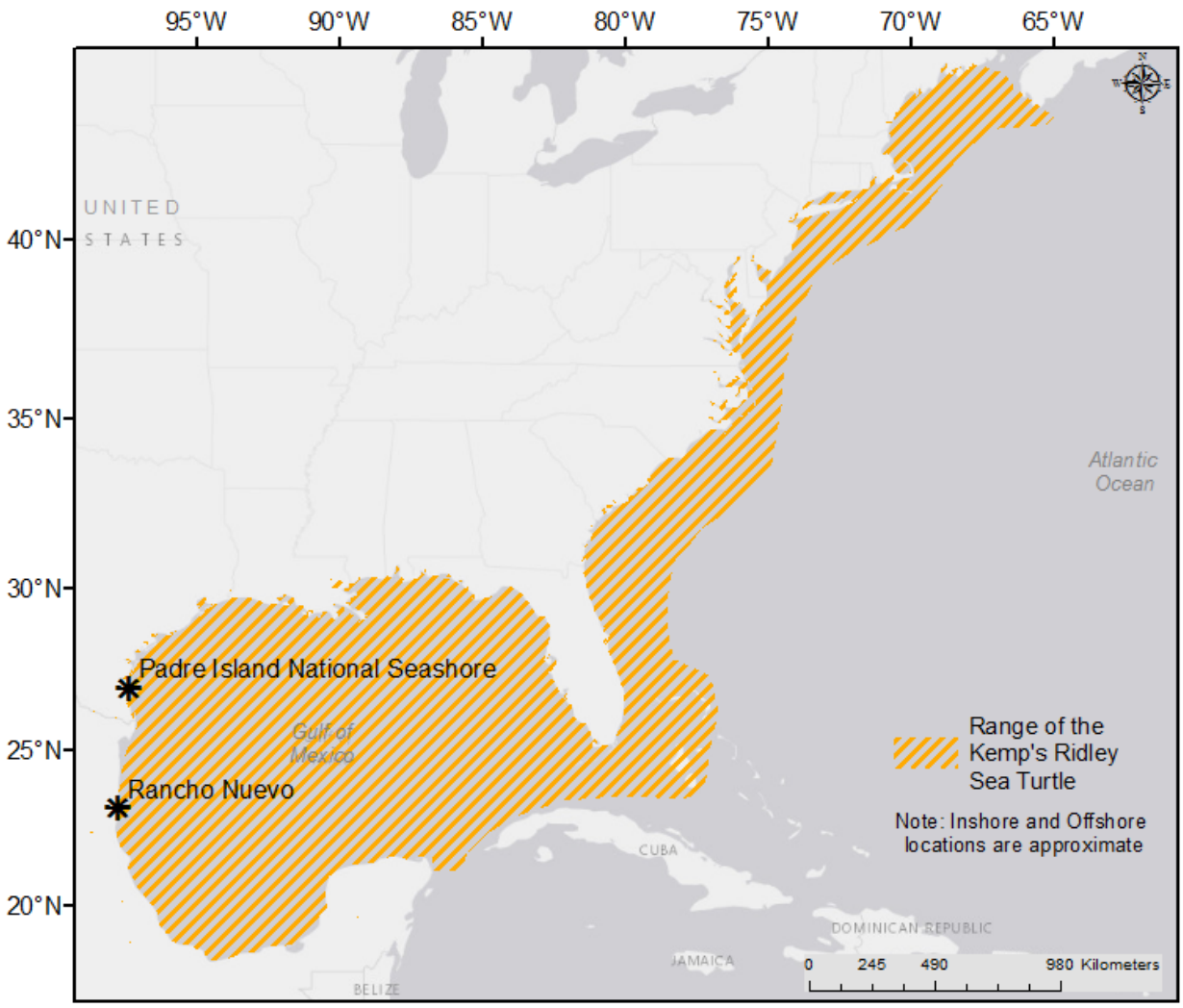

Figure 4: The approximate range of the Kemps ridley sea turtle and the location of the main nesting beaches of the species, Padre Island National Seashore, TX, USA and Rancho Nuevo, Mexico. Derived from NMFS *et al.* (2010).

The beach at Rancho Nuevo, Mexico is a high-energy, dissipative beach (Wright & Short, 1984) characterized by fine grain sand and low dunes stabilized by coastal plants and fine grain sand. Forming reef-like barriers, sand flats parallel the beach (Bevan *et al.*, 2016; NMFS & USFWS, 2015). The dunes in this region are stabilized by bushy coastal vegetation similar to that of Padre Island, Texas, including sea oats and spartina alterniflora (Marquez-M., 1994). Two berms, varying in width from 15-45 m, usually form the beach. On the landward side of the

beach, coastal lagoons with several narrow cuts surround the beach (NMFS & USFWS, 2015). Carranza-Edwards *et al.* (2004) notes that beaches near Rancho Nuevo, Mexico are narrower and steeper in comparison to beaches near the center of the Rio Grande delta (Figure 5). This corresponds to larger particle sizes, poorly sorted sediments and the presence of shell fragments in this region (Carranza-Edwards *et al.*, 2004). Similarly, along the central section of Padre Island, the beaches are steeper, narrower, and characterized by the presence of shell fragments (NMFS *et al.*, 2010; NMFS & USFWS, 2015).

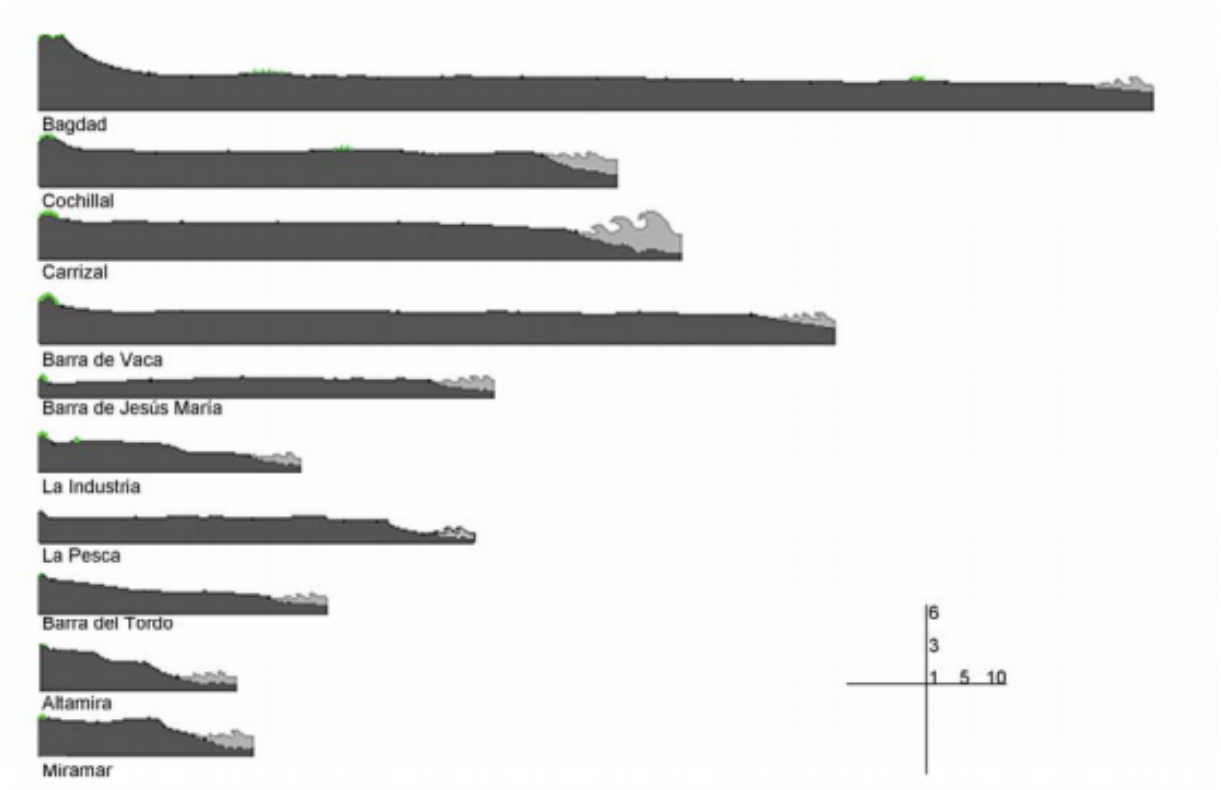

Figure 5: Beach profiles in Tamaulipas, Mexico (2x vertical exaggeration). Rancho Nuevo is located near Barra del Tordo. (Carranza-Edwards *et al.*, 2004).

Nesting Preferences

Environmental factors affect embryo survivorship, hatchling quality, and sex ratio. Therefore, nest site selection largely determines the fitness of a nesting female because it significantly influences hatchling survival (Horrocks & Scott, 1991; Wood & Bjorndal, 2000;

Zavaleta-Lizarraga & Morales-Mavil, 2013). Females respond to various signals, both biotic and abiotic, to attempt to select the most successful site for her eggs, making nest site selection non-random (Weishampel *et al.*, 2006; Zavaleta-Lizarraga & Morales-Mavil, 2013). According to Wood and Bjorndal (2000), sea turtle nest site selection can be divided into three stages: beach selection, emergence of the female, and nest placement. Beach selection and emergence probably depend on offshore cues and beach characteristics, such as slope and dune profile (Wood & Bjorndal, 2000). A number of selective forces drive nest placement both seaward towards the shoreline and landward away from it; nests close to the sea have a higher probability of inundation and egg loss due to erosion while nests further from the sea are more likely to result in predation and hatchling disorientation (Wood & Bjorndal, 2000; Santos *et al.*, 2006).

The biophysical features of beaches that affect nesting preference have long been thoroughly studied, but morphological characteristics influencing nest site selection have not been researched to the same extent (Horrocks & Scott, 1991; Yamamoto *et al.*, 2012). Furthermore, there has been little to no research regarding the connection between beach geomorphology and Kemp's ridley nesting site selection, but studies regarding other species of sea turtles suggest that beach characteristics may be important factors in determining sea turtle nesting site preferences (Santos *et al.*, 2006; Yamamoto *et al.*, 2012).

While it is well known that females prefer to nest on beaches with fine grain sands because it is more difficult to dig egg chambers in coarse, dry sand, Mortimer (1982) predicted that slope and offshore configuration are potentially more important than sand grain properties in nesting preferences, but their relative importance was not quantified (Mortimer, 1990; Mortimer, 1982). One study found that segments of beaches with higher beach face slopes and narrower widths had higher nest densities of loggerhead turtles than beaches with lower slopes and wider

widths (Provancha & Ehrhart, 1987). Research regarding hawksbill turtles found that nest elevation above sea level was positively related to hatching success. Furthermore, this study found that hawksbills nested further from the high tide line on beaches with less steep slopes, suggesting that they prefer to nest at a certain mean elevation above sea level (Horrocks & Scott, 1991). Similarly, Wood and Bjorndal (2000) found that out of the factors slope, temperature, moisture, and salinity, slope had the largest impact on nest site selection of loggerheads, likely because it is correlated with nest elevation. A study in Mexico discovered that green sea turtles prefer beaches with steeper slopes, specifically a steeper berm slope, while hawksbill turtles nest site selection extended to a wider range of beach morphology characteristics (Cuevas *et al.*, 2010). A similar study regarding nest site selection by the green sea turtle in Mexico found that the most utilized nest sites were characterized by beaches at least 1,300 m long with gentle to medium slopes (Zavaleta-Lizarraga & Morales-Mavil, 2013).

Most recently, Dunkin *et al.* (2016) developed a model that accurately predicts loggerhead nesting habitat suitability in Florida using elevation, beach slope, beach width, and dune peak as predictors. Consistent with the findings of several of the aforementioned studies, they found that elevation was the most influential factor for nesting preferences (Dunkin *et al.*, 2016). Similarly, Yamamoto *et al.* (2012) successfully modeled nest density for three different sea turtle species using a limited number of geomorphology variables. This study found that each sea turtle species exhibited a tolerance for beaches with a wide range of measured geomorphology variables but would not nest on beaches outside of this tolerance (Yamamoto *et al.*, 2012).

The specific preference of nesting beach characteristics varies between species, possibly due to the difference in size and weight between each species. This makes the specific preference

of nesting beach characteristics for the Kemp's ridley unidentifiable. Considering the importance that slope and elevation have in regards to nest site selection of various species of sea turtles, it is possible that they are important aspects of Kemp's ridley nesting preference. Additionally, other geomorphology features, such as dune height, rugosity, aspect, beach width, distance from shoreline, and offshore configuration, might also be important aspects of nesting preference for the Kemp's ridley. Marquez-M. (1994) notes that on beaches in Rancho Nuevo, Mexico, the Kemp's ridley usually nests beyond the high tide line in front of the first dune, on the windward slope of the dune or on top of the dune. This report describes the distribution of nests at relative positions along a beach profile, but it fails to quantify the characteristics of each position, such as elevation or distance from shoreline, and to assess alongshore nesting preferences in relation to beach geomorphology characteristics, such as beach slope or width (Marquez-M., 1994).

Imprinting

Some studies suggest that sea turtles return to nest in the region where they were hatched through imprinting or a natal homing mechanism (Shaver *et al.*, 2016b). The previously mentioned PAIS Restoration Program was constructed around this concept, in hopes that released hatchlings would return to PAIS to nest and form a nesting colony. According to Shaver *et al.* (2016b), most nesting turtles observed in south Texas from 1978-2014 were wild-stock turtles (89.4 %), while 7.9% were Padre Island-imprinted head-start turtles and 2.7% were Mexico-imprinted head-start turtles (Figure 6). While Padre Island-imprinted sea turtles are returning to the National Seashore, it is unclear the degree to which imprinting effects nesting beach selection on the National Seashore itself. The nests of imprinted sea turtles are widely distributed along PAIS, suggesting that the location of the release site is not the only determining factor for nest site selection. Furthermore, a recent study by Shaver *et al.* (2017) found that 95%

of documented Kemp's ridleys nested more than once on the Texas coast between 1991 and 2014 on the same or nearby beaches, but only a small portion demonstrated site fidelity, defined as 13.5 km or less between nest sites. On PAIS, the mean distance between nests of females that nested more than once in the same season was 18.7 km, with a range of 0.3 to 77.3 km (Shaver *et al.*, 2017). This variability in nest location within the region further suggests that more factors than solely imprinting affect nest site selection.

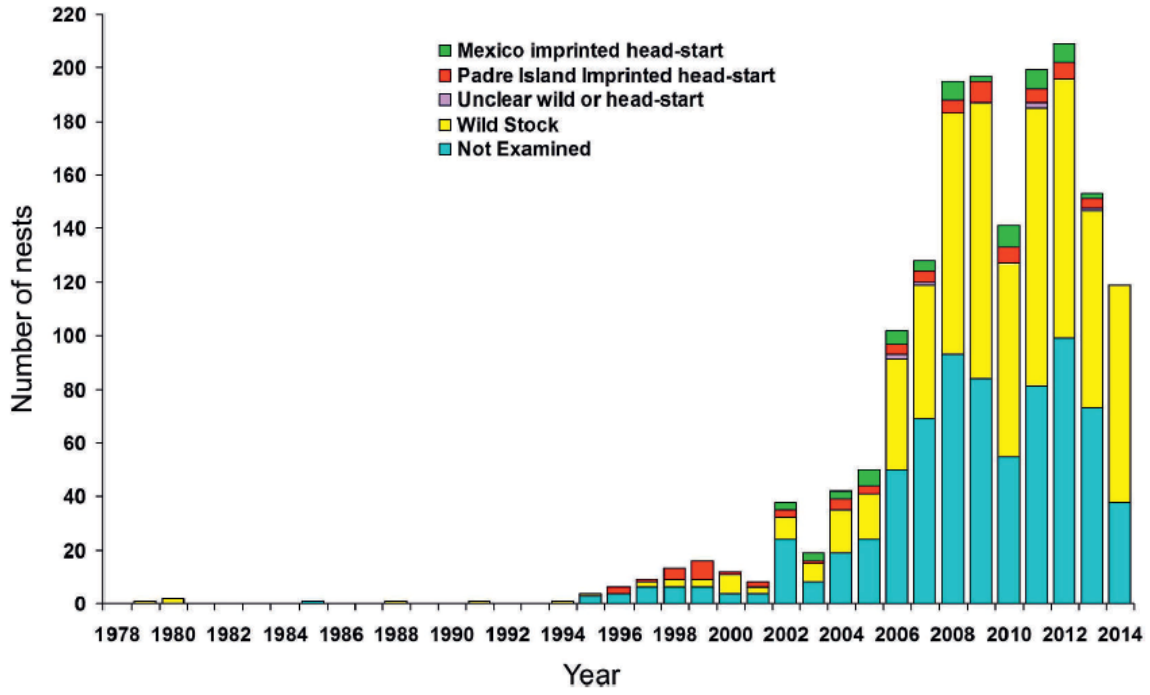

Figure 6: Annual nest counts of Kemp's ridleys found on the Texas coast from 1978-2014 differentiated by wild stock and imprinting location of hatchlings in the PAIS Restoration Program. (Shaver *et al.*, 2016b).

Potential Threats to Terrestrial Habitat

The terrestrial habitat for a sea turtle is a critical, limiting factor for successful reproduction due to the limited area in which suitable environmental conditions occur for nesting, making any threat to the terrestrial environment extremely impactful (Pike, 2013). Sea level rise can cause inundation, sand erosion, and changes in topography that are difficult for

turtles to traverse, which therefore effectively decreases the availability of suitable nesting habitat (Santos *et al.,* 2015; Ussa, 2013; Witt *et al.,* 2010).

According to a vulnerability assessment of PAIS, the most influential factors controlling how Padre Island will respond to sea-level rise are geomorphology and shoreline change (Pendleton *et al.,* 2004). Beach slope, width, elevation, and other morphological features are factors that may be key to nesting preference that are also at risk of SLR-induced changes (Santos *et al.,* 2015; Stutz & Pilkey, 2011; Williams, 2013). It is very probable, therefore, that North and South Padre Islands will undergo changes caused by SLR that put the Kemp's ridley sea turtle terrestrial habitat at risk.

Average annual long-term shoreline rates along Padre Island range from over 2m of retreat per year to 2m of accretion, with the most accretion occurring at the central section of North Padre Island (Paine *et al.,* 2013). Climate change may also increase the magnitude of storm events, which can be extremely destructive to sea turtle habitat (NMFS & USFWS, 2015; Long *et al.,* 2011). A recent study found that the more the shape of a beach profile was changed from its pre-hurricane morphology, the further nesting success declined (Long *et al.,* 2011).

Beach nourishment projects are often completed in response to shoreline erosion caused by hurricanes or other damaging processes. However, beach nourishment efforts may not fully restore the sea turtle nesting habitat to its full potential and, furthermore, can potentially decrease survivorship of eggs and hatchlings. This is because nourishment projects can change beach characteristics such as beach slope and width, sand compaction, gaseous environment, hydric environment, containment levels, nutrient availability, and thermal environment (Crain *et al.,* 1995; Gallaher, 2009).

Study Area

The study area for this research is the beaches of Padre Island National Seashore on North Padre Island and South Padre Island, Texas, USA (Figure 7). North and South Padre Islands are barrier islands that run parallel to the coastline, separated from the mainland by the shallow estuaries of the Upper and Lower Laguna Madre, respectively (Judd *et al.*, 1977; Weise & White, 1980). Collectively, North and South Padre Islands extend 182 km from Corpus Christi to Brazos-Santiago Pass, varying from 450 m to 4.8 km in width (Judd *et al.*, 1977). Port Mansfield Channel is a human-made and jettied channel that separates South Padre Island from North Padre Island (Judd *et al.*, 1977). Padre Island National Seashore, located on North Padre Island, is mostly undeveloped and spans roughly 112 km of coastline, covering 52,745 ha (KellerLynn, 2010).

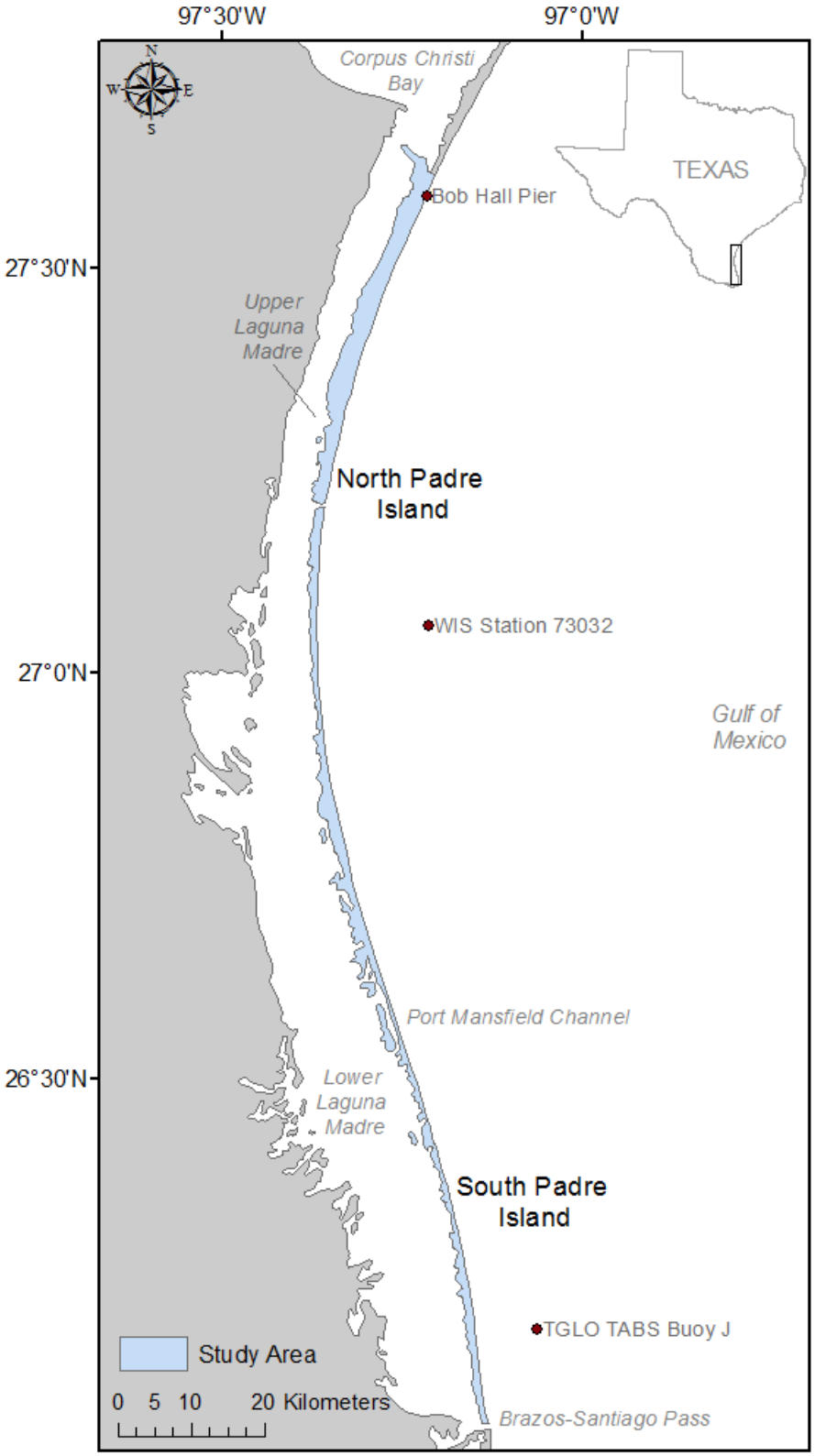

Figure 7: Map of the study area, North and South Padre Islands, Texas, USA.

Geologic History

Padre Island is a fairly young island geologically; according to radiocarbon dating of shells, it is estimated to have begun forming approximately 4,500 years ago (Weise & White, 1980). It is hypothesized that Padre Island began as a submerged sand bar formed from offshore shoals that grew via spit accretion (Weise & White, 1980). Approximately 18,000 years ago during the Last Glacial Maximum, sea level was 90 to 140 meters lower than present-day, thus exposing a large portion of the currently submerged continental shelf (Weise & White, 1980). During this time of low sea level, rivers deposited sediments in the Gulf of Mexico. As glaciers melted and sea level began to rise, the old submerged river-delta deposits eroded and moved towards the shore via wave and current activity (Weise & White, 1980). Sand bars developed and eventually emerged as barrier islands, mostly positioned on the divides between historic river valleys. Longshore currents transported and deposited sand onto the islands, resulting in spit accretion (KellerLynn, 2010; Weise & White, 1980). Aeolian and marine processes helped the island to develop vertically into the modern barrier island, but the same processes continue to re-shape the island today. Though the northern half of the island is currently in a relatively stable state of equilibrium, South Padre Island has been in an erosional or destructive state for some time (KellerLynn, 2010; Weise & White, 1980).

Beach Characteristics and Geomorphology

As a barrier island system, Padre Island is composed of a series of geomorphic zones that are shaped by the forces of tides, winds, and waves (Figure 8). From the Gulf of Mexico moving landward, these geomorphic zones are nearshore, forebeach, backbeach, coppice dunes, active dunes, stabilized blowout dunes, vegetated barrier flat, and back-island sand flats (KellerLynn, 2010). In the barrier flats and storm washover channels, brackish and freshwater marshes and

ponds may form. In the southern area of Padre Island, washover channels cut through the island. Wind-deflation flats separate the barrier island and lagoon systems. The lagoon system includes wind-tidal flats (also referred to as Sabkhas), lagoon-margin sand, and grassflats (KellerLynn, 2010).

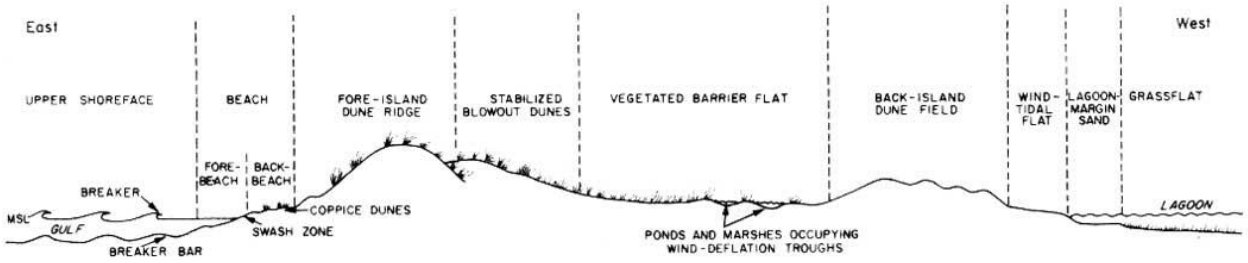

Figure 8: Generalized cross section of North Padre Island displaying the geomorphic zones. (Weise & White, 1980).

The trends in the geomorphology characteristics of the beaches of North and South Padre Islands vary alongshore (KellerLynn, 2010; Weise & White, 1980). The northern section of the island consists of broad beaches, large foredunes, and grasslands and the beaches here are typically higher and wider than the southern section. The beaches are also high-energy and predominately dissipative, characterized by a double-barred beach profile (Weymer, 2012; Wright & Short, 1984). The shape of the Texas Gulf shoreline causes longshore currents to converge near the central section of North Padre Island, where wave fronts are parallel to the shore (Figure 9). This convergence results in the accumulation of sediment and shell fragments, thereby causing the beach to be steeper since slope is directly related to sediment size (Davis, 1977; Watson, 1971; Weise & White, 1980). Therefore, along the central section of the study area, narrower beaches with a steeper topography and a plethora of shells are dominant, making these beaches predominantly reflective (Weymer, 2012; Wright & Short, 1984). The beaches in this area are characterized by extensive foredunes stabilized by vegetation, some of which reach 15m in height (Davis, 1977; KellerLynn, 2010). In the southern section of North Padre Island, the beaches are relatively flat, the foredunes are sparse, and the vegetation is scattered. Washover

channels and blowout dunes are more frequent in this area (KellerLynn, 2010; Judd *et al.*, 1977). The beaches in this region are predominately dissipative or intermediate (Wright & Short, 1984).

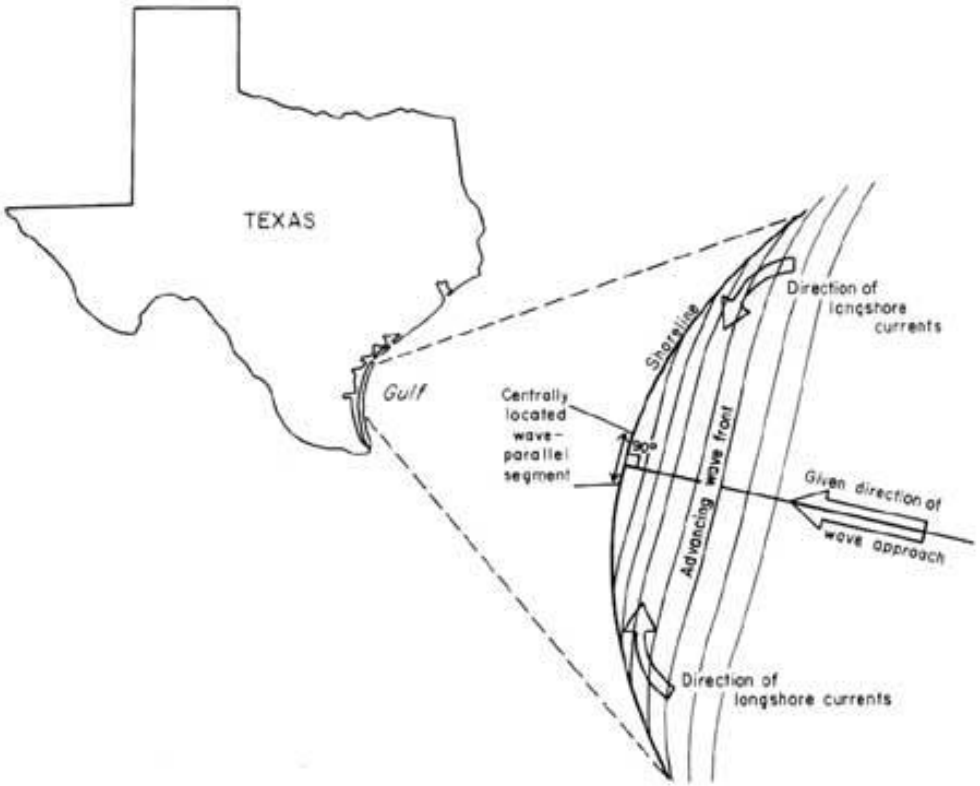

Figure 9: Longshore currents converge near the central section of North Padre Island, causing wave fronts approaching at a 90° angle to be parallel to the shore. (Weise & White, 1980).

On South Padre Island, there is a considerable amount of variability in morphology. It ranges from well-developed foredunes with a height of 12m to washover channels lacking vegetation (Houser & Mathew, 2010). Overall, the beaches in this area are composed of wide backbeach areas and a gentle foreshore (Davis, 1977). South Padre Island has been experiencing widespread erosion due to a substantial loss of sediment supply from the Rio Grande River Delta caused by flow reductions and reservoir sedimentation (Houser & Mathew, 2011). This erosion is exacerbated by extreme storms that breach the dunes and move sediment into Laguna Madre through washover channels (Houser & Mathew, 2011).

There are documented variations in mean grain size along the study area (Davis, 1977) (Figure 10). The southern section of North Padre Island is characterized by fine grain sizes with little temporal or spatial variation. Mean grain size in the northern section of North Padre Island is overall finer than the grain sizes in the other sections of the study area and, like the southern section, shows little variation in time and space. However, the mean grain sizes of the central section of North Padre Island, the site of longshore current convergence, display both temporal and spatial variation, with some sites composed of fine sediments and other sites composed of coarser sediments (Davis, 1977).

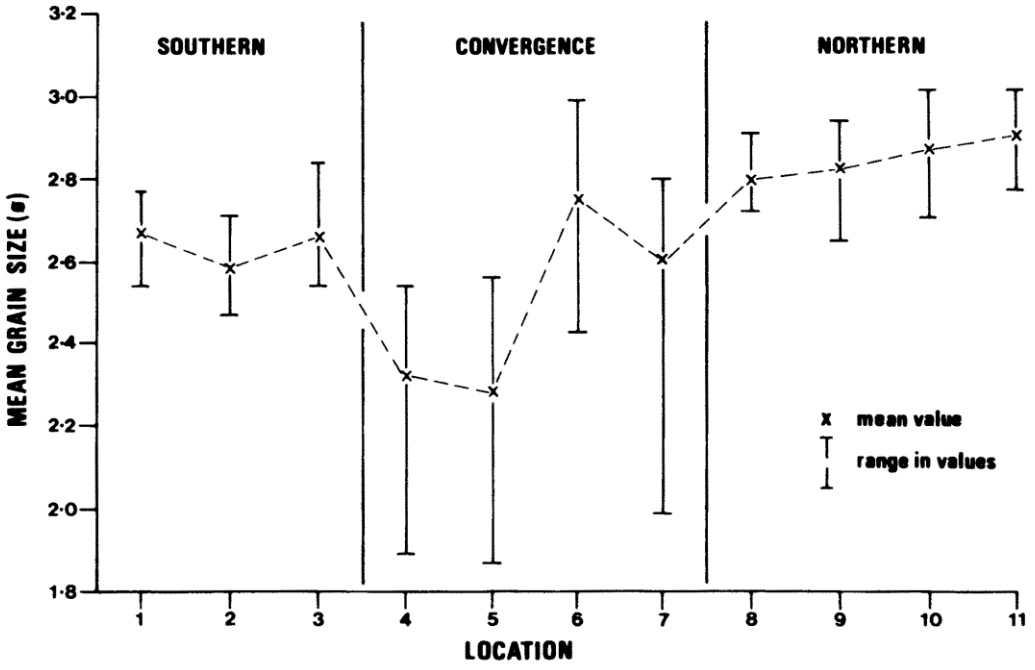

Figure 10: Range and mean values of foreshore mean grain size (φ) for each relative section of Padre Island, with convergence occurring at the central section of North Padre Island. (Davis, 1977).

Physical Processes

As is typical of the Texas Gulf Coast, the tidal range of North and South Padre Islands is small (Weise & White, 1980). North and South Padre Islands are microtidal and diurnal, with a mean diurnal tidal range of 0.43 m and 0.49 m, respectively (Houser & Mathew, 2010; Weise &

White, 1980). Wind tides, which occur when strong winds elevate the water surface, can cause large changes in the water level and are much more influential than astronomical tides (KellerLynn, 2010). Wind tides can produce a rise and fall of water levels by as much as 0.6 m, which can expose or submerge the beach profile and cause erosion or deposition. Similarly, storm tides and waves produced by hurricanes and storms can cause large changes in the beach and foredunes that may take years to recover to pre-storm conditions (Weise & White, 1980).

As previously mentioned, wind is an important driver for waves, currents, tides and aeolian processes in the Gulf of Mexico (Curray, 1960; Weise & White, 1980). South and southeasterly winds occur most frequently in the study area, but northerly winds associated with a cold front dominate during the winter (U.S. Army Corps of Engineers, 2014) (Figure 11). Concurrent with trends in wind direction, waves most frequently approach from the southeast (U.S. Army Corps of Engineers, 2014) (Figure 12). Waves along Padre Island are on average around 1 m in height, but they can be over 2 m high during storms (U.S. Army Corps of Engineers, 2014; Weise & White, 1980).

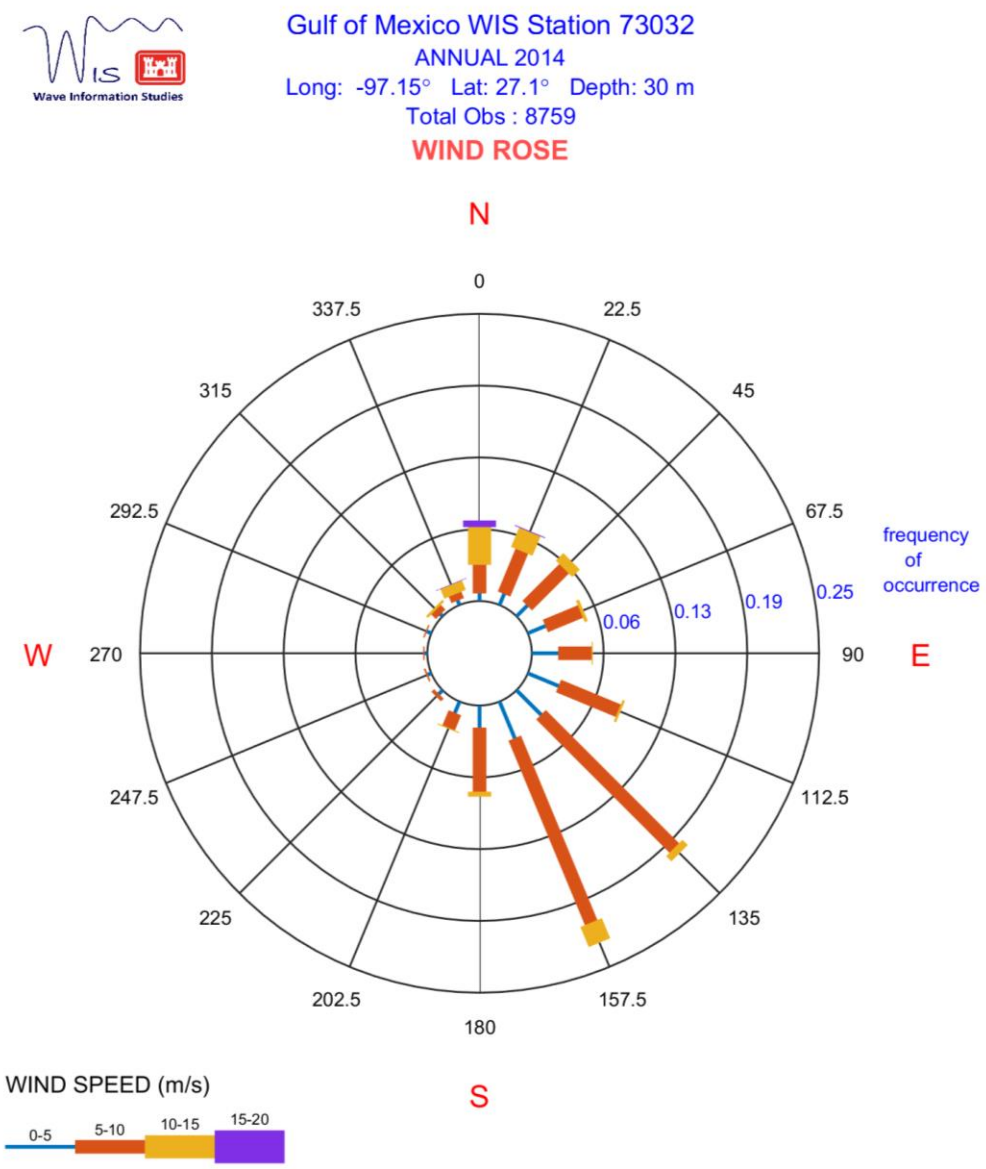

Figure 11: Wind Rose of Gulf of Mexico WIS Station 73032, located near the central section of the study area, for 2014. See Figure 7 for location. (Wave Information Study, http://wis.usace.army.mil/).

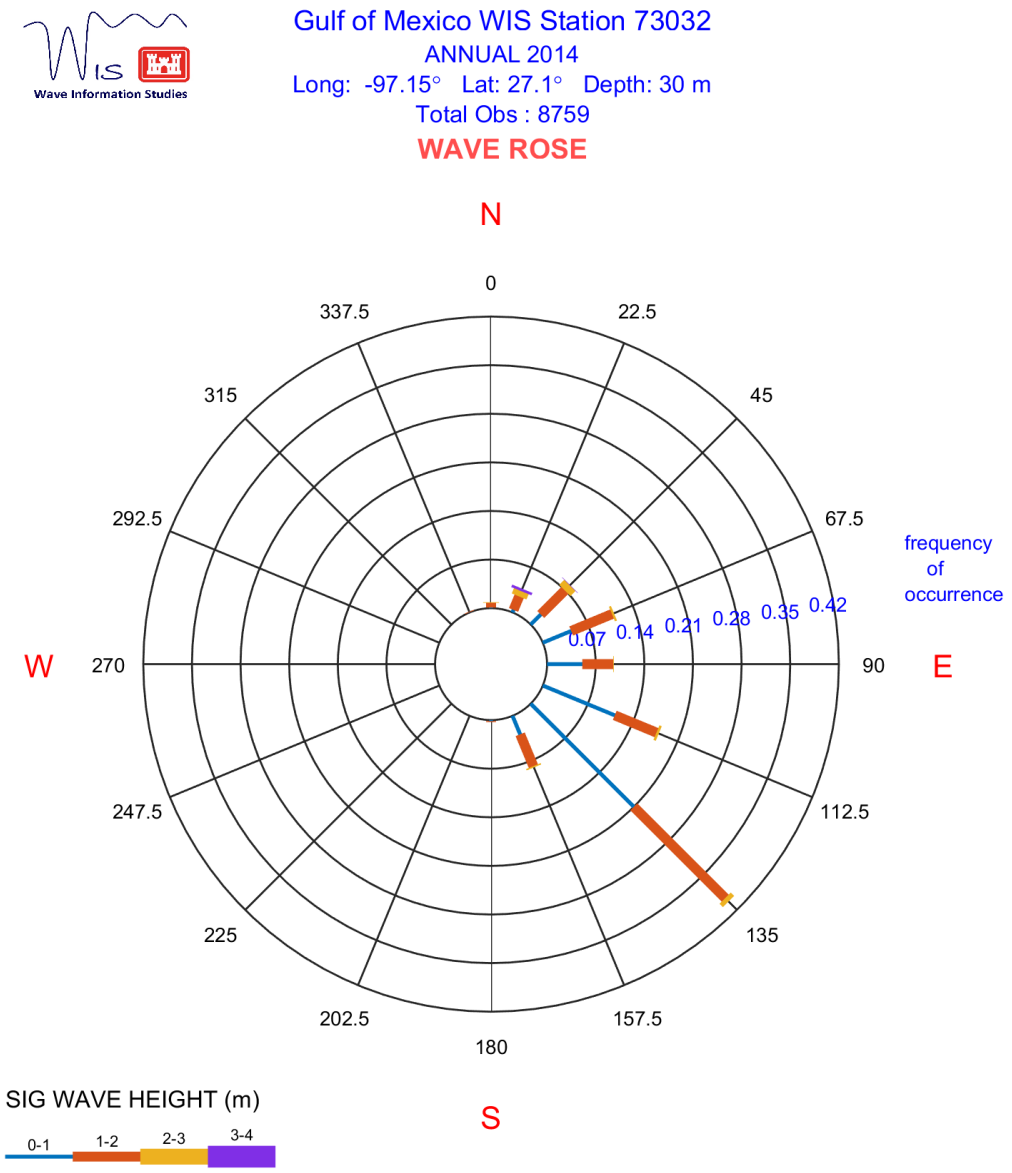

Figure 12: Wave Rose of Gulf of Mexico WIS Station 73032, located near the central section of the study area, for 2014. See Figure 7 for location. (Wave Information Study, http://wis.usace.army.mil/).

METHODS

Light Detection and Ranging (lidar) uses laser pulses to obtain spatially dense and accurate elevation data capable of displaying small differences in elevation across a landscape (Yamamoto *et al.,* 2012). Laser pulses emitted from an aircraft-mounted lidar system reflect from objects both on and above the ground, and any laser pulse that encounters multiple reflection surfaces is split into multiple returns (Houser *et al.,* 2008). The first return is associated with the highest feature, or the first reflection surface that the laser pulse detects, and the last return is associated with the last reflection surface the laser pulse encounters, which may not always be the ground (Starek *et al.,* 2012). The spatial and temporal resolution of lidar data is ideal for extracting topographic information from coastal areas, making lidar data optimal for this study (Houser *et al.*, 2008; Yamamoto *et al.*, 2012).

Figure 13 depicts a flowchart of the methodology of this study, with the green box indicating the prominent steps. Lidar data collected in 2009, 2010, 2011, and 2012, and the coordinates of Kemp's ridley nests for the respective years on North and South Padre Islands, Texas, were compiled and processed. Background points were randomly generated within the study area for assessing the variability of the available nesting area. Next, beach geomorphology characteristics were extracted from the lidar data at each nest coordinate and background point, which were then statistically analyzed using generalized linear models and a random forest to assess both the relationship between nest presence and the geomorphology characteristics and the capacity of geomorphology characteristics in predicting nest presence. To determine if environmental variables influence nesting preferences, average daily environmental conditions for each day during nesting season were also obtained and statistically analyzed with respect to daily nest counts.

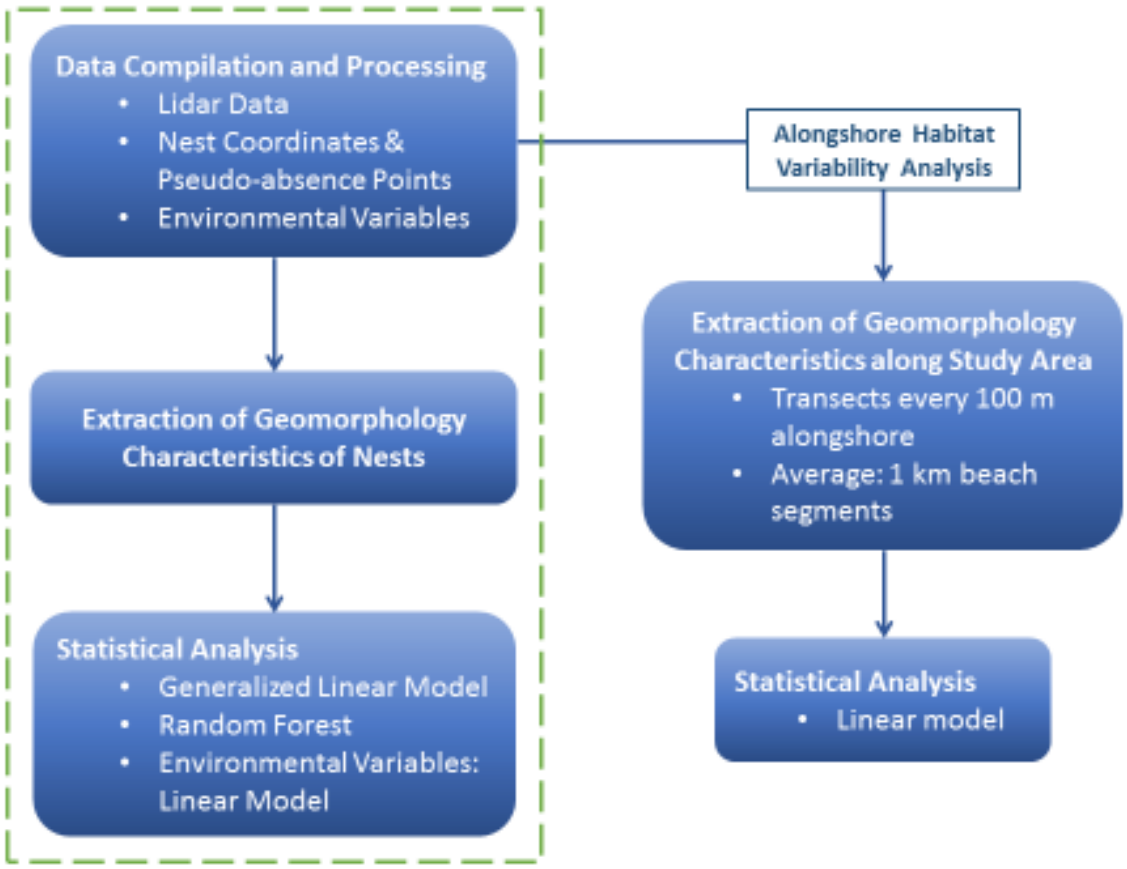

Figure 13: Flowchart of the methodology of the study, with the green box indicating the prominent procedure.

Labeled 'Alongshore Habitat Variability Analysis' in Figure 13, the next portion of the methodology aims to quantify the habitat variability alongshore and assess the relationship between alongshore trends in geomorphology and nest presence. Cross-shore topographic profiles were generated every 100 m alongshore, from which beach geomorphology characteristics were extracted. Subsequently, the profiles were grouped together in 1 km beach segments and the average geomorphology characteristics within each group were statistically analyzed with respect to nest density, resembling the methodologies used in studies regarding other sea turtle species (Cuevas *et al.*, 2010; Long *et al.*, 2011; Provancha & Ehrhart, 1985; Rousoo *et al.*, 2014; Yamamoto *et al.*, 2012; Zavaleta-Lizarraga & Morales-Mavil, 2013).

Data Compilation and Processing

Lidar Data

The Bureau of Economic Geology (BEG), the Center for Space Research, and Texas A&M-Corpus Christi conducted three airborne lidar surveys of the Texas Gulf of Mexico shoreline every year from 2010 through 2012. The 2010 and 2011 surveys were conducted in April at the beginning of Kemp's ridley nesting season while the 2012 survey was conducted in February, a few months prior to the start of nesting season (Paine *et al.*, 2013). Lidar instrument settings for these surveys were as follows: laser pulse rate, 25 kHz; scanner rate, 26 Hz; scan angle, +/- 20 degrees; beam divergence, narrow; altitude, 570 to 1200 m above ground level; and ground speed, 50 to 120 kts (Paine *et al.*, 2013). The horizontal datum is North American Datum of 1983 (NAD83), the ellipsoid is Geodetic Reference System of 1980 (GRS80), and the vertical datum is North American Vertical Datum of 1988 (NAVD88). The projected coordinate system of the data is Universal Transverse Mercator, Zone 14 N (UTM 14 N) (Paine *et al.*2013). BEG transferred the raw flight data into lidar point files, applied bias correction to the first and last return, and converted z-values from height above the GRS80 ellipsoid to elevations with respect to NAVD88 using the Geoid99 geoid model. The BEG has thoroughly performed quality assurance and quality control on the data (Paine *et al.*, 2013) (Table 1).

In 2009, the US Army Corps of Engineers (USACE) Joint Airborne Lidar Bathymetry Technical Center of Expertise (JALBTCX) collected lidar data of the South Texas Gulf of Mexico shoreline for the West Texas Aerial Survey 2009 project. The survey was conducted between February and April, just before Kemp's ridley nesting season (Table 1). The lidar point cloud was gathered at a density sufficient to produce a maximum final post spacing of 1.5 points

per meter (NOAA *et al.*, 2016). The horizontal datum is NAD83, the ellipsoid is GRS80, and the vertical datum is NAVD88 using the Geoid12A geoid model (NOAA *et al.*, 2016). This data has undergone accuracy assessment and quality control by the originator (Table 1). Using NOAA/NOS's VDatum, the data was converted from Geoid12A to Geoid99, the same geoid as the 2010-2012 BEG lidar data. The las2las tool in LAStools (Isenburg, 2017) was used to project the 2009 LAS files into UTM 14 N.

Table 1: Information from NOAA et al. (2016) and Paine et al. (2013) about the accuracy of the lidar data from the USACE and BEG, respectively.

Source	Collection Timeframe	Point Spacing (m)	Horizontal Accuracy (m)	Vertical Accuracy (m)
USACE	02-04/2009	1.5	1	0.15
BEG	04/2010	1	1	0.1
	04/2011			
	02/2012			

The las2las tool in LAStools was used to filter the 2012 lidar data by return points. The 2009-2011 lidar data was already classified by return points. The last return points were used for this project in order to reduce the probability of land cover biasing topography (Starek *et al.*, 2012).

The last return LAS files for each year were imported into ArcMap 10.4.1 as LAS datasets and the statistics for each LAS dataset were calculated. The lidar data for each year was clipped to a polygon of the study area using the Clip tool in ArcGIS. To assess the point density of the last return lidar points, the LAS Point Statistics as Raster tool in ArcGIS, with the method set to pulse count, was used to create point density rasters for each year (Figure 14). The point density rasters were used to check for voids and to determine the ideal resolution for the elevation rasters. The Apply Filter tool in ArcGIS was used to locate any outliers in the data by

identifying data points that exceed a height or slope difference relative to neighboring measurements within 30 meters. To eliminate outliers in the data, the las2las tool in LAStools was used to filter out data above an elevation of 20 meters, a threshold that is above the maximum dune height.

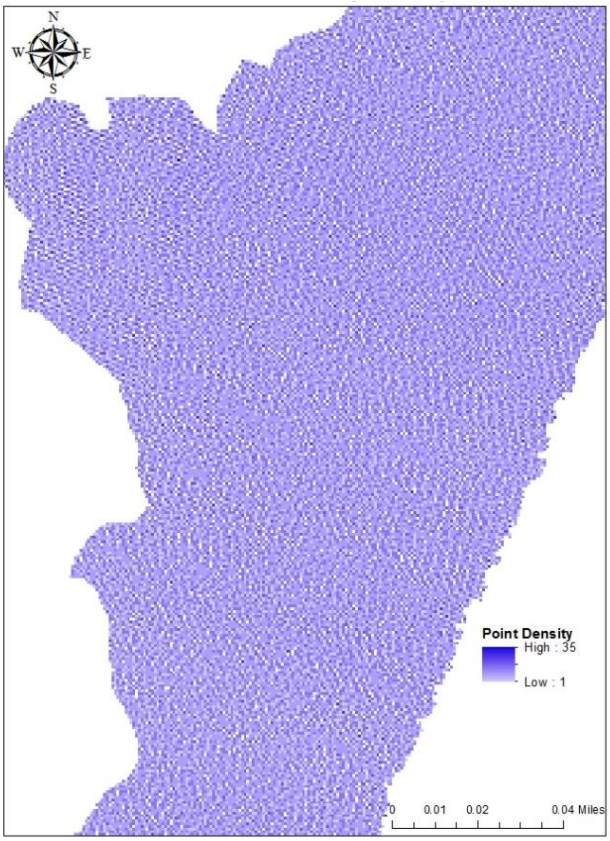

Figure 14: Example of a point density raster with a 1 m x 1 m cell size for the 2010 lidar data.

The data points were classified into ground and vegetation points using LAStools. To assess the effect of filtering point classifications when gridding the lidar data, 1 m x 1 m resolution elevation rasters of all last return points, ground points, and ground and vegetation points were created for a subset of the 2012 data using the LAS Dataset to Raster tool in ArcGIS (Figure 15). The cell assignment method used in the tool was inverse distance weighted (IDW) and the void fill method was natural neighbor interpolation.

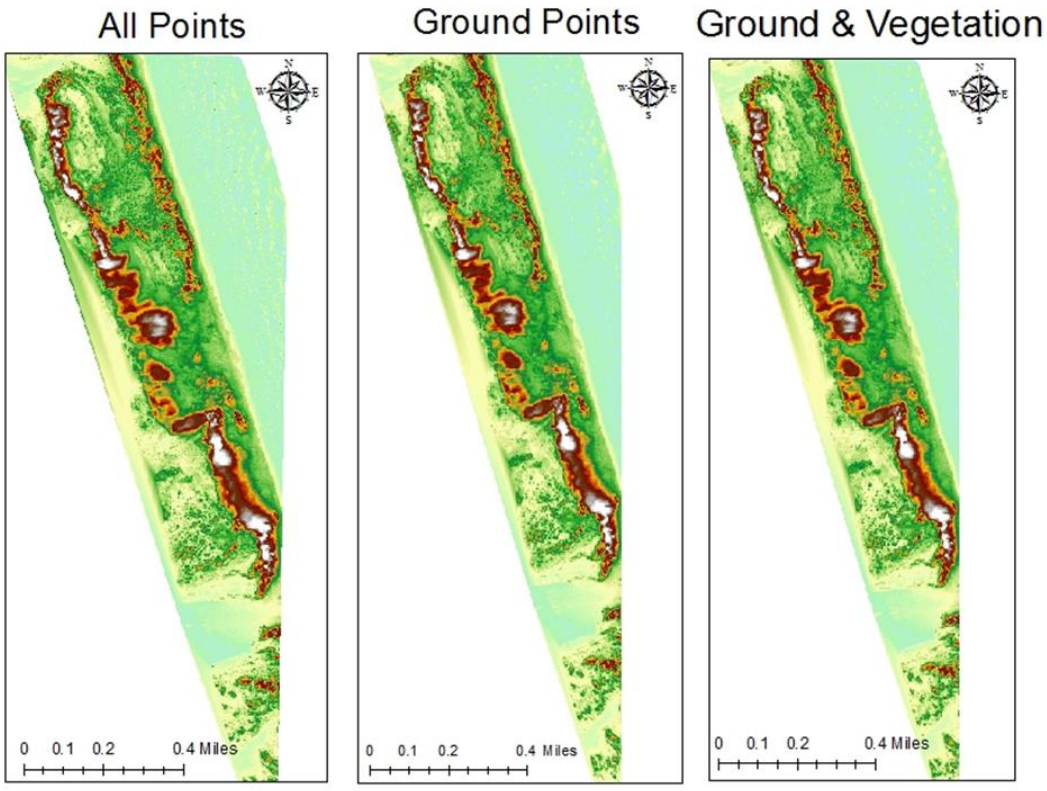

Figure 15: Elevation rasters (1 m x 1 m cell size) created using ground, ground and vegetation, and all point classification filters for a subset of the 2012 data. Red and white indicate areas of high elevation and light green indicates areas of low elevation.

The use of only ground points or of ground and vegetation points caused the dune profiles to be flattened, and otherwise, there were minimal differences between surfaces generated using ground, ground and vegetation, and all point classification filters. Therefore, all last return points for each year were used to generate 1-m x 1-m resolution elevation surfaces. Each LAS file was gridded using an IDW operation developed in the Coastal and Marine Geospatial Lab at Harte Research Institute for Gulf of Mexico Studies. This method generated surfaces with a consistent method for both cell assignment and void fill. The search radius for the IDW operation was 2.5 m and the operation used a maximum of 3 points within that search radius. In ArcGIS, the Mosaic to New Raster tool was used to combine the rasters into a consistent surface for each year.

Bias between surveys in the lidar data was calculated by comparing the elevation of roads, a feature that should maintain a consistent elevation through the years. Most of the study area is undeveloped, so the roads available for this calculation were limited to the northern-most section of North Padre Island and the southern-most section of South Padre Island (Figure 16). Roads were outlined using the Draw tool in ArcGIS and then points were created every 1 meter along the roads using the Create Station Points tool in the ET GeoWizard extension for ArcGIS. Elevation data for each year was extracted from the gridded elevation surfaces to the points using the Extract Values to Points tool in ArcGIS. The difference in elevation between subsequent years was calculated. Due to the limited extent of roads within the study area and the minimal differences between the elevations of the roads for each year, the bias in the lidar data was not corrected (Table 2 & Appendix A).

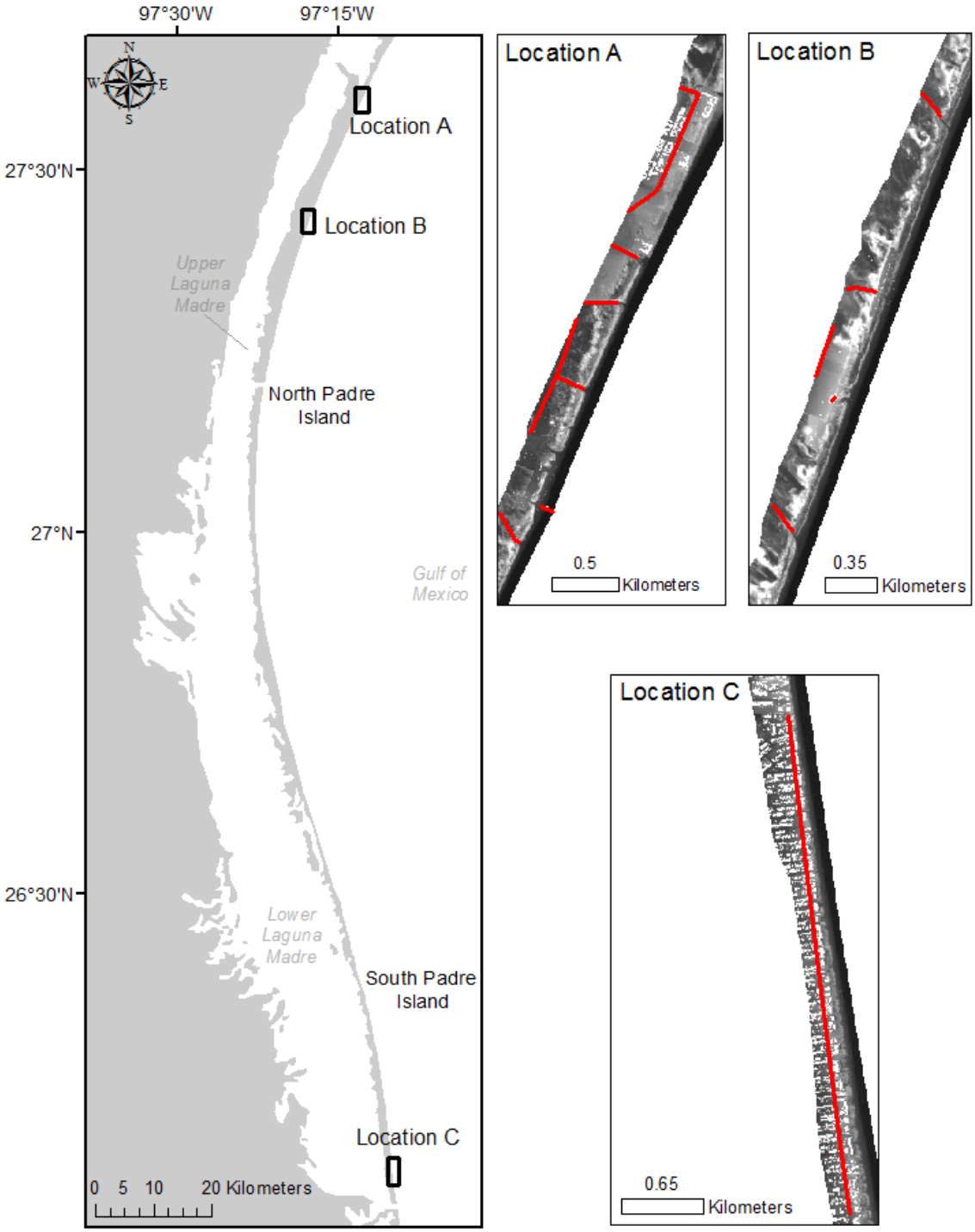

Figure 16: Map depicting the location of the roads used for the calculation of the bias between the surveys in the lidar data. Locations A and B are referred to as the North in Table 2 and Location C is referred to as the South.

Table 2: Mean bias and standard deviation (m above NAVD88) between surveys in the lidar data in the North and South.

Year	Mean Bias: North	Standard Deviation: North	Mean Bias: South	Standard Deviation: South
2012-2011	0.14	0.062	0.017	0.045
2011-2010	-0.041	0.053	0.072	0.045
2010-2009	-0.23	0.044	0.0054	0.044

Nest Coordinates

Padre Island National Seashore Sea Turtle Division employees used Garmin GPS 72 and Garmin GPS 72H to record the coordinates of observed sea turtle nests on North Padre Island, Texas. Se Turtle, Inc. employees used Garmin GPS 72 or the Google Earth to document nest coordinates on South Padre Island, Texas. The coordinates of observed Kemp's ridley nests within the study area for the years 2009-2012 were obtained from Dr. Donna J. Shaver, the coordinator of the Sea Turtle Stranding and Salvage Network in Texas and Chief of Sea Turtle Science and Recovery at Padre Island National Seashore (Table 3). The geographic coordinate system of the data was set to WGS_1984, but the data was then projected to UTM 14 N, the coordinate system of the lidar data. Of the total 573 nest coordinates, 8 points (1.39%) were determined to be outliers and were excluded from the study. These coordinates, comprised of three points from 2012, four points from 2011, and 1 point from 2010, were located outside of the study area within the Gulf of Mexico, likely due to an instrumentation error when the nest coordinates were recorded.

Table 3: The number of Kemp's ridley nests confirmed within the study area from 2009 to 2012.

Year	North Padre Island	South Padre Island
2009	117	33
2010	74	28
2011	117	39

2012	106	59

Comparisons of various species distribution modeling techniques demonstrate that presence-absence models typically perform better than presence-only models (Barbet-Massin *et al.*, 2012; Edith *et al.*, 2006). Presence-absence models are increasingly used when only presence data is available by creating artificial absence data, referred to as pseudo-absence or background data (Barbet-Massin *et al.*, 2012; Edith *et al.*, 2006). Background data establishes the characteristics of the study area while the presence data provides the attributes of the area in which a species is more likely to be present (Phillips *et al.*, 2009). Background points were created for this study by using the Create Random Points tool in ArcGIS to randomly generate points within the study area (Barbet-Massin *et al.*, 2012; VanDerWal *et al.*, 2009). The background points were created on a 10:1 ratio to the nest coordinates in order to better capture the distribution of the features of the entire system. Furthermore, Barbet-Massin *et al.* (2012) found that model accuracy increased until an asymptote when the ratio of background to presence points reached 10:1 for generalized linear models and random forests.

Environmental Variables

A study by Shaver and Rubio (2008) concluded that adult female and male Kemp's ridleys are primarily inhabitants of near-shore waters with relatively shallow depths. Therefore, meteorological and physical data measured on Bob Hall Pier, located on North Padre Island, should be representative of the environmental conditions of adult females in nearby waters in the northern section of the study area (Figure 7). Similarly, environmental data from TGLO TABS Buoy J should characterize the environmental conditions of adult females in nearby waters in the southern section of the study area (Figure 7). However, historic data for TGLO TABS Buoy J was not available for the entire period of this study. After comparing the data from Bob Hall Pier

to the available data from TGLO TABS Buoy J, it was determined that the average daily data from Bob Hall Pier was representative of the average daily conditions at South Padre Island, Texas, so the data from Bob Hall Pier was used for the entire study area (Table 4).

Table 4: Mean difference between the average daily environmental variables measured at Bob Hall Pier and TGLO TABS Buoy J during nesting season in 2012. The average TGLO TABS Buoy J data was subtracted from the average Bob Hall Pier data.

	Mean Difference
Wind Speed (knots)	3.18
Wind Direction (degrees)	-3.13
Gust Speed (knots)	2.64
Water Temperature (°F)	3.66

Environmental conditions during nesting season each year were obtained from Bob Hall Pier (NWLON Station 8775870), including wind speed, wind direction, gust speed, atmospheric temperature, barometric pressure, water temperature, water level, and sigma of water level (NOAA, 2017). The daily average, maximum, and minimum for each of these variables was calculated and was associated with the daily nest count. It is important to note that information regarding air temperature, barometric pressure, and water temperature was missing for 5/16/2010 – 6/27/2010 and information regarding wind speed and gust speed was missing for 5/16/2010.

Extraction of Geomorphology Characteristics

Shoreline, potential line of vegetation, and landward dune boundaries were mapped to delineate the beach and the foredune complex within the study area for geomorphology characteristic extraction (Figure 17). Through the analysis of lidar data and beach profiles, Gibeaut *et al.* (2002) and Gibeaut and Caudle (2009) found that the wet/dry boundary typically occurs at 0.6 m above mean sea level on the Texas Gulf Coast. This elevation was mapped as the shoreline for each year. The potential vegetation line is the lowest elevation dune vegetation may

thrive along the Texas Gulf shore and is 1.2 m above mean sea level. The wet/dry line is the seaward boundary of the beach and potential vegetation line is the landward boundary of the beach and seaward boundary of the fordune. The ArcGIS Contour List tool was used to map the contours, and the contours were smoothed using a 5 m tolerance with the Polynomial Approximation with Exponential Kernel (PAEK) method of the Smooth Line tool in ArcGIS.

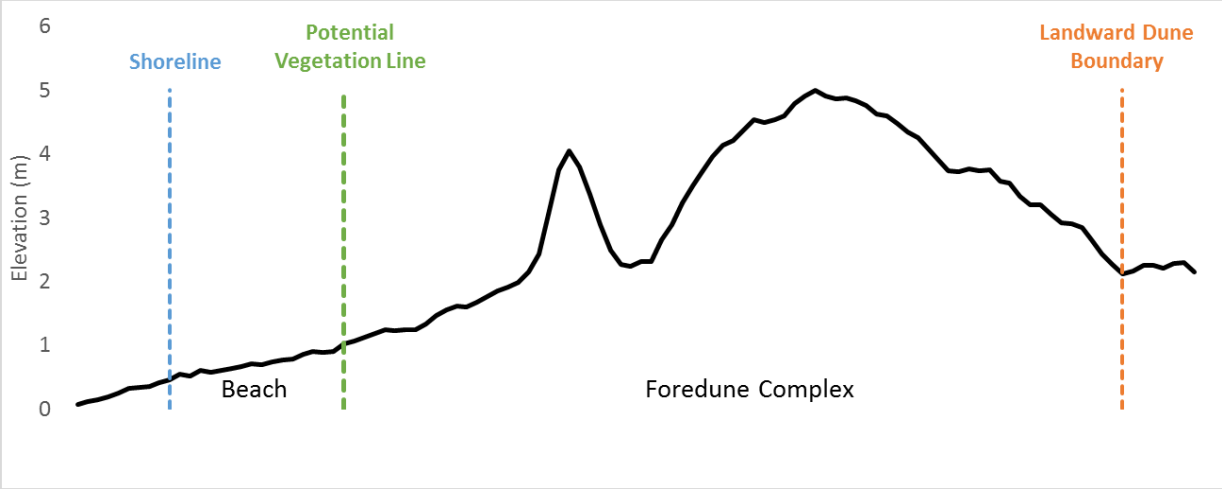

Figure 17: Example of a beach profile with shoreline, potential vegetation line, and landward dune boundaries delineating the beach and foredune complex.

The landward dune boundaries for the 2010-2012 data were mapped by the Coastal and Marine Geospatial Lab at Harte Research Institute, as outlined in Paine *et al.* (2013). The same systematic qualitative criteria used to generate the landward dune boundaries for 2010-2012, outlined in Appendix B, was used to create a landward dune boundary for 2009. The following criteria were used to determine inclusion in the fordune complex: change in slope from steep on the foredune to gentle on the back-barrier dune; elevation about 2 m above mean sea level; provides storm-surge protection; morphology is elongate parallel to the shoreline; proximity to the shoreline; density clusters of dune forms; and connection to other forms classified as foredunes (Appendix B).

The following procedure, which involves the use of basic tools in ArcGIS and ET Geowizard Extension of ArcGIS, was applied to the nest coordinates and background points for each year to extract the associated beach geomorphology characteristics. A seaward baseline was created by using the Buffer tool in ArcGIS to generate a 150 m buffer around each shoreline and then using the Draw tool in ArcGIS to create a new line feature along the buffer. Using the same methodology, a secondary baseline was created landward of the study area. The Perpendiculars to Polyline tool in ET Geowizard Extension of ArcGIS was used to cast lines from the nest coordinates to the seaward baseline and then the Intersect tool in ArcGIS was employed to create points where the aforementioned lines intersect the baseline. Transects were cast from these points to the landward baseline using the Perpendiculars to Polyline tool, producing across-shore transects that run through each presence and background point (Figure 18). The transects were split at the potential vegetation line, shoreline, and landward dune boundary using the Split Polyline with Layer tool in ET Geowizard Extension of ArcGIS. The segment that extends from the potential vegetation line to the shoreline was selected using the Select by Location tool in ArcGIS and exported as a new shapefile, resulting in transects of the beach (Figure 18). The segment of transect that extends from the landward dune boundary to the potential vegetation line was also selected using the Select by Location tool in ArcGIS and exported as a new shapefile, producing transects of the dune complex (Figure 18).

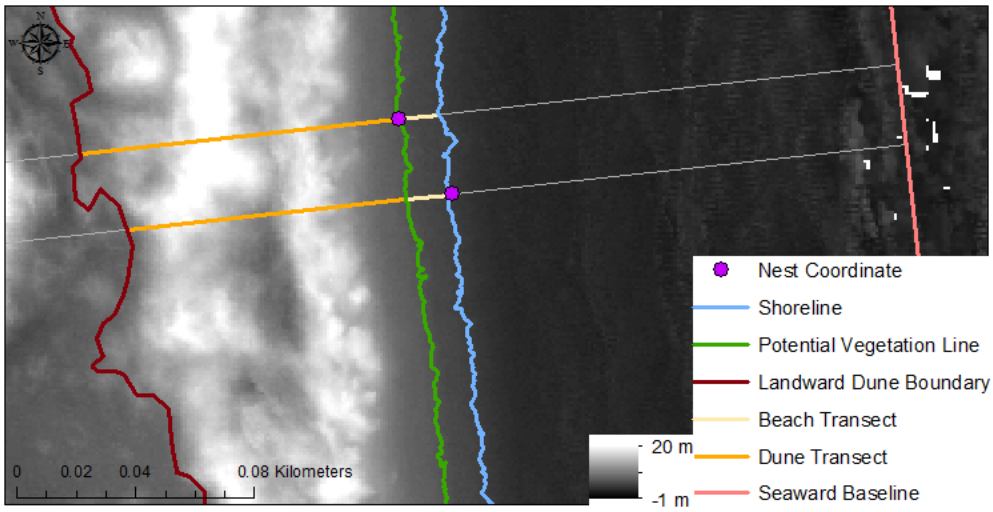

Figure 18: Example of across-shore transects that intersect nest coordinates and the derived beach and dune transects.

Points were created every 1 m along both the beach and dune profiles using the Create Station Points tool in ET Geowizard, and then elevation values were attributed to the points using the Extract Values to Points tool in ArcGIS. The Points to Polyline tool and the PolylineZ Characteristics tool in ET Geowizard were applied to convert the points to polylineZ features and to derive various characteristics of the 3D profiles, respectively. The resulting geomorphology characteristics include average beach slope, maximum beach slope, 3D beach width, dune peak height, maximum dune slope upward from potential vegetation line, average dune slope upward from potential vegetation line, and 3D dune width (Table 5).

Table 5: Description of each geomorphology characteristic derived for each nest coordinate and background point.

Geomorphology Characteristic	**Description**
Beach Width	Distance (m) between the potential vegetation line and the shoreline
Beach Slope	Average slope (degrees) of the profile from the shoreline to the potential line of vegetation; maximum, minimum, and average values
Dune Height	Highest point (m) between the landward dune boundary and the potential line of vegetation
Dune Width	Distance (m) between the potential vegetation line and the landward dune boundary

Dune Slope	Average upward slope (degrees) going from the potential line of vegetation toward the landward dune boundary; maximum, minimum, and average values
Distance from Shoreline	Distance (m) from nest position to the shoreline (negative value on the seaward side of the shoreline)
Rugosity	Surface roughness or the standard deviation of elevation
Aspect	Compass direction that a slope faces
Elevation	Elevation (m) above NAVD88

In order to calculate the distance of each nest and background point from the shoreline (Table 5), the Perpendiculars to Polyline tool in ET Geowizard was used to generate a line from each point to the baseline and Calculate Geometry in the attribute table of the shapefile in ArcGIS was used to calculate the length of each line. The segment of profile that extends from the shoreline to the seaward baseline was selected using the Select by Location tool in ArcGIS and exported as a new shapefile. The length of each line was calculated using Calculate Geometry in the attribute table of the shapefile in ArcGIS. Using the Spatial Join tool in ArcGIS, the shapefiles were combined and the difference in length between related lines was calculated using Calculate Geometry in ArcGIS. This methodology option accounted for the placement of nests on the seaward side of the shoreline, which resulted in a negative distance from shoreline value. Background points with a distance from shoreline value outside the range of the distance from shoreline values attributed to the presence points were deemed as outside of the study area and were excluded from statistical analyses.

An aspect raster for each year was generated using the Aspect tool in ArcGIS. Rugosity rasters for each year were created using the Focal Statistics tool in ArcGIS by calculating the standard deviation of elevation in a 3 x 3 m window. Using the Extract Values to Points tool in

ArcGIS, values from the aspect, slope, and elevation rasters were extracted to the nest coordinates and background points of respective years (Table 5).

Statistical Analysis

To better understand the dynamics of the system, preliminary statistical analyses were conducted. The Optimized Hot Spot Analysis tool in ArcGIS, which identifies statistically significant spatial clusters of high values and low values, was used on each year of nest coordinates, as well as all years combined. This tool aggregates incident data, identifies an appropriate scale of analysis, and corrects for multiple testing and spatial dependence. The Getis_Ord Gi* statistic is calculated for each feature in the dataset, and the resulting high and low z-scores are indicative of hot spots and cold spots, respectively. The resulting maps identified statistically significant hot spots and cold spots of nests and classified the general spatial trends in nesting.

Boxplots were created in R that compare the median and interquartile range of each geomorphology characteristic differentiated by nest presence and pseudo-absence. These boxplots served as tools that can be used to recognize if the Kemp's ridleys are nesting within a subset of the available habitat. Additionally, a correlation matrix composed of pairwise scatterplots and associated Pearson correlation coefficients was calculated in R to assess the collinearity between the geomorphology characteristics and to preliminarily pinpoint any geomorphology characteristics with a relationship to nest presence. Collinearity between variables can skew generalized linear models, so this information was taken into consideration during model development and selection.

Generalized Linear Model

Due to the binomial distribution of the response variable, generalized linear models for each year and all years combined were developed in R, with nest presence/absence as the dependent variable and the geomorphology characteristics as the explanatory variables. Models utilizing all of the explanatory variables were dredged in order to pinpoint the variables that comprise the relatively best model options. The relatively best models options were then generated and evaluated using McFadden's pseudo R-squared value, K-fold cross-validation prediction error, and a boxplot of the predictions differentiated by the observation value. McFadden's pseudo R-squared value is defined as $R^2_{McFadden} = 1 - \frac{\log(L_c)}{\log(L_{null})}$, where L_c denotes the likelihood value from the current fitted model and L_{null} denotes the corresponding value for the null model (McFadden, 1974). In K-fold cross-validation, the observations are split into K partitions, the model is trained on K-1 partitions, and the test error is predicted on the left out partition k (Zuur *et al.*, 2009). This process is repeated for each partition and the result is the average test error of all partitions (Zuur *et al.*, 2009).

Because the sampling type and ratio of the background data can greatly affect the model, these components were taken into consideration when developing the model (Barbet-Massin *et al.*, 2012; VanDerWal *et al.*, 2009). As mentioned in section Data Acquisition and Processing, background points were generated at a ratio of 10:1 to the presence points. However, using this ratio as an input into the model would likely cause the model to be biased to predict the background points instead of the presence points. Therefore, models were developed using a 10:1, 5:1, 2:1, and equal ratios of background points to presence points in order to gauge the effect of variations in ratio background points on model accuracy (Barbet-Massin et al, 2012; VanDerWal *et al.*, 2009). Models were also as created using background points with geographic

exclusions of 25 m, 50 m, and 100 m to assess the impact of variations in sampling technique (Barbet-Massin et al, 2012; VanDerWal *et al.*, 2009). The models generated using 5:1, 2:1, and equal ratios of background to presence points were re-constructed 100 times, resampling the background points each iteration, in order to fully take into consideration the distribution of the background points. The geographic exclusions were created by using the Buffer tool in ArcGIS to create 25 m, 50 m, and 100 m buffers around each nest coordinate, which subsequently eliminated the background points that fall within each range. McFadden's pseudo R-squared value, K-fold cross-validation prediction error, and a boxplot of the predictions differentiated by the observation value for each model were compared in order to evaluate model performance.

Spatial Autocorrelation

The analysis of spatial data is often complicated by spatial autocorrelation, a phenomenon that occurs when the values of variables sampled at nearby locations are not independent of each other (Dormann *et al.*, 2007; Crase *et al.*, 2014). In order to determine if there was spatial autocorrelation in the presence/absence data, a spline correlogram of the raw data was created in R (Zuur *et al.*, 2009; Crase *et al.*, 2014). A spline correlogram is a graphical representation of Moran's I for different distance classes that is smoothed using a spline function. A spline correlogram of the Pearson residuals of the model was also created in R to determine if any spatial autocorrelation was explained by the explanatory variables (Zuur *et al.*, 2009). If positive spatial autocorrelation is present in the Pearson residuals of the model, then the explanatory variables did not explain the spatial autocorrelation. In this case, a Generalized Linear Mixed Model (GLMM) that accounts for spatial autocorrelation would need to be developed.

Random Forest

In order to assess the capacity of geomorphology characteristics in predicting the presence or absence of Kemp's ridley nests, a random forest model was applied to the full study dataset (2009-2012). Random forests are machine learning classification and regression tools that are composed of a combination of trees created by using bootstrap samples of training data and random feature selection in tree induction (Breiman, 2001; Svetnik *et al.*, 2003). A random forest model was determined to be a suitable option due to the size of the dataset and the ability to gain insights into variable importance. The predictand of the model was the presence or background of a nest site while the predictors were the geomorphology characteristics. The relative importance of each predictor in the model was quantified, providing even more insight into the relationships within the system.

Because the sampling type and ratio of the background data can greatly affect the model, these components were taken into consideration when developing the random forest model (Barbet-Massin et al, 2012; VanDerWal *et al.*, 2009). A subset of the background points of equal ratio to the presence points was constructed and then the data was further split into 75% for testing and 25% for training. The random forest model was built and then a loop was established to perform 100 iterations of each step. This effectively bootstraps the background data so that the entire distribution is assessed. The outputs for each iteration were captured as text files. In order to assess the accuracy of each model, a confusion matrix was generated as an output for both the test and training subsets of each model. The accuracy, sensitivity, and specificity were used to assess and compare the performance of each model iteration. Variable importance plots were constructed in order to determine the role of each explanatory variable.

Environmental Variables

A correlation matrix was created in R to assess the collinearity between the explanatory variables and to preliminarily evaluate the relationship between daily nest count and the average daily environmental conditions. Statistical measures of the average daily environmental conditions associated with nesting days were compared to those of non-nesting days for all the years of data combined in order to further pinpoint any trends.

Linear models were generated for each year and all years combined with daily nest count as the dependent variable and the average daily environmental conditions as the explanatory variables. Environmental conditions include including wind direction, wind speed, gust speed, water level, water sigma, water temperature, air temperature, and barometric pressure. For the 2010 dataset, barometric pressure, air temperature, and water temperature were excluded since there was missing data. The models were dredged and their Akaike Information Criterion (AICc) values were compared in order to pinpoint which models were the relatively best options. The linear model options were assessed using the p-value of both the model and variables, the adjusted R-squared value, and a plot of the residuals.

Power and exponential models predicting daily nest count also were developed in R using a non-linear least squares approach with daily average wind speed as the explanatory variable. The goodness of fit of each model was compared by computing the residual sum-of-squares and the complement of its proportion to the total sum-of-squares, or the multiple R-squared value. Models were also evaluated based upon AICc values and plots of the residuals. The non-linear models were compared to the top linear model using the same evaluation criteria in order to determine the relatively best model option.

Alongshore Habitat Variability Analysis

To assess the variability of the geomorphology of the study area, cross-shore profiles were generated every 100 m alongshore and subsequently divided into groups, which were then compared. Cross-shore profiles of the study area were created using the Create Station Lines tool in ET Geowizard Extension for ArcGIS. The profiles were created at 100 meter intervals perpendicular to the baseline. The Split Polyline with Layer tool in ET Geowizard Extension for ArcGIS was used to split the profiles at the dune boundary and shoreline. Select Layer by Location in ArcGIS was used to select the lines that extend from the dune boundary to the shoreline, which were then exported as a new shapefile. The final output was cross-shore profiles every 100 meters along the study area that extend from the landward foredune boundary to the shoreline (Figure 19).

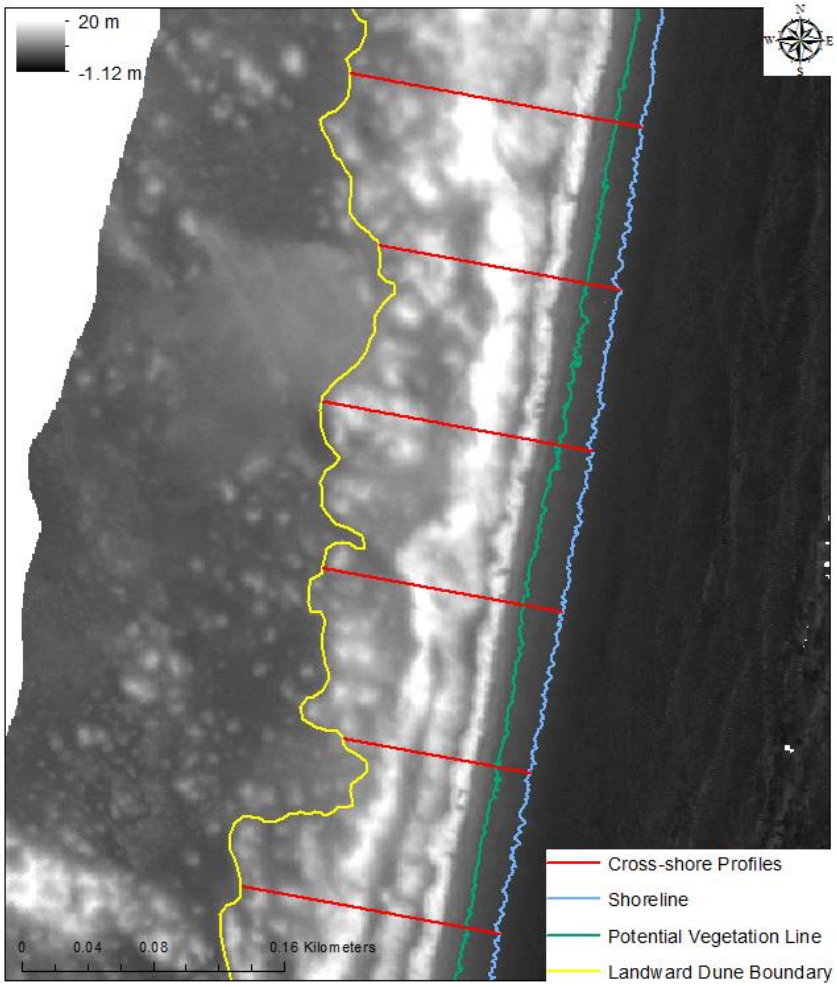

Figure 19: Example of the cross-shore profiles every 100 m alongshore that extend from the shoreline to the landward dune boundary.

Using the procedure outlined in Extraction of Geomorphology Characteristics, the geomorphology features of dune width, dune height, dune slope, beach slope and beach width were extracted to each profile. The profiles for each year were divided into groups using the Group Analysis tool in ArcGIS. The profiles were grouped using K nearest neighbors based upon the geomorphology characteristics and spatial distribution of the profiles, and the optimal number of groups was evaluated using the Calinski-Harabasz pseudo F-statistic. The average, maximum, and minimum value for each geomorphic characteristic, as well as nest frequency, was calculated for each group and compared.

Next, resembling the methodology of other studies regarding other sea turtle species, the study area was divided into sections and the average geomorphology characteristics and nest abundance for each section was calculated and statistically analyzed (Cuevas *et al.*, 2010; Long *et al.*, 2011; Provancha & Ehrhart, 1985; Rousoo *et al.*, 2014; Yamamoto *et al.*, 2012; Zavaleta-Lizarraga & Morales-Mavil, 2013). Blocks 1000 meters in length were created alongshore the study area, and nest abundance and the average of the geomorphic variables of the profiles within each block was calculated. The average geomorphology characteristics alongshore were plotted in order to further assess habitat variability.

The data was statistically analyzed using a linear model in R, with nest abundance acting as the dependent variable and the geomorphology characteristics acting as the explanatory variables. For each year and all years combined, a model was created with all of the geomorphology characteristics acting as the explanatory variables, which was subsequently dredged to identify the relatively best model options based on AICc values. The top models were developed and evaluated based upon the mean square error, p-value, and adjusted R-squared value.

RESULTS

Preliminary Statistical Analysis

The use of the Optimized Hot Spot Analysis tool on the nest coordinates of each year and all years combined resulted in the presence of a hot spot near the central section of Padre Island, Texas each year (Figure 20). In particular, the analysis of all years combined exposed a notable hot spot along the central section of Padre Island and a cold spot along the northern half of South Padre Island.

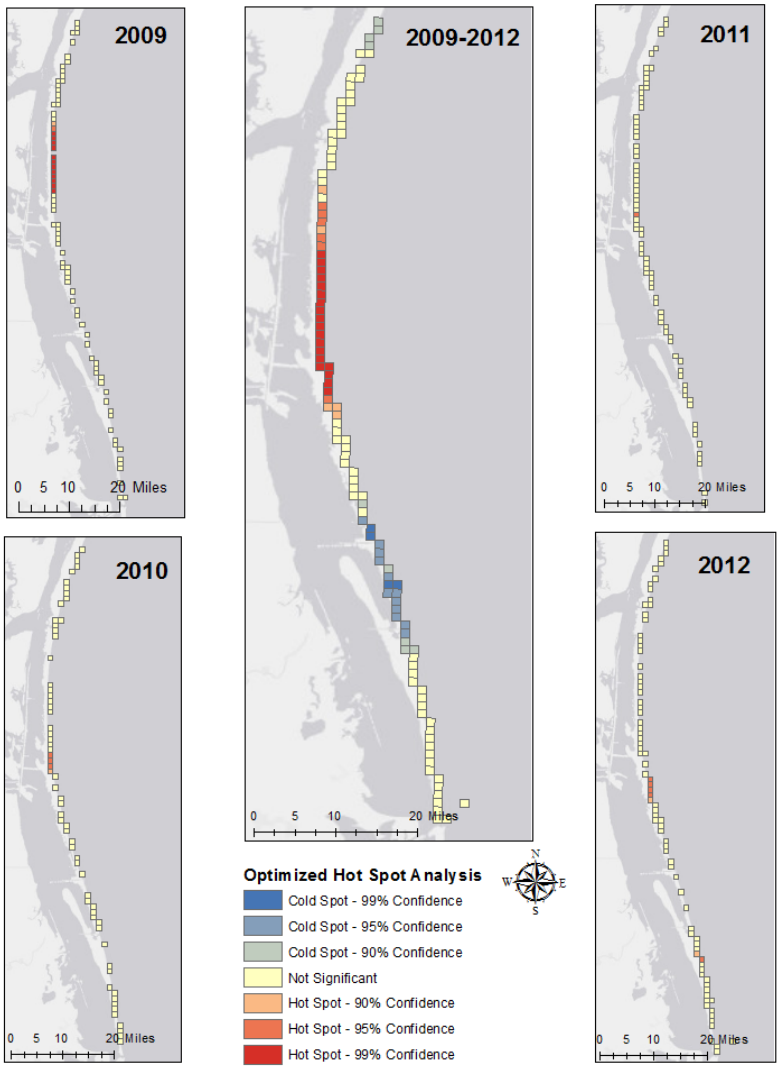

Figure 20: Statistically significant hot spots and cold spots for each year of data produced using the Optimized Hot Spot Analysis tool in ArcGIS.

Boxplots of each geomorphology characteristic differentiated by nest presence contrast the range of geomorphology values used by the Kemp's ridley sea turtle with the total range of available nesting area (Figures 21-27). In Figures 21-27, the lines of each box, moving from the bottom to the top of each figure, indicate the 1st, 2nd, and 3rd interquartile range. The points above and below the tails represent potential outliers, or values beyond the quartiles by one-and-a-half the interquartile range. For most of the geomorphology characteristics, the extent used by the Kemp's ridley for nesting is limited in comparison to the breadth of the entire study area; the Kemp's ridley tends to avoid extreme values. The median value for presence points is lower than the median value for the background points for the variables elevation, distance from shoreline, maximum dune slope, dune width, and average beach slope (Figures 21-27). In particular, the interquartile range of the presence points does not overlap with the interquartile range of the background data for elevation and distance from shoreline, indicative of a distinct preference of the species (Figures 21-22). Furthermore, Tables C1-C5 in Appendix C list statistical measures of each geomorphology characteristic for the nest coordinates for each year and all years of data combined, which provides a detailed quantification of the terrestrial habitat range of the Kemp's ridley sea turtle.

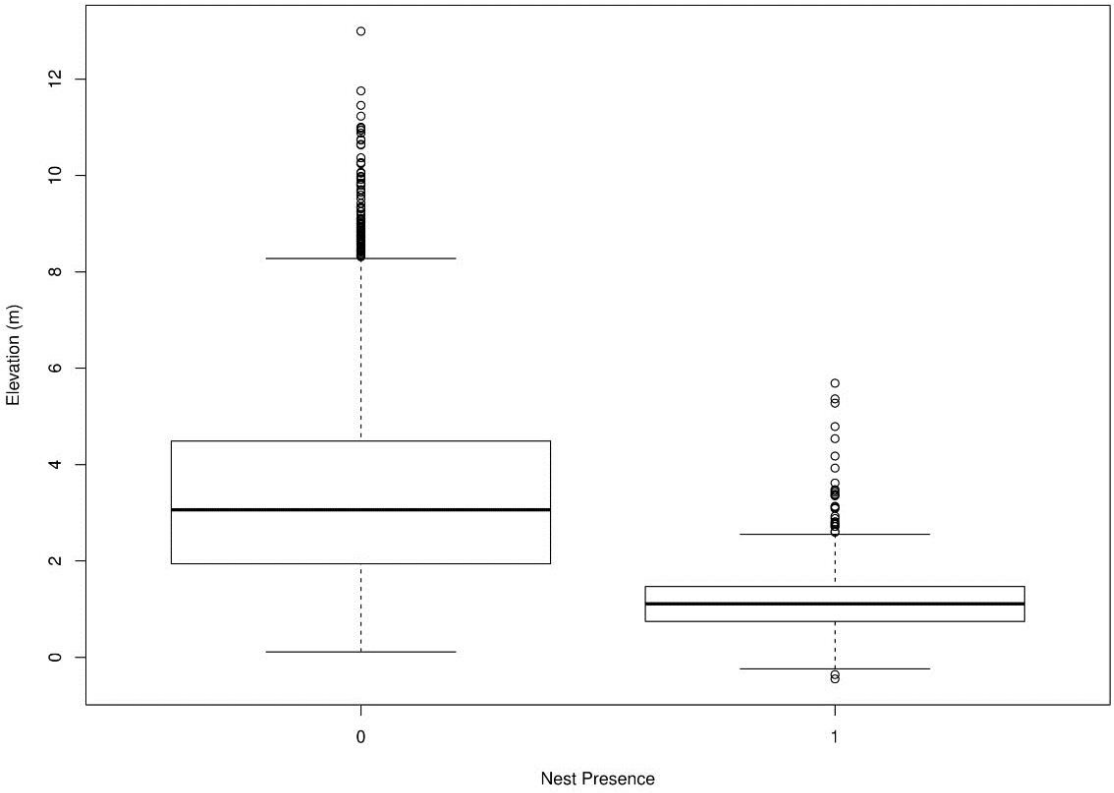

Figure 21: Boxplot of elevation (m) differentiated by background (0) and nest presence (1) data.

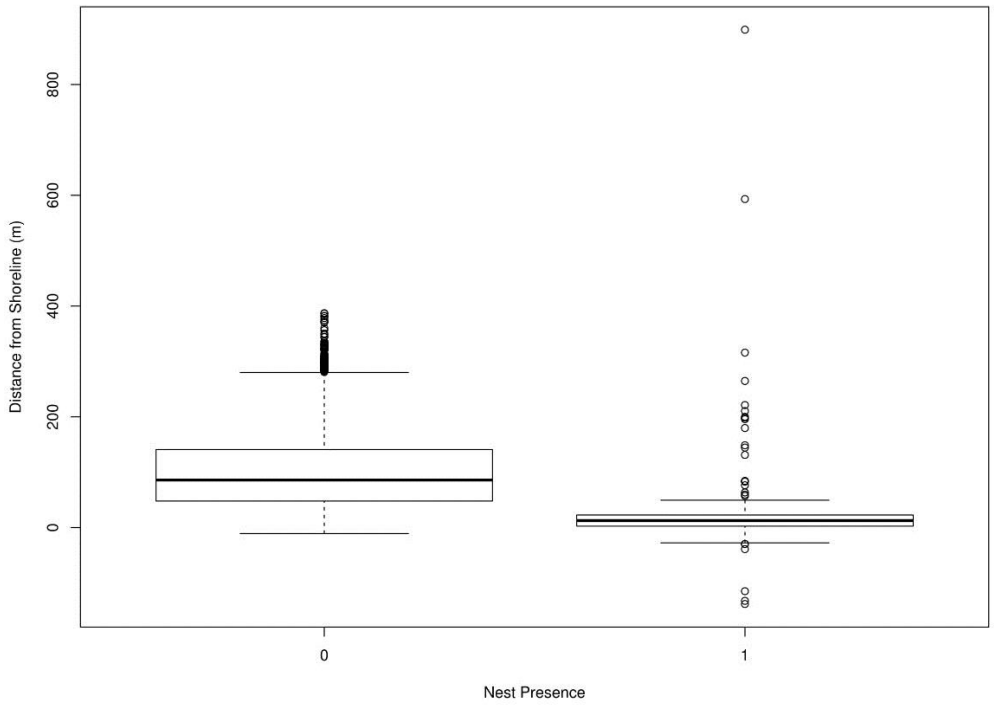

Figure 22: Boxplot of distance from shoreline (m) differentiated by background (0) and nest presence (1) data.

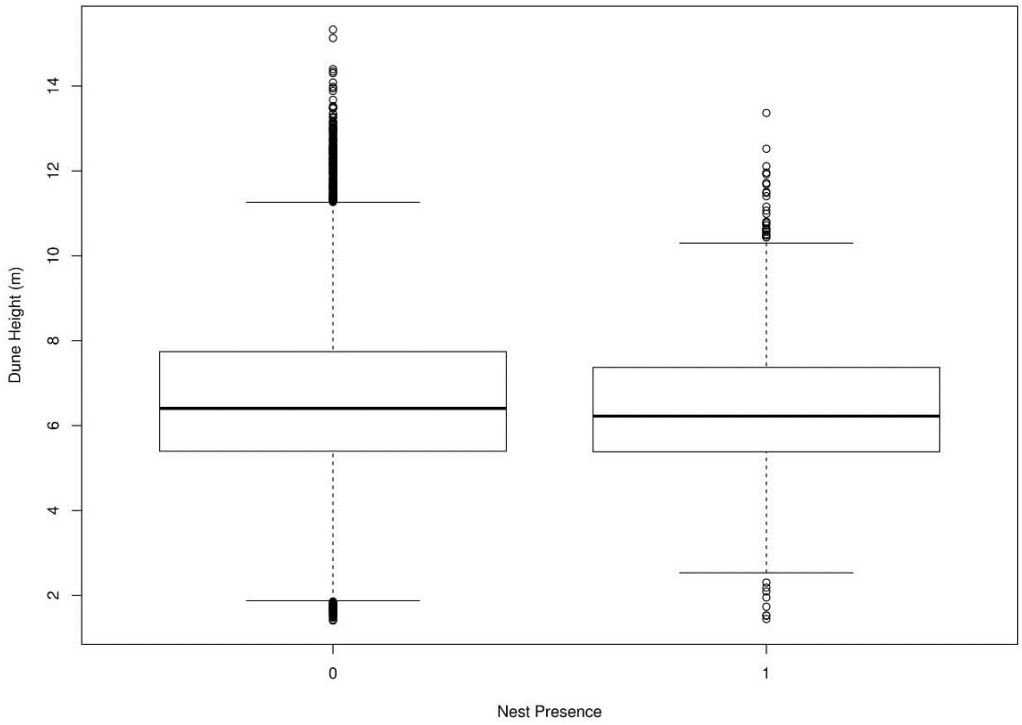

Figure 23: Boxplot of dune height (m) differentiated by background (0) and nest presence (1) data.

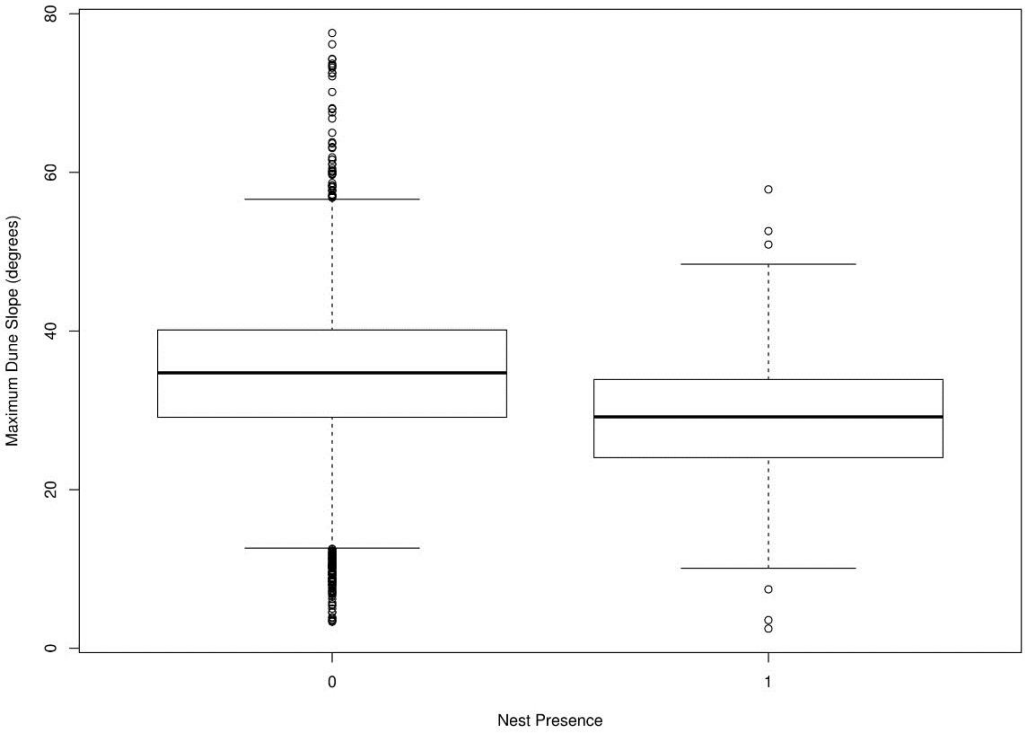

Figure 24: Boxplot of maximum dune slope (degrees) differentiated by background (0) and nest presence (1) data.

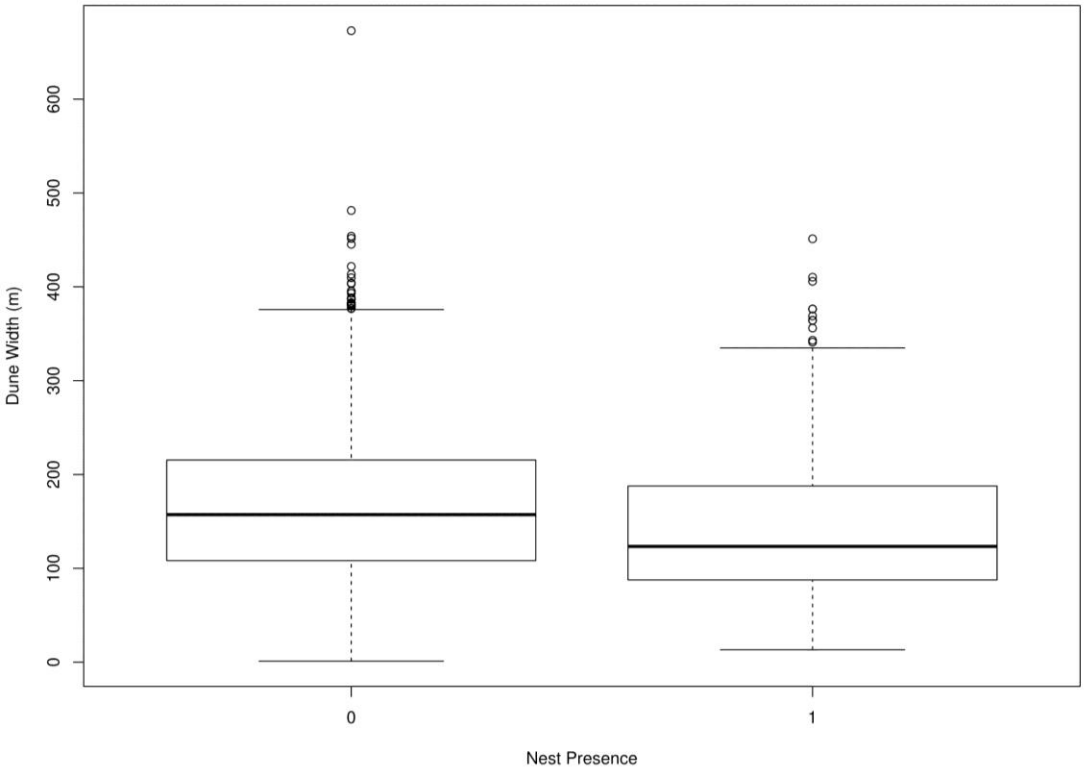

Figure 25: Boxplot of dune width (m) differentiated by background (0) and nest presence (1) data.

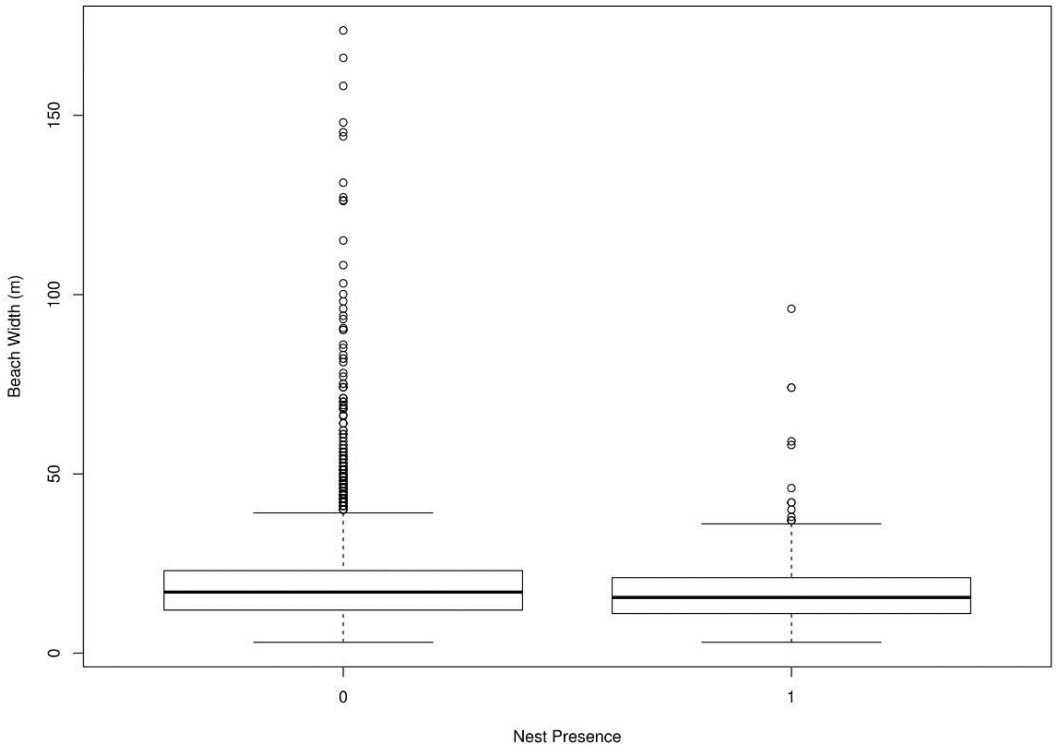

Figure 26: Boxplot of beach width (m) differentiated by background (0) and nest presence (1) data.

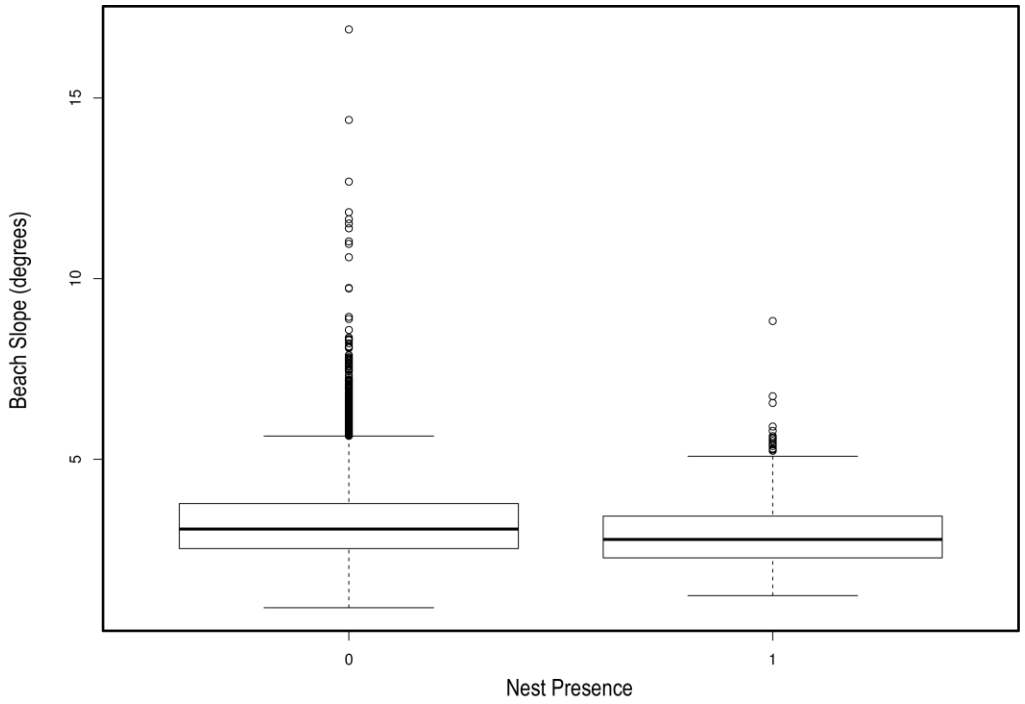

Figure 27: Boxplot of beach slope (degrees) differentiated by background (0) and nest presence (1) data.

A correlation matrix of the variables revealed collinearity between the following pairs of variables: maximum dune slope and average dune slope, maximum beach slope and average beach slope, and elevation and rugosity (Figure 28). There was also a notable relationship between elevation and dune height, as well as between elevation and distance from shoreline.

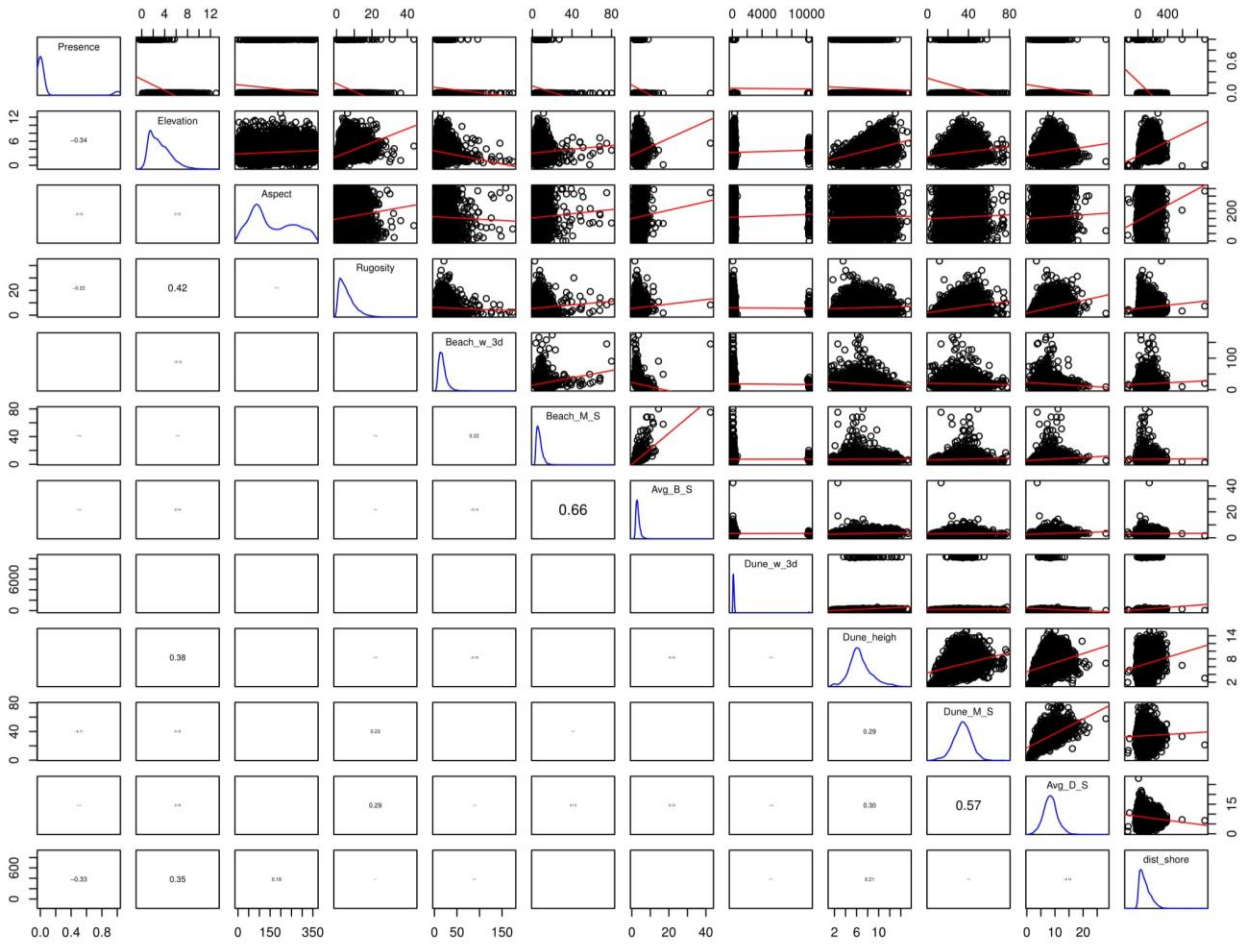

Figure 28: Correlation matrix showing pairwise scatterplots (upper right) and Pearson correlation coefficients (lower left) for each pair of geomorphic variables for all years combined.

Generalized Linear Model

Several generalized linear models were generated that predicted the presence or absence of nests for all of the years of data combined (Table 6). One of the top models, Model 1, included the significant variables (p-value < 0.001) of elevation, dune height, average beach slope, maximum dune slope, and beach width (Table 6). This model had a pseudo R-squared value of 0.46, meaning it accounted for approximately 46% of the variability of nest presence and absence. Another one of the top models for all of the years combined, Model 2, included the significant variables (p-value < 0.001) of distance from shoreline, dune height, maximum dune slope, and average beach slope (Table 6). This model had a pseudo R-squared value of 0.411,

meaning it accounted for approximately 41% of the variability of nest presence and absence. Elevation and distance from shoreline are the most important variables in the first and second models, respectively. A model containing the other significant variables without elevation or distance from shoreline, Model 3, only had a pseudo R-squared value of 0.097 (Table 6).

Table 6: Various generalized linear models and their respective McFadden's pseudo R-squared values and K-fold cross validation prediction errors. These models were produced using all of the years of data combined.

Model Number	**Generalized Linear Model**	**McFadden's Pseudo R-Squared**	**K-fold Cross-Validation Prediction Error**	**Ratio of Background: Presence Points**
1	5.9 – 1.64*elevation + 0.21*dune height – 0.36*avg beach slope – 0.075*max dune slope – 0.034*beach width	0.460	0.117	1:1
2	4.9 – 0.037*distance from shoreline + 0.13*dune height – 0.088*max dune slope – 0.43*avg beach slope	0.411	0.106	1:1
3	3.16 + 0.077*dune height – 0.29*avg beach slope – 0.086*max dune slope	0.097	0.220	1:1
4	5.8 – 1.79*elevation + 0.22*dune height – 0.44*avg beach slope – 0.074*max dune slope – 0.04*beach width	0.450	0.111	2:1
5	5.23 – 2.05*elevation + 0.26*dune height – 0.47*avg beach slope – 0.069*max dune slope – 0.05*beach width	0.448	0.075	5:1
6	4.375 – 2.16*elevation + 0.23*dune height – 0.37*avg beach slope – 0.065*max dune slope – 0.05*beach width	0.417	0.051	10:1

The first three models were generated using an equal ratio of background points to nest coordinates, but models were also generated using 10:1, 5:1, and 2:1 ratios. The model created using a 10:1 ratio (Model 6) had a pseudo R-squared value of 0.417, the model created using a

5:1 ratio (Model 5) had a pseudo R-squared value of 0.448, and the model created using a 2:1 ratio (Model 4) had a pseudo R-squared value of 0.450 (Table 5). The accuracy of the aforementioned models in predicting nest presence versus nest absence was assessed via boxplots of the predictions differentiated by nest presence (Figures 29-34). The results indicate that the ratio of background to presence points acts as a factor for model accuracy in predicting presence and absence; as the ratio of background points to presence points decreases, the accuracy of the predictions for nest presence increases and the accuracy of the predictions for nest absence decreases (Figures 29 & 32-34). It is also important to note that the median prediction value for the presence points increases in accuracy at a faster rate than the median prediction value for the absence points decreases in accuracy, resulting in a somewhat balanced accuracy in the model created using an equal ratio. This is further validated by comparing the statistical measures of the confusion matrices for the models created using varying ratios of background to presence points (Appendix D). Therefore, a 1:1 ratio of background to present points is optimal for the purposes of this study, as it produces the most accurate model for predicting nest presence without exceedingly hindering the accuracy for predicting nest absence.

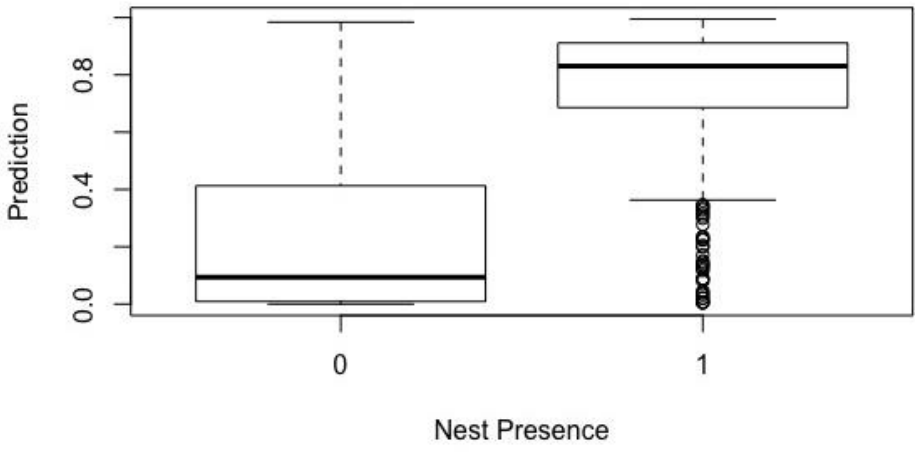

Figure 29: Boxplot of the predictions of Model 1 in Table 5 differentiated by nest presence.

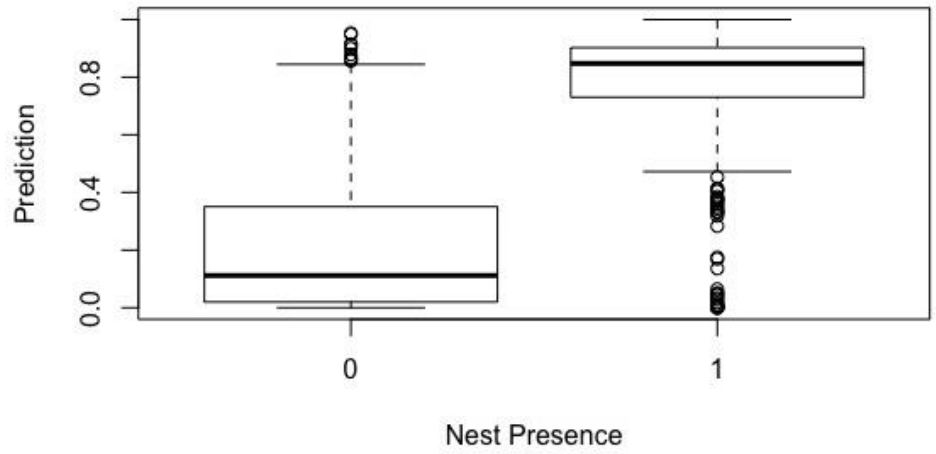

Figure 30: Boxplot of the predictions of the Model 2 in Table 5 differentiated by nest presence.

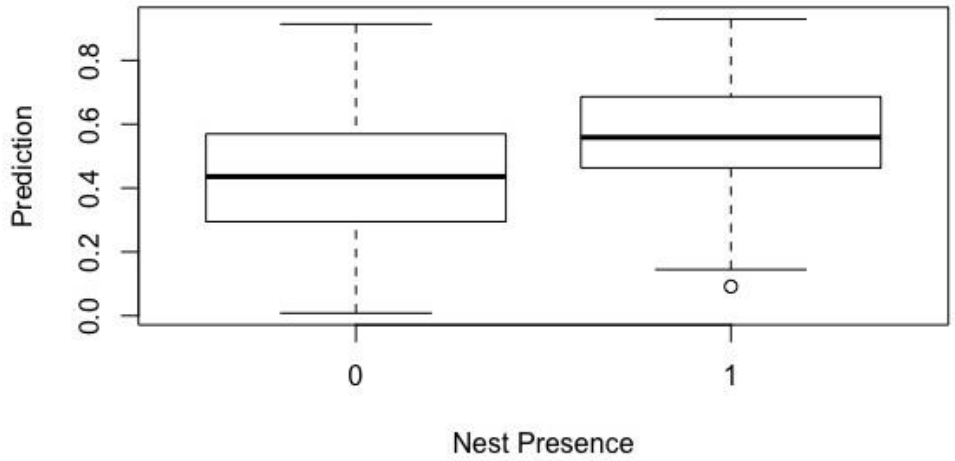

Figure 31: Boxplot of the predictions of the Model 3 in Table 5, which excludes elevation and distance from shoreline, differentiated by nest presence.

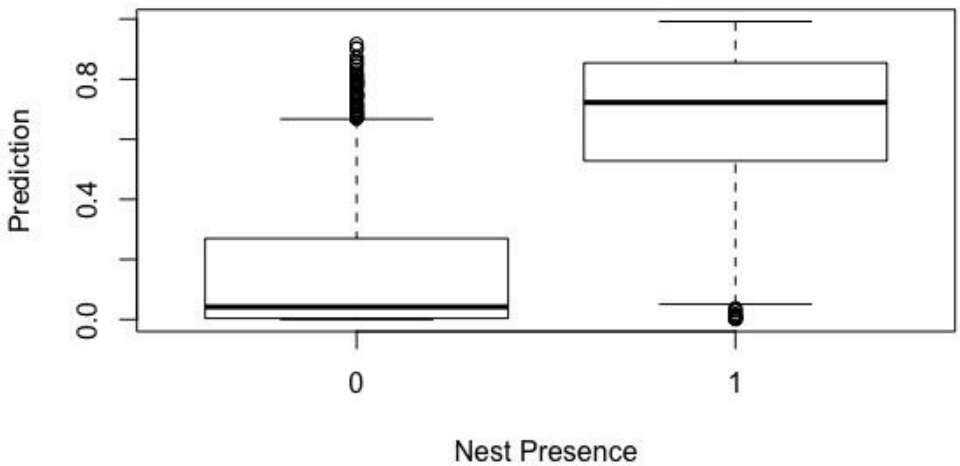

Figure 32: Boxplot of the predictions of Model 4 in Table 5, which was generated using a 2:1 ratio of background to presence points, differentiated by nest presence.

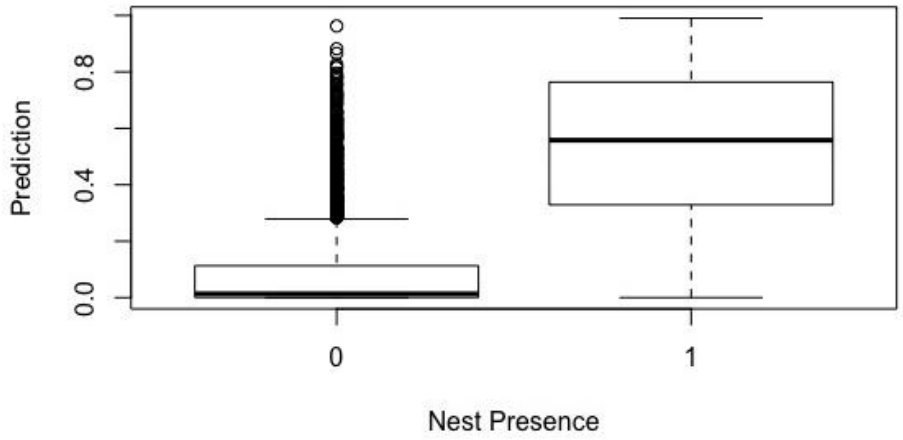

Figure 33: Boxplot of the predictions of Model 5 in Table 5, which was generated using a 5:1 ratio of background to presence points, differentiated by nest presence.

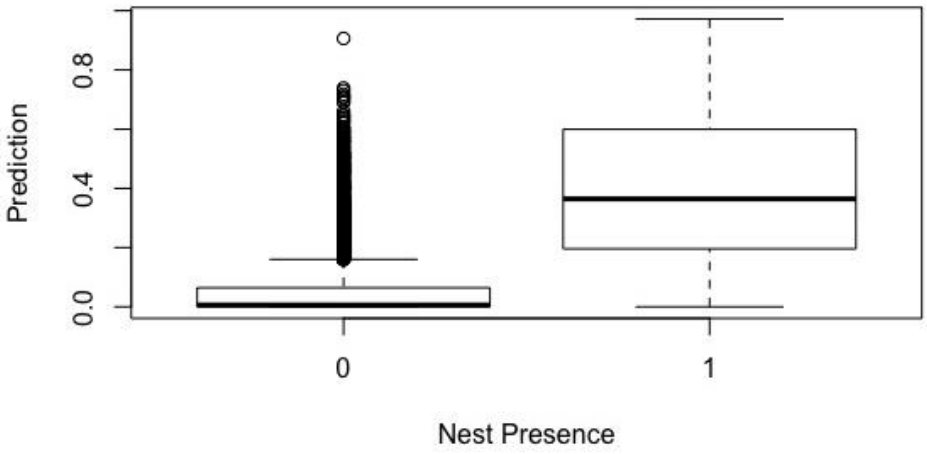

Figure 34: Boxplot of the predictions of Model 6 in Table 5, which was generated using a 10:1 ratio of background to presence points, differentiated by nest presence.

Geographic exclusions were applied to the background points input into model 6 of Table 6 to limit the proximity of the background points to the nest coordinates. The subsequent McFadden's pseudo R-squared values and K-fold cross-validation prediction errors were compared to assess the impact of background sampling technique on model performance (Figures 35-36). The McFadden's pseudo R-squared value increased as the size of the geographic exclusion increased, but the K-fold cross validation prediction error increased as well, meaning increased geographic exclusions resulted in models that explained more variation but were less accurate (Figures 35-36).

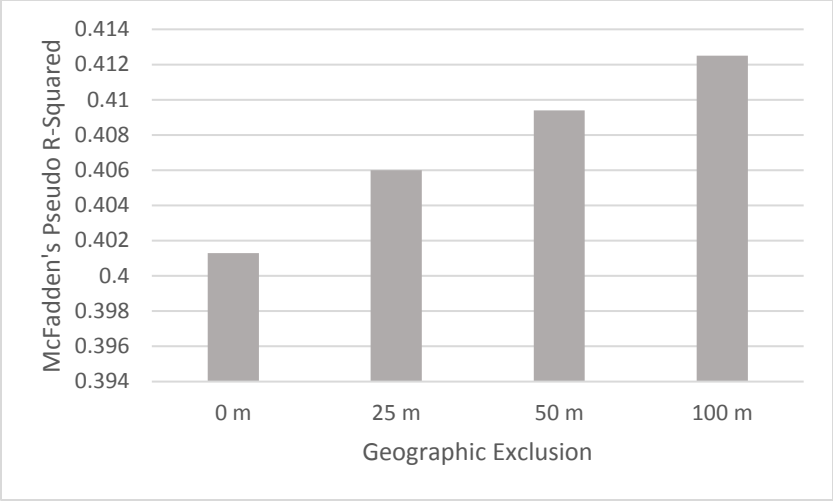

Figure 35: McFadden's pseudo R-squared value for models created using varying geographic exclusions.

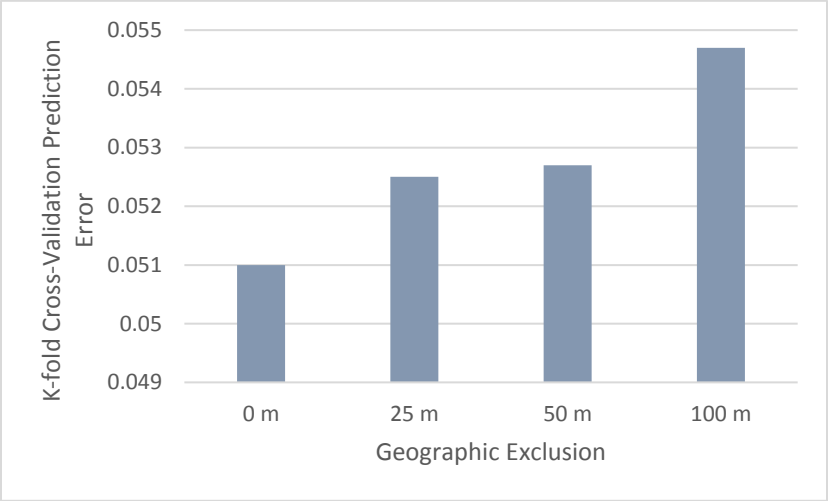

Figure 36: K-fold cross-validation prediction error for models created using varying geographic exclusions.

Overall, differences between the models generated using varying geographic exclusions were minute and corresponded with the findings of Barbet-Massin *et al.* (2012), which were that geographic exclusions decrease the accuracy of GLMs and, therefore, using a random selection sampling technique of background points is ideal. Consequently, the optimal generalized linear models for this study are models characterized by a 1:1 ratio of background to presence points and background points created using a random sampling technique. Models 1 and 2 in Table 5 were determined to be the best overall models for all the years of data combined.

Generalized linear models were produced for each year of data using a 1:1 ratio of background to presence points without a geographic exclusion. Each of these were characterized by McFadden's pseudo R-squared values and K-fold cross-validation prediction errors (Table 7). The top model for each year contained a distinct combination of explanatory variables, but elevation, dune height, and maximum dune slope were consistently present in each (Table 7).

Table 7: Top generalized linear model for each year using nest presence/absence as the dependent variable and the geomorphology characteristics as the explanatory variables.

Year	Generalized Linear Model	McFadden's Pseudo R-Squared	K-fold Cross-Validation Prediction Error
2009	1.51 – 1.77*elevation + 0.21*dune height – 0.06*max dune slope + 0.42*avg beach slope – 0.0075*aspect	0.379	0.054
2010	3.94 – 0.93*elevation + 0.52*dune height – 0.06*max dune slope – 1.05*avg beach slope – 0.019*dune width	0.362	0.056
2011	5.6 – 3.32*elevation + 0.27*dune height – 0.08*max dune slope – 0.048*beach width	0.524	0.044
2012	6.13 – 2.8*elevation + 0.22*dune height – 0.1*max dune slope – 0.076*beach width – 0.0054*aspect	0.532	0.0415

Spatial Autocorrelation

The spline correlogram of the raw data for all years of data combined revealed positive spatial autocorrelation between nests up to 250 m apart (Figure 37). The spline correlogram of the Pearson residuals of the top generalized linear model for all the years combined (first model in Table 4) exhibited little spatial autocorrelation between nests, even within a short distance (Figure 38). This suggests that the spatial autocorrelation in the data was explained by the explanatory variables in the model (Zuur *et al.*, 2009; Crase *et al.*, 2014). Therefore, the generalized linear model does not need to be adapted to account for spatial autocorrelation (Zuur *et al.*, 2009).

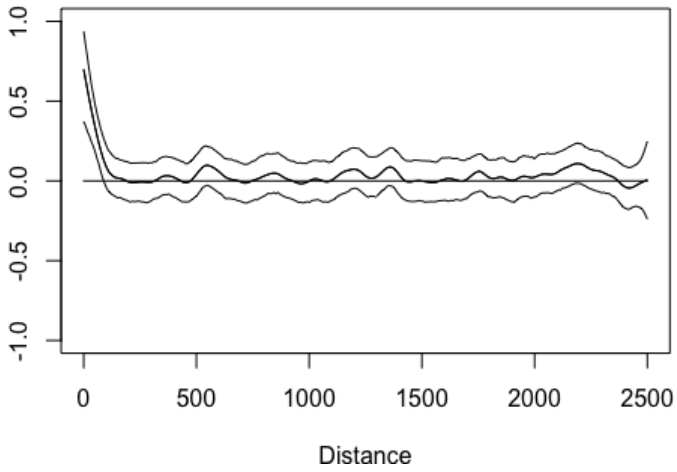

Figure 37: Spline correlogram of the raw data with 95% pointwise bootstrap confidence intervals.

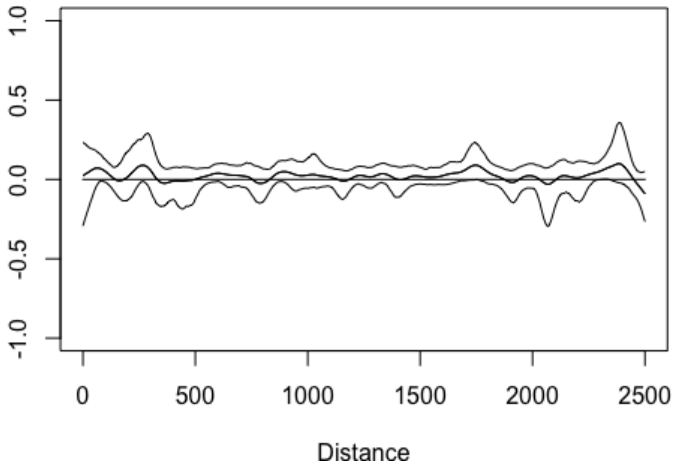

Figure 38: Spline correlogram of the residuals of the GLM with 95% pointwise bootstrap confidence intervals.

Random Forest

A random forest model was successfully created with an accuracy of 0.896, a sensitivity of 0.914, and a specificity of 0.879 (Table 8). This model was generated using an equal ratio of pseudo absence points to presence points. A Receiving Operating Characteristic (ROC) curve of the random forest model shows the false positive rate versus the true positive rate (Figure 39). The closer the false positive rate is to 0 and the closer the true positive rate is to 1, the more accurate the model. Furthermore, variable importance plots for the random forest demonstrate the relative ranking of each predictor in importance (Figure 40). Elevation and distance from

shoreline proved to be the most important variables, but maximum dune slope and average beach slope were relatively important as well.

Table 8: Results of the random forest model generated using an equal ratio of background points to presence points. These values are the average values of the 100 iterations.

Accuracy	0.896
Kappa	0.792
P-value	< 2e-16
Sensitivity	0.914
Specificity	0.879
Positive Prediction Value	0.885
Negative Prediction Value	0.909
Prevalence	0.506
Detection Rate	0.522
Balanced Accuracy	0.896

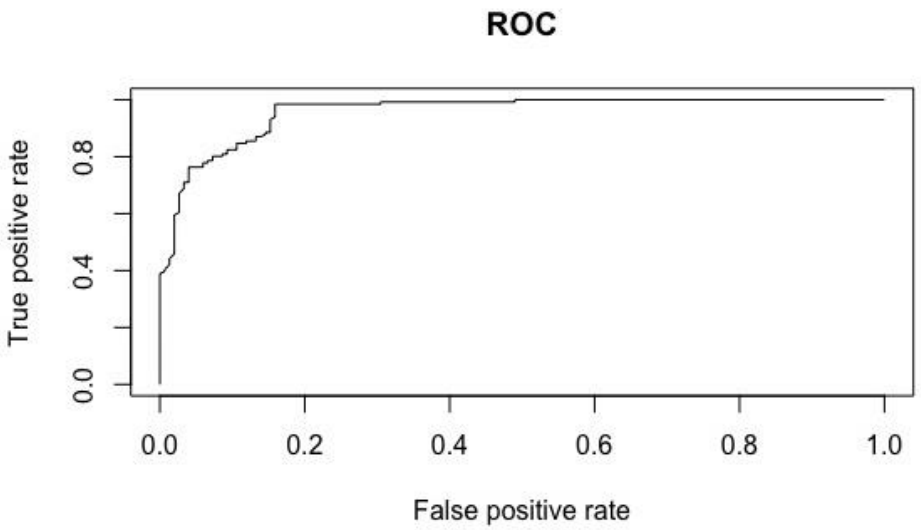

Figure 39: Receiver operating characteristic (ROC) curve of the random forest model.

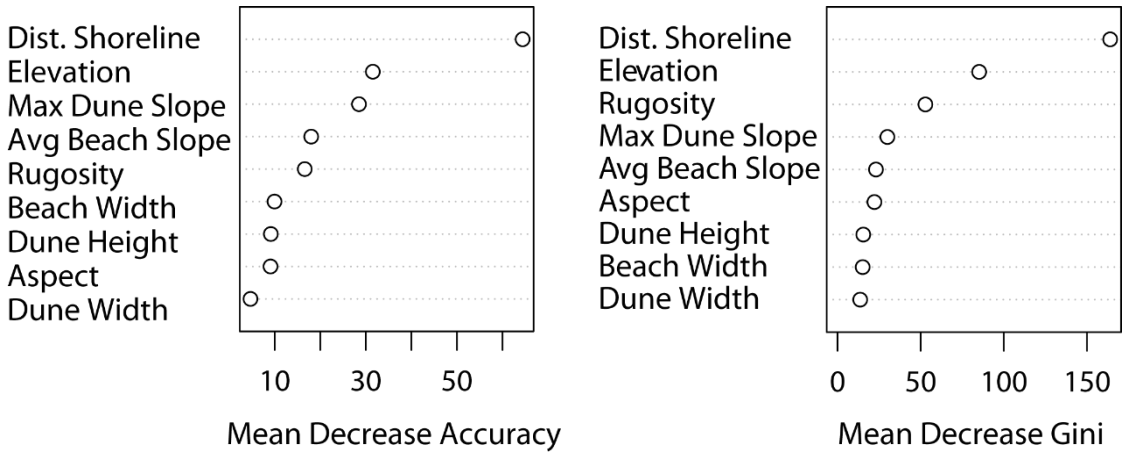

Figure 40: Variable importance plots of the random forest model. The figure on the left shows the mean decrease in accuracy of the model due to the exclusion of each variable and the figure on the right shows the relative importance of each variable.

A random forest model was also generated using a 10:1 ratio of background points to presence points (Table 9). In comparison to the random forest generated using an equal of background points to presence points, the sensitivity, or accuracy of predicting presence points, of this model was much lower. This is indicative that the higher ratio of background to presence points biases the model against the presence data, which is consistent with the trends between the generalized linear models created using varying ratios of background to presence points (Tables 8-9). Therefore, the top random forest model for this study was the model created using an equal ratio of background to presence points because it was more accurate in predicting nest presence without exceedingly hindering the accuracy in predicting nest absence.

Table 9: Results of the random forest model generated using a 10:1 ratio of pseudo absence points to presence points.

Accuracy	0.948
Kappa	0.607
P-value	1.05e-09
Sensitivity	0.530
Specificity	0.987
Positive Prediction Value	0.787

Negative Prediction Value	0.958
Prevalence	0.0843
Detection Rate	0.0569
Balanced Accuracy	0.759

Environmental Variables

The correlation matrix of the environmental variables for all years of data combined revealed collinearity between the following pairs of variables: water temperature and air temperature, and wind speed and gust speed (Figure 41).

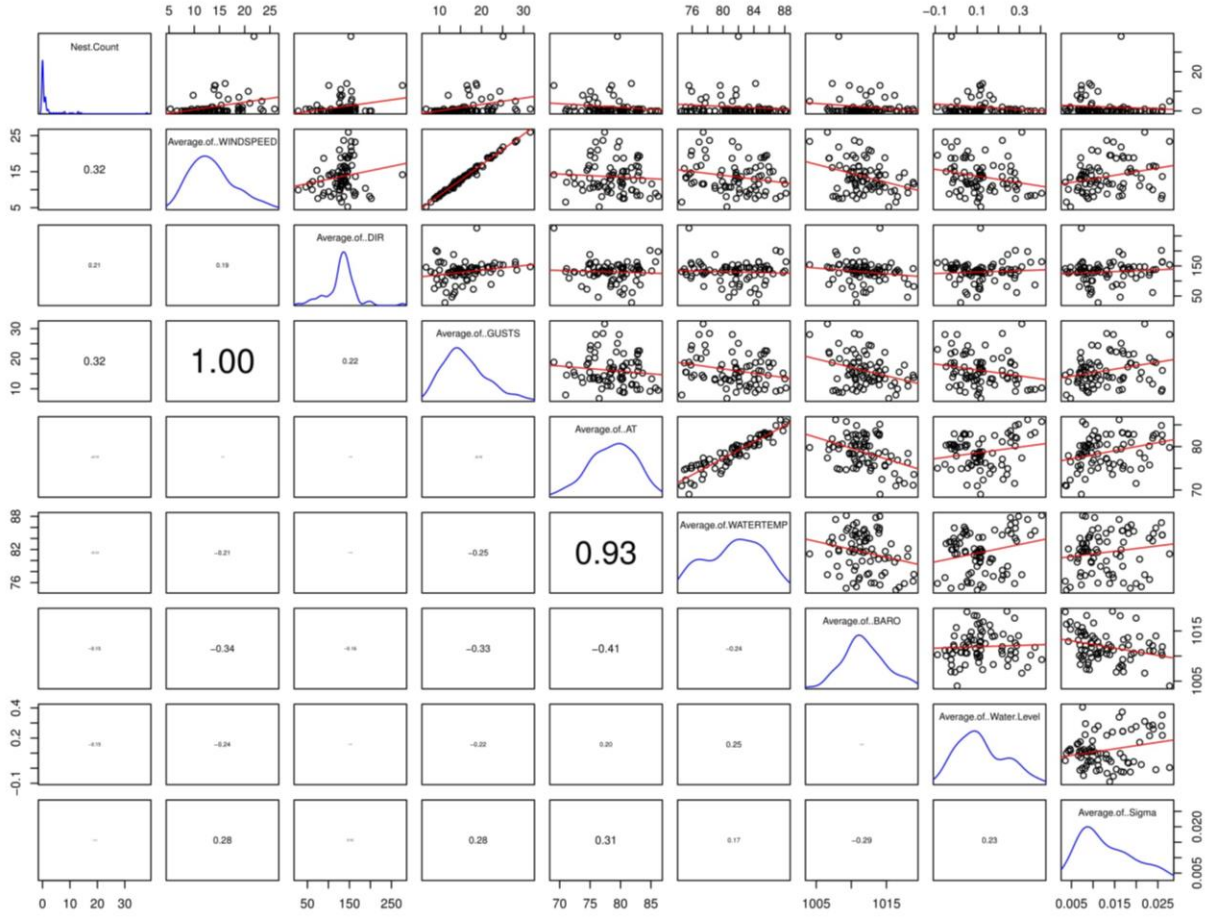

Figure 41: Correlation matrix comprised of pairwise scatterplots (upper right) and Pearson correlation coefficients (lower left) for each pair of environmental variables for all years of data combined.

Comparing the statistical measures of the average daily environmental conditions for non-nesting days during nesting season, nesting days, and nesting days with more than two nests

revealed stark differences for the environment variables of wind speed and gust speed (Table 10). For nesting days, the median wind speed was 16.0 knots and the median gust speed was 18.7 knots. This is a sharp contrast to the median wind speed and gust speed values for non-nesting days, 12.3 knots and 14.3 knots, respectively. Furthermore, 75% of nesting days with two or more nests were characterized by wind speeds of at least 14.4 knots and by gust speeds of at least 17.1 knots, while only 25% of non-nesting days were characterized by comparable wind speeds and gust speeds (Table 10). This suggests that nesting is more likely to occur if wind speeds and gust speeds surpass a certain magnitude.

Table 10: Statistical measures of the average daily environmental conditions for non-nesting days, nesting days, and nesting days with more than two nests.

	Non-Nesting Days		**Nesting Days**		**Nesting Days (>2 Nests)**	
	Wind Speed (kn)	Gust Speed (kn)	Wind Speed (kn)	Gust Speed (kn)	Wind Speed (kn)	Gust Speed (kn)
Average	12.62	14.72	15.84	18.53	16.53	19.37
1st Quartile	9.78	11.35	13.41	15.57	14.44	17.13
2nd Quartile	12.28	14.25	16.04	18.69	16.73	19.25
3rd Quartile	15.09	17.65	18.57	21.56	18.83	22.29

Several linear models were generated that predict daily nest count using daily average environmental conditions as the explanatory variables (Table 11). The top two models were comprised of the explanatory variables of wind speed and gust speed, which are collinear, and were characterized by comparative adjusted R-squared values, p-values, and F-statistics (Table 11). Models generated using across-shore wind speed (wind direction of east or west) and alongshore wind speed (wind direction of north or south) were characterized by lower adjusted R-squared values and p-values in comparison to the model generated using wind speed of all

directions (Table 11). Plots of the residuals of the top two linear models reveal an increasing trend, suggestive that a non-linear model might be a better fit for the data (Figures 42-43).

Table 11: Linear models and their associated statistics using daily nest count as the dependent variable and daily average environmental characteristics as the explanatory variables.

Linear Model	**Adjusted R Squared**	**P-value**	**F-statistic**
-3.05 + 0.344*wind speed	0.1086	8.55e-10	40.01
-3.02 + 0.29*gust speed	0.108	9.64e-10	39.74
-1.92 + 0.24*across-shore wind speed	0.0864	0.000348	13.49
-3.38 + 0.37*alongshore wind speed	0.0969	9.595e-06	20.74

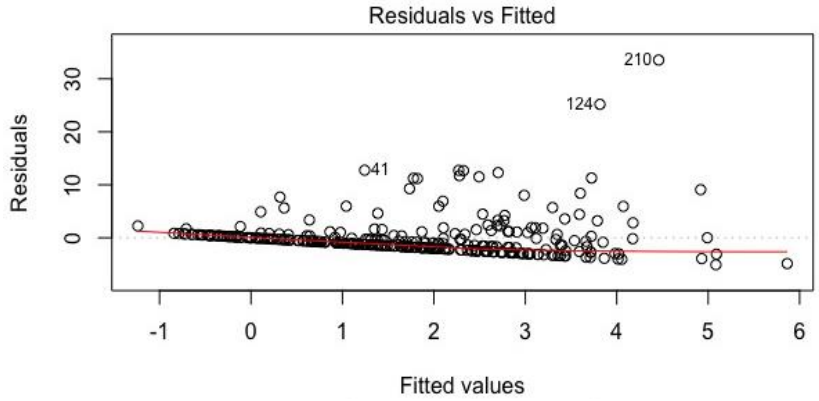

Figure 42: Plot of the residuals versus fitted values for the linear model generated using wind speed.

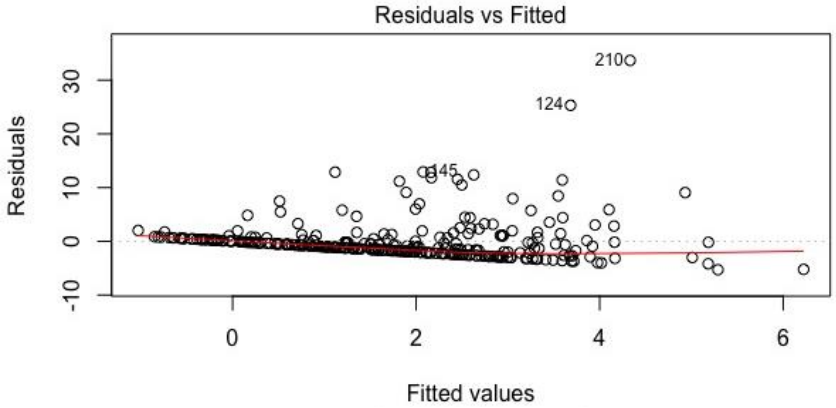

Figure 43: Plot of the residuals versus fitted values for the linear model generated using gust speed.

Non-linear models, specifically power and exponential models, were developed in R using wind speed as the explanatory variable and daily nest count as the dependent variable. The

multiple R-squared and AICc values of the non-linear models were comparable to that of the linear model that used wind speed as the explanatory variable, yet the values associated with the linear model were slightly more favorable (Table 12). Furthermore, the power and exponential models did not explain the trend in the residuals (Figures 44-45). The plots of the residuals for the non-linear models reveal an increasing trend in the residuals similar to the trend of the residuals for the linear model (Figures 42 & 44-45). Therefore, the relatively best model option that uses environmental conditions to predict daily nest count is the linear model with the explanatory variable of wind speed.

Table 12: The multiple R-squared and AICc values of the linear, power, and exponential models with wind speed as the explanatory variable.

Model Type	**Model**	**Multiple R-squared**	**AICc**
Linear	-3.05 + 0.344*wind speed	0.1114	1774.075
Power	-15.7 + 9.1*(wind speed^0.25)	0.1016	1777.619
Exponential	-0.31 + 1.12*e^(-1.709 + 0.153*wind speed)	0.1107	1774.338

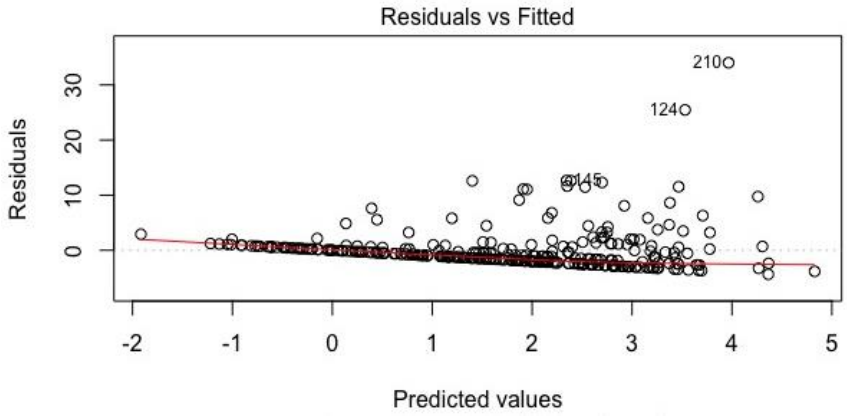

Figure 44: Plot of the residuals versus fitted values for the power model generated using wind speed.

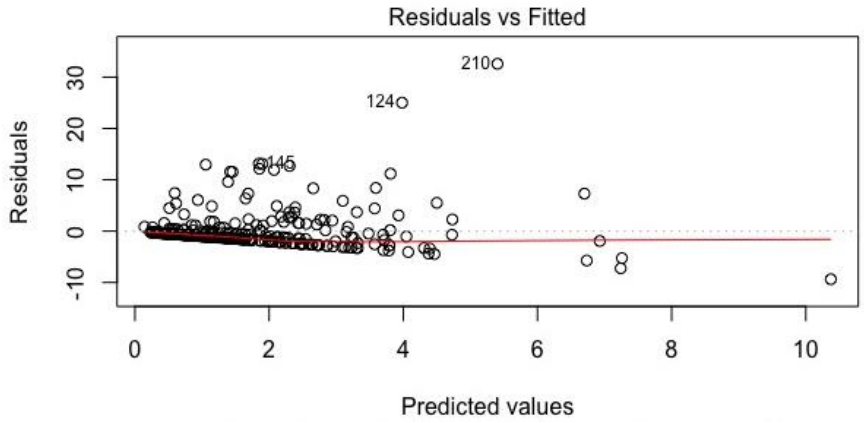

Figure 45: Plot of the residuals versus fitted values for the exponential model generated using wind speed.

Alongshore Habitat Variability Analysis

The optimal number of groups for the cross-shore profiles created every 100 m alongshore, which was evaluated using the Calinski-Harabasz pseudo F-statistic, was four for 2009-2011 and five for 2012. Tables 13-16 list the average value of each geomorphology characteristic and nest frequency for each group of profiles each year, providing a quantification of the general trends in geomorphology alongshore. A detailed quantification of the variations in geomorphology alongshore is furnished by plots of each geomorphology characteristic derived from the cross-shore profiles versus distance alongshore, located in Appendix E. Figures 46-49 display the location of each group of profiles per year. Each year, nest frequency was highest in one of the groups of profiles located in the central section of the study area (Figures 46-49). This section was characterized by beaches that were narrower and steeper than average and by dunes that had an above average height, with the exception of 2011 where the steepest beach slope was located in the northernmost region.

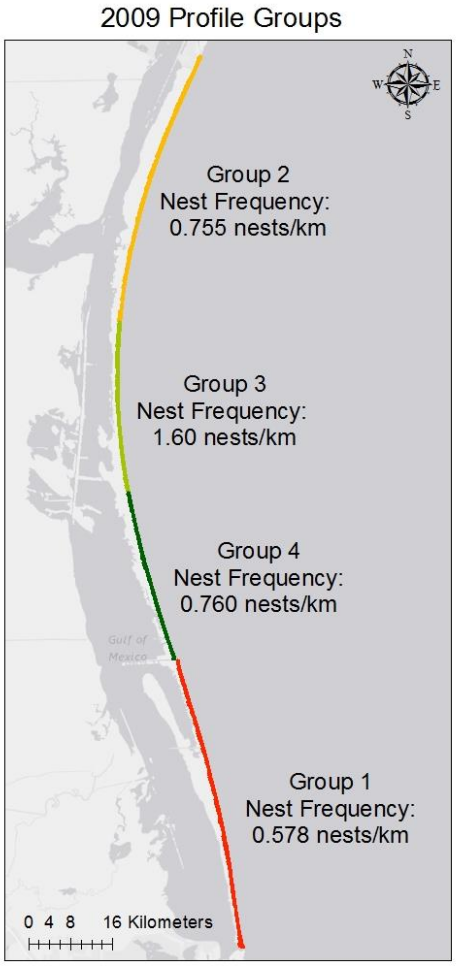

Figure 46: Map depicting the location of each group (cluster) of profiles for 2009 labeled with the corresponding nest frequency (nests/km).

Table 13: Table listing the average of each geomorphology characteristics for each group of profiles for 2009, listed in order from North to South.

Group	Average Dune Slope (degrees)	Beach Width (m)	Average Beach Slope (degrees)	Dune Width (m)	Dune Height (m)	Nests Frequency (nests/km)
2	7.29	16.45	2.29	170.69	6.63	0.75
3	7.03	10.60	3.58	204.75	7.73	1.60
4	8.36	11.45	3.18	124.57	5.99	0.76
1	6.04	16.43	2.66	143.26	5.61	0.58

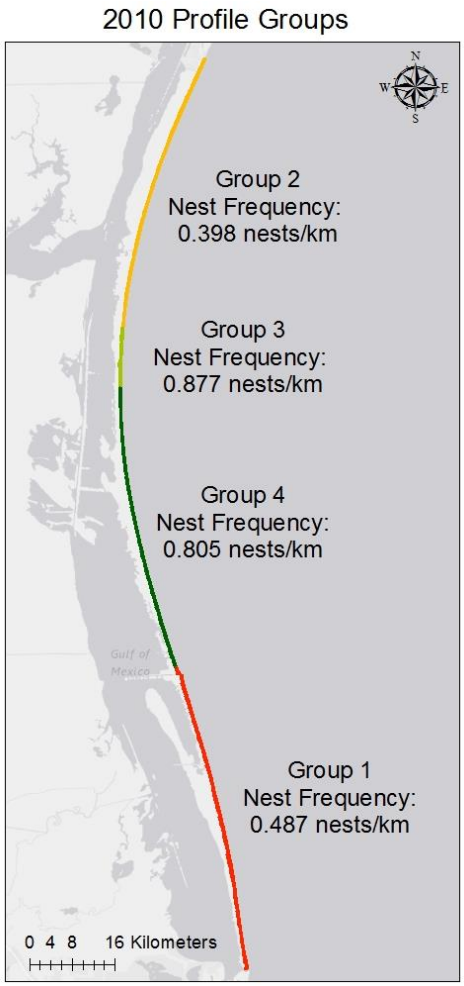

Figure 47: Map depicting the location of each group (cluster) of profiles for 2010 labeled with the corresponding nest frequency (nests/km).

Table 14: Table listing the average of each geomorphology characteristics for each group of profiles for 2010, listed in order from North to South.

Group	Average Dune Slope (degrees)	Beach Width (m)	Average Beach Slope (degrees)	Dune Width (m)	Dune Height (m)	Nest Frequency (nests/km)
2	10.35	23.53	2.66	63.93	5.28	0.40
3	7.81	10.32	4.32	134.81	8.15	0.88
4	9.86	17.46	3.31	71.11	5.86	0.81
1	2.50	27.95	6.58	117.82	5.38	0.49

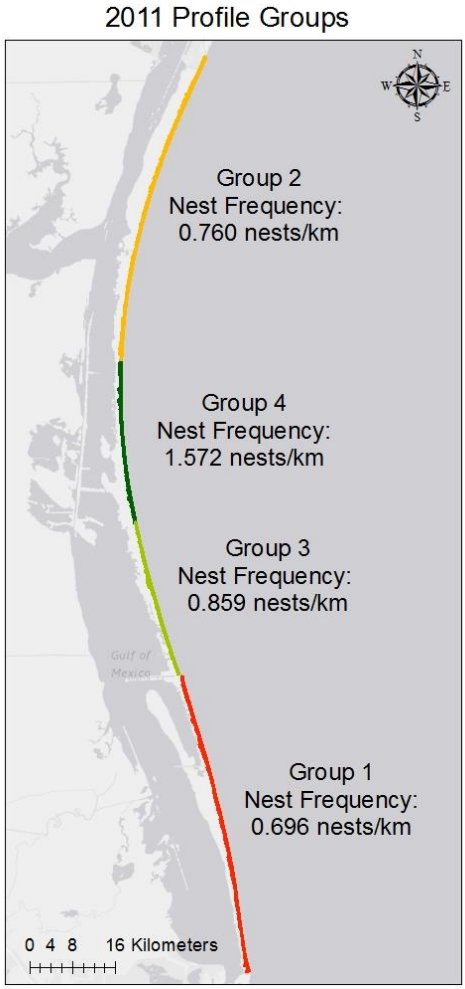

Figure 48: Map depicting the location of each group (cluster) of profiles for 2011 labeled with the corresponding nest frequency (nests/km).

Table 15: Table listing the average of each geomorphology characteristics for each group of profiles for 2011, listed in order from North to South.

Group	Average Dune Slope (degrees)	Beach Width (m)	Average Beach Slope (degrees)	Dune Width (m)	Dune Height (m)	Nest Frequency (nests/km)
2	8.10	20.13	3.58	158.84	6.72	0.76
4	7.88	20.87	3.00	174.00	7.58	1.57
3	8.85	22.51	2.58	123.77	6.03	0.86
1	6.76	36.12	2.32	134.27	5.74	0.70

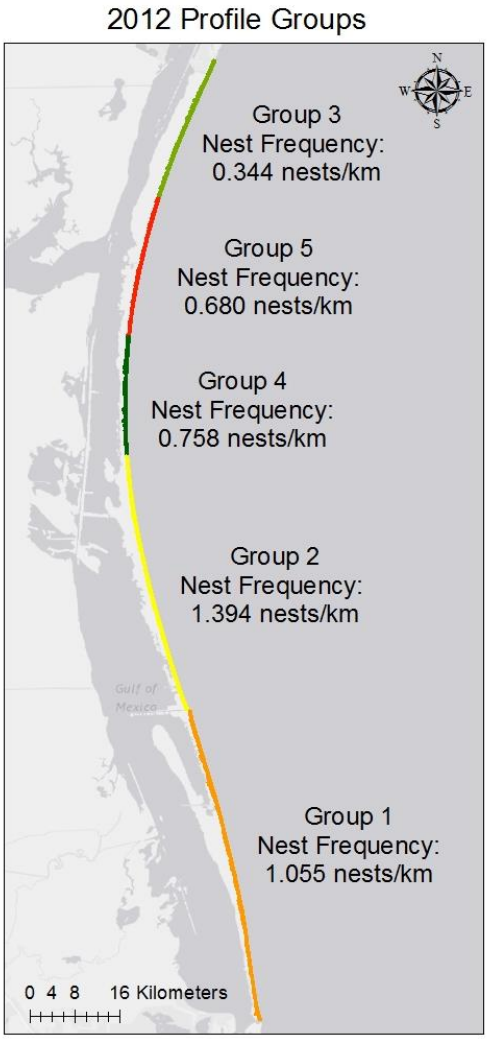

Figure 49: Map depicting the location of each group (cluster) of profiles for 2012 labeled with the corresponding nest frequency (nests/km).

Table 16: Table listing the average of each geomorphology characteristics for each group of profiles for 2012, listed in order from North to South.

Group	Average Dune Slope (degrees)	Beach Width (m)	Average Beach Slope (degrees)	Dune Width (m)	Dune Height (m)	Nest Frequency (nests/km)
3	7.84	21.95	2.81	157.53	6.31	0.34
5	8.59	19.10	2.71	137.96	6.46	0.68
4	7.08	10.18	3.83	200.89	7.91	0.76
2	9.26	13.70	3.20	114.61	6.37	1.39
1	6.61	18.13	2.96	143.42	5.79	1.06

Statistical analyses of nest abundance and the associated average geomorphology characteristics within the 1 km beach segments for each year and all years combined resulted in linear models with low adjusted R-squared values, high p-values and high errors (Table 17). The models for each year and all years combined were each comprised of a unique combination of explanatory variables. For each year and all years combined, each variable in the top linear model was significant with an alpha of 0.1. In comparison to the aforementioned GLMs, these models are not effective at predicting nest presence or absence, possibly due to the limited number of nests over the extensive study area.

Table 17: Table listing the top linear model for each year and all years combined for the statistical analysis of nest abundance and average geomorphology characteristics within 1 km beach segments.

Year	**Linear Model**	**Adjusted R-Squared**	**P-value**	**Mean Square Error**
2009	0.2 + 0.31*avg beach slope + 0.0039* dune width – 0.028*max dune slope	0.084	0.0004	0.97
2010	1.9 – 0.068*avg dune slope – 0.018*beach width – 0.0036*dune width	0.032	0.034	0.63
2011	0.394 + 0.0033*dune width	0.034	0.0078	0.99
2012	-2.98 + 4.31*avg beach elevation – 0.016*beach width	0.032	0.022	1.11
All	-1.85 – 0.011*beach width + 0.081*dune height + 2.48*avg beach elevation	0.038	1.32e-06	0.96

DISCUSSION

Kemp's ridley nest presence was successfully modeled using a small number of geomorphology characteristics. The top generalized linear models were able to explain 40-46% of the variability of nest presence with a relatively low prediction error (Table 6), and the final random forest model was highly accurate with a true positive rate above 85% (Table 8). The random forest model was superior in performance compared to the generalized linear models. This indicates that ranges of the geomorphology characteristics may be more important for Kemp's ridley nesting than linear trends, or that the relationship between nest presence and the explanatory variables is non-linear.

The generalized linear models generated using a higher ratio of background to presence points were characterized by lower pseudo R-squared values and lower K-fold cross validation prediction errors in comparison to the generalized linear models constructed using a lower ratio of background to presence points (Table 6). However, as the ratio of background to presence points increased, model accuracy in predicting presence points decreased while accuracy in predicting background points increased (Figures 29 & 32-34).

Similarly, the random forest model generated using a 10:1 ratio of background points to presence points had a higher accuracy in predicting background points with a lower sensitivity in comparison to the random forest model generated using an equal ratio (Tables 9-10). This is indicative that the models generated using higher ratios of background to presence points are biased towards predicting the background points. Furthermore, generalized linear models created using a geographic exclusion sampling technique of the background points decreased the accuracy of the model, indicating that a random selection sampling technique of background points is a good method to build presence/absence models (Figures 35-36). Therefore, the

optimal generalized linear models for this study were generated using a 1:1 ratio of background points to presence points with background points that were randomly sampled, making Models 1 and 2 of Table 6 the top generalized model options. Similarly, the top random forest model was created using an equal ratio of background to presence points (Table 8).

For both the random forest model and the top generalized linear models, elevation and distance from shoreline were the most important variables. The optimized generalized linear models included the aforementioned geomorphology characteristics as significant variables. Furthermore, the generalized linear model generated without the variables of elevation or distance from shoreline was less accurate in predicting nest presence and absence and only accounted for 9% of the variability (Table 6). Similarly, the variable importance plots for the random forest model indicate that elevation and distance from shoreline contributed the most to the accuracy of the model and were the relatively most important variables (Figure 40). This is indicative that site specific characteristics, or where Kemp's ridleys nest on a given beach, are more important than the other beach geomorphology characteristics. This is further supported by the results of the alongshore habitat variability analysis, which revealed that alongshore trends in the geomorphology characteristics did not significantly influence nest presence (Table 17).

However, the alongshore habitat variability analysis may have been ineffective at predicting nest presence due to the relatively small number of nests in comparison to the extensive size of the study area. Maximum dune slope and average beach slope were both relatively important variables in the random forest model and were significant variables in the top generalized linear models, exhibitive of a degree of importance for nesting preferences (Table 6 & Figure 40).

Kemp's ridleys preferred to nest at a median elevation of 1.04 m above mean sea level and a median distance from shoreline of 12.79 m, which corresponds to the area near the potential vegetation line (Appendix A). This is consistent with the description of the nesting habits of the species by Marquez-M. (1994) that the Kemp's ridley usually nests in front of the first dune, on the windward slope, or on top of the dune. Kemp's ridleys also exhibited a preference for a limited range of the available habitat and avoided nesting on beaches with extreme values for maximum dune slope, average beach slope, and beach width (Figures 21-27). Additionally, nesting occurred at a median value for each geomorphology characteristic that is lower than the median value of the background points, suggestive of an aversion to maximum values of geomorphology characteristics (Figures 21-27). Figures 50 and 51 are examples of profiles that would not be preferred for nesting because they are characterized by extreme values for the beach geomorphology characteristics. On the other hand, Figures 52 and 53 are examples of profiles that would be preferred for nesting because they are characterized by beaches with moderate widths and slopes as well as prominent foredune complexes.

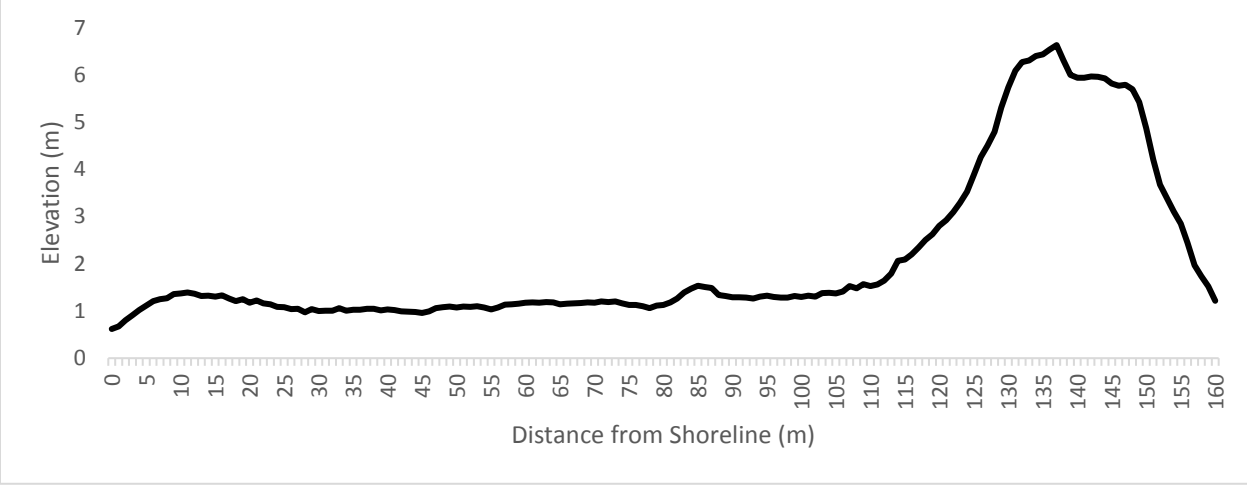

Figure 50: Example of a profile that would not be preferred for nesting due to the wide, flat beach.

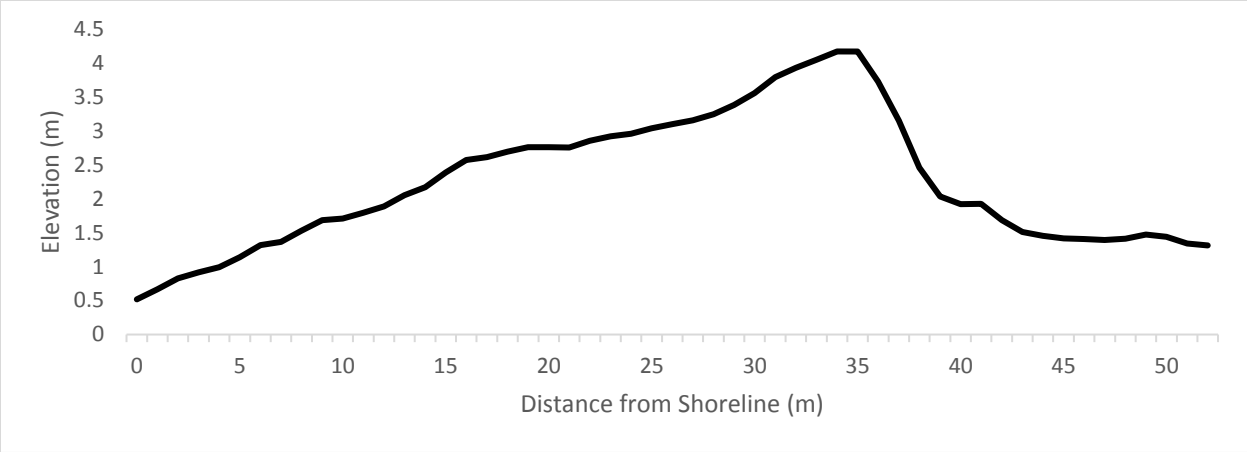

Figure 51: Example of a profile that would not be preferred for nesting due to the narrow, steep beach and high average dune slope.

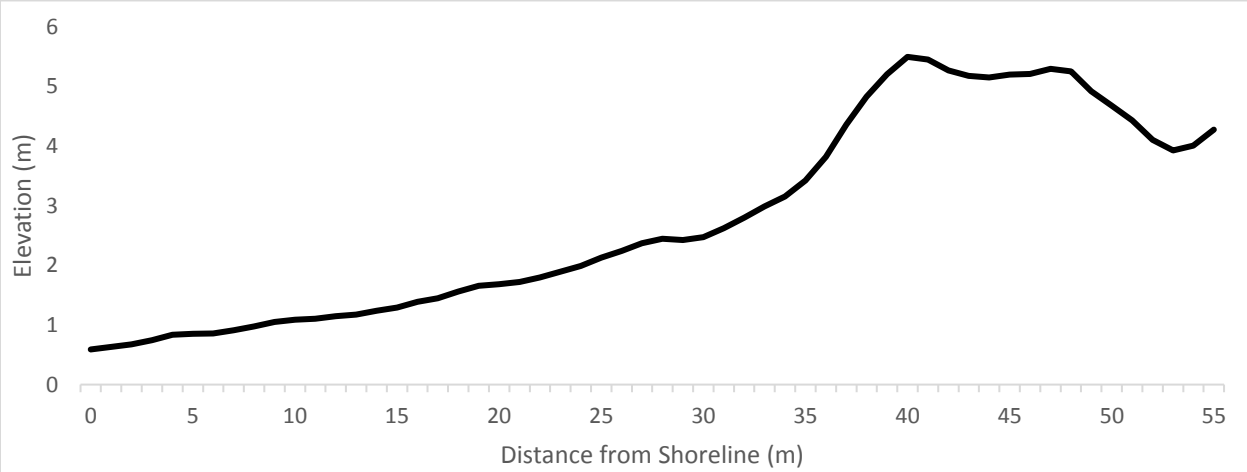

Figure 52: Example of a profile that would be preferred for nesting due to the moderate beach slope and width and prominent dune complex.

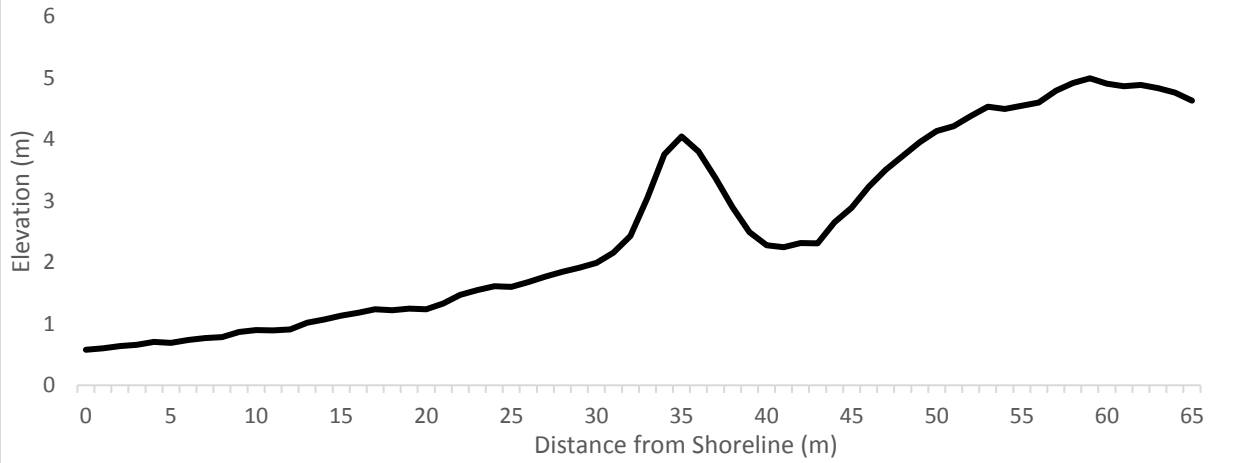

Figure 53: Example of a profile that would be preferred for nesting due to the moderate beach slope and width and prominent dune complex.

Spatially, Kemp's ridleys nested at higher frequencies along the central section of the study area; the beaches in this region are on average narrower, steeper and characterized by higher dune peaks in comparison to the northern and southern sections of the study area (Figures 46-49 & Tables 13-16). However, this is not indicative that this region is characterized by more extreme values for beach geomorphology characteristics in comparison to the other regions (Appendix E). The results of the Optimized Hot Spot Analysis tool in ArcGIS concur with this finding, with a considerable hot spot occurring along the central section of the study area for all the years of data combined (Figure 30). The beaches along the central section of the study area resemble the main nesting site of the Kemp's ridley, the beaches of Rancho Nuevo, Mexico, which are also narrower and steeper in comparison to nearby beaches (Carranza-Edwards et al., 2004) (Figure 4). Both regions are also characterized by the presence of shell fragments (Carranza-Edwards et al., 2004; NMFS *et al.*, 2010; NMFS & USFWS, 2015). The resemblance between the beaches of the central section of Padre Island, TX and Rancho Nuevo, Mexico reinforces the spatial nesting trends found in this study.

These results largely resemble the findings of research regarding other sea turtle species. Yamamoto *et al.* (2012) found that loggerhead, green, and leatherback sea turtles each exhibited tolerances for ranges of values of geomorphology characteristics, but they would not nest on beaches with values outside of these tolerances. This is consistent with the findings of this research, which concluded that Kemp's ridleys exhibited an aversion to beaches outside of a certain range of values of geomorphology characteristics (Figures 21-27). Studies regarding both the loggerhead and hawksbill sea turtles found that these species prefer to nest at a certain elevation above mean sea level (Horrocks & Scott, 1991; Wood & Bjorndal, 2000). Furthermore, Dunkin *et al.* (2016) developed a model that successfully predicted loggerhead habitat suitability

using geomorphology characteristics, of which elevation proved to be the most influential factor. Similarly, Kemp's ridley nest presence was successfully modeled using beach geomorphology characteristics, and elevation and distance from shoreline, which are collinear variables, were the most important.

Environmental Conditions for Nesting

The results of this study also indicate that the Kemp's ridley exhibited a preference for nesting on days with higher wind speeds and gust speeds, concurrent with the findings of Jimenez-Quiroz *et al.* (2005) and Shaver *et al.* (2017). A comparison of statistical measures of the environmental conditions for non-nesting days, nesting days, and nesting days with two or more nests suggested that nesting becomes more likely once wind speeds and gust speeds reach a certain magnitude. Seventy-five percent of nesting days with two or more nests were characterized by wind speeds of at least 14.4 knots and by gust speeds of at least 17.1 knots (Table 10). In comparison, only 25% of non-nesting days during nesting season were characterized by comparable wind speeds and gust speeds (Table 10). Furthermore, models predicting daily nest count using daily average wind speed and gust speed as explanatory variables were significant and explained over 10% of the variability in daily nest count (Tables 11-12). It is possible that wind speed acts as a cue or stimuli for Kemp's ridleys to initiate an arribada, since higher wind speeds are advantageous because they produce cooler sand temperatures and reduce predation risk (Jimenez-Quiroz *et al.*, 2005; Shaver *et al.*, 2017; Shaver & Rubio, 2008).

Sources of Error

Potential sources of error include the accuracy of both the nest coordinates and the lidar data. Both the Garmin GPS 72 and GPS 72H have a typical GPS accuracy of less than 15 meters

with an RMS of 95% and a typical DGPS accuracy of 3 to 5 meters with an RMS of 95% (Garmin, 2002; Garmin, 2009). The horizontal accuracy of the lidar data is less than 1 m and the vertical accuracy is less than 0.15 m (Table 1). The bias in the lidar data, though minimal, was not corrected and constitutes another source of error (Table 2 & Appendix A). In particular, the accuracy of the nest coordinates measured on South Padre Island using Google Earth is questionable. Google makes no claims as to the accuracy of the coordinates in Google Earth, and imagery is acquired from several sources with varying projections and spectral characteristics. However, a recent study by Wang *et al.* (2017) found that the RMSE of Google Earth roadway elevations was 2.27 meters and concluded that elevation data provided by Google Earth is a reliable data source for transportation applications.

Additionally, in-situ nests, or nests not located during beach monitoring and nest location efforts, were not included in this study. The beaches of these nests could be characterized by geomorphology characteristics that fall outside the current quantification of the Kemp's ridley habitat range, which would thereby change the range of the species and alter the statistical models. However, the patrol effort along the study area is considerable and the number of in-situ nests is likely minimal (Shaver *et al.*, 2016b). This means that the nests analyzed in this study are representative of a majority of nests within the study area, and it is feasible to assume that any in-situ nests would only minutely alter the results of this study.

Applicability for Kemp's Ridley Management and Conservation

There are variety of species management and conservation applications for the results of this study that would help protect the Kemp's ridley sea turtle and its habitat. The methods developed in this study can be used to monitor Kemp's ridley habitat availability along the Texas coast as both human (i.e. beach nourishment) and natural processes (i.e. sea-level rise and

extreme storm events) alter beach geomorphology characteristics. Resource managers and city planners can use these results to limit degradation to Kemp's ridley terrestrial habitat during beach nourishment and maintenance projects by ensuring the geomorphology characteristics of all managed beaches fall within the habitat range of the species. For instance, beaches can be managed to resemble Figures 52-53 and can be further altered if they resemble Figures 50-51.

Furthermore, this quantification of Kemp's ridley terrestrial habitat and nesting preferences can be used to locate beaches with optimal nesting habitat for any future relocation efforts and to assist with a critical habitat designation for the species. The results of this study can also be applied to Kemp's ridley nest location efforts. Monitoring can be focused on areas where Kemp's ridleys are most likely to nest, such as near the potential line of vegetation and along the central section of Padre Island, Texas, and searches can be strengthened on days with higher wind speeds, especially on days with wind speeds greater than 15 knots.

CONCLUSIONS

This project assessed the relationship between beach geomorphology and Kemp's ridley nest site selection on North and South Padre Islands, Texas, USA and determined the influence of environmental conditions on Kemp's nest presence. The following objectives were achieved:

- Identify the terrestrial habitat variability of the Kemp's ridley sea turtle on the beaches of North and South Padre Islands, Texas;
- Quantify the influence of beach geomorphology characteristics on Kemp's ridley nest site selection;
- Assess the impact of daily average environmental conditions, such as wind speed and direction, on Kemp's ridley daily nest abundance.

The results of this study include new information regarding the Kemp's ridley sea turtle that will be beneficial for species conservation practices and management decisions. Although the Kemp's ridley nests on beaches with a wide range of geomorphology characteristics, the species exhibited an aversion to beaches outside a certain range of values (Figures 21-27). Furthermore, the Kemp's exhibited a preference for nesting near the potential vegetation line, or the lowest dune elevation at which vegetation will grow, and on days with higher wind speeds.

Future Research

Future work should incorporate the results of this study into a habitat suitability model in order to map Kemp's ridley habitat along the Texas Gulf Coast, especially as beaches respond to threats, such as extreme storms and sea-level rise, and the extent of Kemp's ridley habitat potentially changes. In addition, applying this study to the main nesting beach of Rancho Nuevo, Mexico would be informative of any regional differences in Kemp's ridley nesting preferences. This would also serve as a method of further validating the results of this study. In hopes of

explaining more of the variability, a future project could also combine geomorphology characteristics with other parameters, such as sand characteristics, artificial lighting, and extent of human use, in a more comprehensive model predicting Kemp's ridley nest presence. Similarly, current and tidal data could be combined with wind speed and gust speed data to attempt to better understand the timing of Kemp's ridley arribadas. Furthermore, future work could assess if individuals exhibit fidelity for beaches within a narrow range of geomorphology characters, even if they do not necessarily exhibit site fidelity.

LITERATURE CITED

Barbet-Massin, M., Jiguet, F., Albert, C. H., & Thuiller, W. (2012). Selecting backgrounds for species distribution models: how, where and how many? *Methods in Ecology and Evolution, 3*(2), 327–338. https://doi.org/10.1111/j.2041-210X.2011.00172.x

Bevan, E., Wibbels, T., Najera, B. M. Z., Sarti, L., Martinez, F. I., Cuevas, J. M., Gallaway, B. J., Pena, L. J., and Burchfield, P. M. (2016). Estimating the historic size and current status of the Kemp's ridley sea turtle (Lepidochelys kempii) population. *Ecosphere*, 7(3), 1–15.

Breiman, L. (2001). Random Forests. *Machine Learning*, *45*(1), 5–32. https://doi.org/10.1023/A:1010933404324

Brubaker, K. M., Myers, W. L., Drohan, P. J., Miller, D. A., and Boyer, E. W. (2013). The Use of Lidar Terrain Data in Characterizing Surface Roughness and Microtopography. *Applied and Environmental Soil Science*, 2013, e891534. https://doi.org/10.1155/2013/891534

Caillouet, C. W., Shaver, D. J., and Landry, A. M. (2015). Kemp's ridley sea turtle (Lepidochelys kempii) head-start and reintroduction to padre island national seashore, Texas. *ResearchGate*, 10(1), 309–377.

Carranza-Edwards, A., Rosales-Hoz, L., Chávez, M. C., & de la Garza, E. M. (2004). Environmental geology of the coastal zone. In *Environmental Analysis of the Gulf of Mexico* (pp. 351–372). Texas A&M University Press.

Crain, D. A., Bolten, A. B., and Bjorndal, K. A. (1995). Effects of Beach Nourishment on Sea Turtles: Review and Research Initiatives. *Restoration Ecology*, 3(2), 95–104. https://doi.org/10.1111/j.1526-100X.1995.tb00082.x

Crase, B., Liedloff, A., Vesk, P. A., Fukuda, Y., & Wintle, B. A. (2014). Incorporating spatial autocorrelation into species distribution models alters forecasts of climate-mediated range shifts. *Global Change Biology, 20*, 2566–2579. https://doi.org/10.1111/gcb.12598

Cuevas, E., Liceaga-Correa, M. de los Á., and Mariño-Tapia, I. (2010). Influence of Beach Slope and Width on Hawksbill (Eretmochelys imbricata) and Green Turtle (Chelonia mydas) Nesting Activity in El Cuyo, Yucatán, Mexico. *Chelonian Conservation and Biology*; Lawrence, 9(2), 262–267.

Curray, J. R. (1960). Sediments and history of Holocene transgression, continental shelf, northwest Gulf of Mexico. In F. P. Shepard, F. B. Phleger, & T. H. van Andel (Eds.), *Recent Sediments, Northwest Gulf of Mexico* (pp. 221–266). Tulsa, Oklahoma: American Association of Petroleum Geologists.

Davis, R. A. (1977). Beach sedimentology of Mustang and Padre Islands: A time-series approach. *The Journal of Geology*, 86(1), 35–46.

Dormann, C. F., McPherson, J. M., Araújo, M. B., Bivand, R., Bolliger, J., Carl, G., Wilson, R. (2007). Methods to account for spatial autocorrelation in the analysis of species distributional data: a review. *Ecography*, *30*(5), 609–628. https://doi.org/10.1111/j.2007.0906-7590.05171.x

Dunkin, L., Reif, M., Altman, S., & Swannack, T. (2016). A Spatially Explicit, Multi-Criteria Decision Support Model for Loggerhead Sea Turtle Nesting Habitat Suitability: A Remote Sensing-Based Approach. *Remote Sensing*, *8*(573). Retrieved from http://www.mdpi.com/2072-4292/8/7/573/pdf

Elith, J., H. Graham, C., P. Anderson, R., Dudík, M., Ferrier, S., Guisan, A., Hijmans, R. J., Huettmann, F., Leathwick, J. R., Lehmann, A., Li, J., Lohmann, L. G., Manion, G., Moritz, C., Nakamura, M., Nakazawa, Y., Overton, J. M. M., Townsend, P., Phillips, S. J., Richardson, K., Scachetti-Pereira, R., Schapire, R. E., Soberon, J., Williams, S., Wisz, M.S., E. Zimmermann, N. (2006). Novel methods improve prediction of species' distributions from occurrence data. *Ecography*, *29*(2), 129–151. https://doi.org/10.1111/j.2006.0906-7590.04596.x

Frey, A., Dutton, P. H., Shaver, D. J., Walker, J. S., and Rubio, C. (2014). Kemp's ridley Lepidochelys kempii nesting abundance in Texas, USA: a novel approach using genetics to improve population census. *Endangered Species Research*, 23, 63–71.

Gallaher, A. A. (2009). The effects of beach nourishment on sea turtle nesting densities in Florida (Ph.D.). University of Florida, United States -- Florida. Retrieved from http://search.proquest.com/naturalscicollection/docview/848633089/abstract/4E9081CEB28D475EPQ/1

Gallaway, B. J., Gazey, W. J., Caillouet Jr., C. W., Plotkin, P. T., Grobois, F. A. A., Amos, A. F., Burchfield, P. M., Carth, R. R., Martinez, M. A. C., Cole, J. G., Coleman, A. T., Cook, M., DiMarco, S., Epperly, S. P., Fujiwara, M., Gamez, D. G., Graham, G. L., Griffin, W. L., Martinez, F. I., Lamont, M. M., Lewison, R. L., and Lohmann, K. (2016a). Development of a Kemp's Ridley Sea Turtle Stock Assessment Model. *Gulf of Mexico Science*, 2016(2), 138–157.

Gallaway, B. J., Gazey, W. J., Wibbels, T., Bevan, E., Shaver, D. J., and George, J. (2016b). Evaluation of the Status of the Kemp's Ridley Sea Turtle After the 2010 Deepwater Horizon Oil Spill. *Gulf of Mexico Science*, 2016(2), 192–205.

Garmin. (2002). GPS 72 Personal Navigator Owner's Manual & Reference Guide. Garmin Ltd. Retrieved from http://static.garmin.com/pumac/GPS72_OwnersManual.pdf

Garmin. (2009). GPS 72H Owner's Manual. Garmin Ltd. Retrieved from http://static.garmincdn.com/pumac/GPS72H_OwnersManual.pdf

Gibeaut, J. C., & Caudle, T. (2009). Defining and Mapping Foredunes, the Line of Vegetaiton, and Shorelines along the Texas Gulf Coast (Final Report prepared for Texas General Land Office). Retrieved from

http://www.beg.utexas.edu/coastal/presentations_reports/Final%20Report%20GLO%2007_005_22.pdf

Gibeaut, J. C., Gutiérrez, Roberto, and Hepner, Tiffany. (2002). Threshold conditions for episodic beach erosion along the southeast Texas coast. *Gulf Coast Association of Geological Societies Transactions*, 52, 323–335.

Herrera, Andres. (1947). Screenshot of a video of an arribada in Rancho Nuevo, Mexico in 1947. Retrieved from: https://www.youtube.com/watch?v=x1hoIxrAcQ8.

Horrocks, J. A., and Scott, N. M. (1991). Nest site location and nest success in the hawksbill turtle Eretmochelys imbricata in Barbados, West Indies. *Marine Ecology Progress Series*, 69, 1–8.

Houser, C., Hapke, C., and Hamilton, S. (2008). Controls on coastal dune morphology, shoreline erosion and barrier island response to extreme storms. *Geomorphology*, 100, 223–240.

Houser, C., and Mathew, S. (2010). Alongshore variation in foredune height in response to transport potential and sediment supply: South Padre Island, Texas. *Geomorphology*, 125(1), 62–72.

Intergovernmental Panel on Climate Change. (2013). Sea Level Change. In J. A. Church, P. U. Clark, J. M. Gregory, S. Jevrejeva, A. Levermann, M. A. Merrifield, G.A. Milne, R. S. Nerem, P. D. Nunn, A. J. Payne, W. T. Pfeffer, D. Stammer, A. S. Unnikrishnan (Eds.), Climate Change 2013: The Physical Science Basis. Contribution of Working Group I to the Fifth Assessment Report of the Intergovernmental Panel on Climate Change. Cambridge, UK and New York, NY, USA: Cambridge University Press. Retrieved from http://www.ipcc.ch/pdf/assessment-report/ar5/wg1/WG1AR5_Chapter13_FINAL.pdf

Isenburg, Martin. (2017). LAStools – efficient LiDAR processing software (version 2.1). Obtained from https://rapidlasso.com/LAStools/

IUCN. (1996). Lepidochelys kempii: Marine Turtle Specialist Group: The IUCN Red List of Threatened Species 1996: e.T11533A3292342. https://doi.org/10.2305/IUCN.UK.1996.RLTS.T11533A3292342.en

Jimenez-Quiroz, M. D. C., Filonov, A., Tereshchenko, I., and Marquez-Millan, R. (2005). Time-Series Analyses of the Relationship Between Nesting Frequency of the Kemp's Ridley Sea Turtle and Meteorological Conditions. *Chelonian Conservation and Biology*, 4(4).

Judd, F. W., Lonard, R. I., and Sides, S. L. (1977). The vegetation of South Padre Island, Texas in relation to topography. *Southwestern Naturalist*, 22(1), 31–48.

KellerLynn, K. (2010). Padre Island National Seashore: Geologic Resources Inventory Report. (No. Natural Resource Report NPS/NRPC/GRD/NRR—2010/246). National Park Service.

Laloë, J.-O., Cozens, J., Renom, B., Taxonera, A., and Hays, G. C. (2014). Effects of rising temperature on the viability of an important sea turtle rookery. *Nature Climate Change*, 4(6), 513–518. https://doi.org/10.1038/nclimate2236

Long, T. M., Angelo, J., and Weishampel, J. F. (2011). Lidar-derived measures of hurricane- and restoration-generated beach morphodynamics in relation to sea turtle nesting behaviour. *International Journal of Remote Sensing*, 32(1), 231–241. https://doi.org/10.1080/01431160903439973

Marquez-M., R. (1994). Synopsis of biological data on the Kemp's ridley turtle, Lepidochelys kempi, (Garman, 1880) (No. NOAA Technical Memorandum NMFS-SEFSC-343) (p. 91). Retrieved from https://www.boem.gov/ESPIS/3/3446.pdf

McFadden, D. (1974) Conditional logit analysis of qualitative choice behavior. Pp. 105-142 in P. Zarembka (ed.), *Frontiers in Econometrics*. Academic Press.

Mitasova, H., Overton, M. F., Recalde, J. J., Bernstein, D. J., and Freeman, C. W. (2009). Raster-based analysis of coastal terrain dynamics from multitemporal lidar data. *Journal of Coastal Research*, 252, 507–514. https://doi.org/10.2112/07-0976.1

Mortimer, J. A. (1982). Factors influencing beach selection by nesting sea turtles. In K. A. Bjorndal (Ed.), Biology and conservation of sea turtles (pp. 45–51). Washington, DC: Smithsonian Institution Press Pages.

Mortimer, J. A. (1990). The Influence of Beach Sand Characteristics on the Nesting Behavior and Clutch Survival of Green Turtles (Chelonia mydas). American Society of Ichthyologists and Herpetologists, *Copeia*, 1990(3), 802–817.

National Marine Fisheries Service, and U.S. Fish and Wildlife Service. (2015). Kemp's Ridley Sea Turtle 5-Year Review: Summary and Evaluation. NOAA.

National Marine Fisheries Service, U.S. Fish and Wildlife Service, and SEMARNAT. (2010). Draft Bi-National Recovery Plan for the Kemp's Ridley Sea Turtle, Secon Revision. Silver Spring, Maryland: National Marine Fisheries Service. Retrieved from http://www.nmfs.noaa.gov/pr/pdfs/recovery/turtle_kempsridley_draft2.pdf

National Oceanic Atmospheric Administration. (2017). Water Level Reports - NOAA Tides and Currents. Retrieved March 1, 2017, from https://tidesandcurrents.noaa.gov/reports.html?id=8775870

National Oceanic Atmospheric Administration, National Ocean Service, Department of Commerce, and Office for Coastal Management. (2016). United States Interagency Elevation Inventory. Retrieved January 31, 2017, from https://coast.noaa.gov/inventory/

National Research Council, Division on Earth and Life Studies, Commission on Life Sciences, and Committee on Sea Turtle Conservation. (1990). Decline of the Sea Turtles: Causes and Prevention. National Academies Press.

Nicholls, R. J., and Cazenave, A. (2010). Sea-Level Rise and Its Impact on Coastal Zones. *Science*, 328(5985), 1517–1520. https://doi.org/10.1126/science.1185782

Paine, J., Caudle, T., and Andrews, J. (2013). Shoreline, Beach, and Dune Morphodynamics, Texas Gulf Coast (No. 09-242-000-3789). Bureau of Economic Geology. Retrieved from http://www.beg.utexas.edu/coastal/data/ciapGulfShorelineLidar_screen.pdf

Paris, P., Starek, M. J., Hardin, E., Kurum, O., Overton, M., and Mitasova, H. (2013). Lines in the Sand: Geomorphic and Geospatial Characterization and Interpretation of Sandy Shorelines and Beaches. *Geography Compass*, 7(5), 315–343. https://doi.org/10.1111/gec3.12041

Pendleton, E. A., Thieler, E. R., Williams, S. J., and Beavers, R. L. (2004). Coastal Vulnerability Assessment of Padre Island National Seashore (PAIS) to Sea-Level Rise. U.S. Geological Survey. Retrieved from https://pubs.usgs.gov/of/2004/1090/images/pdf/pais.pdf

Phillips, S. J., Dudík, M., Elith, J., Graham, C. H., Lehmann, A., Leathwick, J., & Ferrier, S. (2009). Sample selection bias and presence-only distribution models: implications for background and background data. *Ecological Applications*, *19*(1), 181–197. https://doi.org/10.1890/07-2153.1

Pike, D. A. (2013). Climate influences the global distribution of sea turtle nesting. *Global Ecology and Biogeography*, 22(5), 555–566. https://doi.org/10.1111/geb.12025

Plotkin, P. T. (2007). Biology and Conservation of Ridley Sea Turtles. JHU Press.

Provancha, J. A. and L. M. Ehrhart. (1987). Sea turtle nesting trends at Kennedy Space Center and Cape Canaveral Air Force Station, Florida, and relationships with factors influencing nest-site selection. Pp 33–44. In Witzell, W. N., editor. (Ed.). Ecology of East Florida Sea Turtles: Proceedings of the Cape Canaveral, Florida Sea Turtle Workshop Miami, Florida February 26–27, 1985 NOAA Technical Report NMFS 53. Seattle, WA.

Putman, N. F., Mansfield, K. L., He, R., Shaver, D. J., and Verley, P. (2013). Predicting the distribution of oceanic-stage Kemp's ridley sea turtles. *Biology Letters*, 9(5), 20130345. https://doi.org/10.1098/rsbl.2013.0345

Rousoo, S., Sanchez, C. C., and Aragon, C. D. L. (2014). Quantifying Sea Turtle Nesting Habitat: Using Beach Profiling and Nest Distribution as a Conservation Tool. NOVA Publishers. Retrieved from http://www.academia.edu/9157948/QUANTIFYING_SEA_TURTLE_NESTING_HABITAT_USING_BEACH_PROFILING_AND_NEST_DISTRIBUTION_AS_A_CONSERVATION_TOOL

Santos, K. C., Tague, C., Alberts, A. C., and Franklin, J. (2006). Sea Turtle Nesting Habitat on the US Naval Station, Guantanamo Bay, Cuba: A Comparison of Habitat Suitability Index Models. Chelonian Conservation and Biology, 5(2):175-187.

Santos, K. C., Livesey, M., Fish, M., and Lorences, A. C. (2015). Climate change implications for the nest site selection process and subsequent hatching success of a green turtle population. *Mitigation and Adaptation Strategies for Global Change*, 1–15. https://doi.org/10.1007/s11027-015-9668-6

Scott, T., Masselink, G., and Russell, P. (2011). Morphodynamic characteristics and classification of beaches in England and Wales. *Marine Geology*, 2011. https://doi.org/http://dx.doi.org/10.1016/j.margeo.2011.04.004

Seney, E. E., and Landry, A. M. (2008). Movements of Kemp's ridley sea turtles nesting on the upper Texas coast: implications for management. *Endangered Species Research*, 4(1–2), 73–84.

Shaver, D. J., and Caillouet Jr., C. W. (2015). Reintroduction of Kemp's Ridley (Lepidochelys kempii) Sea Turtle to Padre Island National Seashore, Texas and Its Connection to Head-Starting. *Herpetological Conservation and Biology*, 10 (Symposium), 378–435.

Shaver, D. J., Hart, K. M., Fujisaki, I., Bucklin, D., Iverson, A. R., Rubio, C., Backof, T. F., Burchfield, P. M., Miron, R. d. J. D., Dutton, P. H., Frey, A., Pena, J., Gamez, D. G., Martinez, H. J., Ortiz, J. (2017). Inter-nesting movements and habitat-use of adult female Kemp's ridley turtles in the Gulf of Mexico. *PLOS ONE*, 12(3).

Shaver, D. J., Hart, K. M., Fujisaki, I., Rubio, C., Sartain, A. R., Peña, J., Burchfield, P. M., Gamez, D. G., Ortiz, J. (2013). Foraging area fidelity for Kemp's ridleys in the Gulf of Mexico. *Ecology and Evolution*, 3(7), 2002–2012. https://doi.org/10.1002/ece3.594

Shaver, D. J., Hart, K. M., Fujisaki, I., Rubio, C., Sartain-Iverson, A. R., Pena, J., Gamez, D. G., Miron, Burchfield, P. M., Martinez, H. J., Ortiz, J. (2016a). Migratory corridors of adult female Kemp's ridley turtles in the Gulf of Mexico. *Biological Conservation*, 194, 158–167.

Shaver, D. J., and Rubio, C. (2008). Post-nesting movement of wild and head-started Kemp's ridley sea turtles Lepidochelys kempii in the Gulf of Mexico. *Endangered Species Research*, 4, 43–55.

Shaver, D. J., Rubio, C., Walker, J. S., George, J., Amos, A. F., Reich, K., Jones, C., Shearer, T. (2016b). Kemp's Ridley Sea Turtle (Lepidochelys kempii) Nesting on the Texas Coast: Geographic, Temporal, and Demographic Trends Through 2014. *Gulf of Mexico Science*, 2016(2), 158–178.

Shaver, D. J., Schroeder, B. A., Byles, R. A., Burchfield, P. M., Pena, J., Marquez, R., and Martinez, H. J. (2005). Movements and Home Ranges of Adult Male Kemp's Ridley Sea Turtles in the Gulf of Mexico Investigated by Satellite Telemetry. *Chelonian Conservation and Biology*, 4(4), 817–827.

Starek, Michael J., Vemula, R., and Slatton, K. C. (2012). Probabilistic Detection of Morphologic Indicators for Beach Segmentation With Multitemporal Lidar Measurements. *IEEE Transactions on Geoscience and Remote Sensing*, 50(11).

Stutz, M. L., and Pilkey, O. H. (2011). Open-Ocean Barrier Islands: Global Influence of Climatic, Oceanographic, and Depositional Settings. *Journal of Coastal Research*, 207–222. https://doi.org/10.2112/09-1190.1

Svetnik, V., Liaw, A., Tong, C., Culberson, J. C., Sheridan, R. P., & Feuston, B. P. (2003). Random Forest: A Classification and Regression Tool for Compound Classification and QSAR Modeling. *Journal of Chemical Information and Computer Sciences*, *43*(6), 1947–1958. https://doi.org/10.1021/ci034160g

Taylor, E. B. (2014). Increasing resilience of urban development on Texas barrier islands. Retrieved from https://repositories.tdl.org/tamucc-ir/handle/1969.6/554

Texas Bureau of Economic Geology. (2007). Padre Island National Seashore: A Guide to the Geology, Natural Environments, and History of a Texas Barrier Island (The Dynamic Barrier Island). Retrieved August 2, 2016, from https://www.nps.gov/parkhistory/online_books/pais/1980-17/sec3.htm

Texas Bureau of Economic Geology. (2013). Coastal Studies. Retrieved February 9, 2017, from http://www.beg.utexas.edu/coastal/morphodynamics.php

Tissot, P., and Dell, L. (2016). Coastal Currents and Waves along the Texas Coastal Bend: Measurements and Model Comparisons. 96th American Meteorological Society Annual Meeting. Retrieved from https://ams.confex.com/ams/96Annual/webprogram/Paper290365.html

U.S. Army Corps of Engineers. (2014). Wave Information Studies Products for GOM Station 73032. Tyler Hesser, Project Manager. Retrieved from http://wis.usace.army.mil/wis_products.html?dmn=gulf&staid=73032&lat=27.1&lon=-97.15&dep=-30

U.S. Fish and Wildlife Service. (1999). Multi-Species Recovery Plan for South Florida: Kemp's Ridley Sea Turtle (pp. 649–664). Retrieved from https://www.fws.gov/verobeach/MSRPPDFs/KempsRidley.pdf

U.S. Geological Survey. (n.d.). Sea-level Rise Hazards and Decision Support, Shoreline Change and Land Loss. Retrieved August 16, 2016, from http://wh.er.usgs.gov/slr/shorelinechange.html

U.S. Global Change Research Program. (2014). Climate Change Impacts in the United States: The Third National Climate Assessment (No. doi:10.7930/J0Z31WJ2) (p. 841). Retrieved from http://s3.amazonaws.com/nca2014/high/NCA3_Climate_Change_Impacts_in_the_United%20States_HighRes.pdf?download=1

Ussa, M. (2013, March 29). Evaluating the Effects of Sea Level Rise on Sea Turtle Nesting Sites: A Case Study of the Archie Carr National Wildlife Refuge. FIU Electronic Theses and Dissertations. Retrieved from http://digitalcommons.fiu.edu/cgi/viewcontent.cgi?article=1959andcontext=etd

VanDerWal, J., Shoo, L. P., Graham, C., & Williams, S. E. (2009). Selecting background data for presence-only distribution modeling: How far should you stray from what you know? *Ecological Modeling*, *220*, 589–594.

Wang, Y., Zou, Y., Henrickson, K., Wang, Y., Tang, J., & Park, B.-J. (2017). Google Earth elevation data extraction and accuracy assessment for transportation applications. PLoS One, 12(4). Retrieved from http://journals.plos.org/plosone/article/file?id=10.1371/journal.pone.0175756&type=printable

Watson, R. T. (1971). Origin of Shell Beaches, Padre Island, Texas. *Journal of Sedimentary Petrology*, 41(4), 1105–1111.

Weise, B. R., and White, W. A. (1980). Padre Island National Seashore: A Guide to the Geology, Natural Environments, and History of a Texas Barrier Island (No. Guidebook 17 Bureau of Economic Geology, University of Texas at Austin). Austin, TX: University of Texas, Bureau of Economic Geology. Retrieved from file:///C:/Users/mculver1/Downloads/Weise_White_1980_PadreIslandNationalSeashoreAGuidetotheGeologyNaturalEnvironmentsandHistoryofaTexasBarrierIsland.pdf

Weishampel, J. F., Bagley, D. A., and Ehrhart, L. M. (2006). Intra-Annual Loggerhead and Green Turtle Spatial Nesting Patterns. *Southeastern Naturalist*, 5(3), 453–462.

Weishampel, Z. A., Cheng, W.-H., and Weishampel, J. F. (2016). Sea turtle nesting patterns in Florida vis-à-vis satellite-derived measures of artificial lighting. *Remote Sensing in Ecology and Conservation*, 2(1), 59–72. https://doi.org/10.1002/rse2.12

Weymer, B. (2012, July 16). A Geologic Characterization of the Alongshore Variability in Beach-Dune Morphology: Padre Island National Seashore, Texas (Thesis). Retrieved from http://oaktrust.library.tamu.edu/handle/1969.1/ETD-TAMU-2012-05-10723

White, S. A., and Wang, Y. (2003). Utilizing dems derived from lidar data to analyze morphologic change in the North Carolina coastline. *Remote Sensing of Environment*, 85(1), 39–47. https://doi.org/10.1016/S0034-4257(02)00185-2

Williams, S. J. (2013). Sea-Level Rise Implications for Coastal Regions. *Journal of Coastal Research*, 184–196. https://doi.org/10.2112/SI63-015.1

Wilks, D. S. (2006). Statistical methods in the atmospheric sciences (2nd ed., Vol. 100). Boston, MA: Academic press.

Witt, M. J., Hawkes, L. A., Godfrey, M. H., Godley, B. J., and Broderick, A. C. (2010). Predicting the impacts of climate change on a globally distributed species: the case of the loggerhead turtle. *Journal of Experimental Biology*, 213(6), 901–911. https://doi.org/10.1242/jeb.038133

Wood, D. W., and Bjorndal, K. A. (2000). Relation of Temperature, Moisture, Salinity, and Slope to Nest Site Selection in Loggerhead Sea Turtles. American Society of Ichthyologists and Herpetologists, *Copeia*, 1, 119–128.

Wright, L., and Short, A. (1984). Morphodynamic variability of surf zones and beaches: A synthesis. *Marine Geology*, 56, 93–118. https://doi.org/10.1016/0025-3227(84)90008-2

Yamamoto, K. H., Powell, R. L., Anderson, S., and Sutton, P. C. (2012). Using Lidar to quantify topographic and bathymetric details for sea turtle nesting beaches in Florida. *Remote Sensing of Environment*, 125, 125–133.

Zavaleta-Lizárraga, L., and Morales-Mávil, J. E. (2013). Nest site selection by the green turtle (Chelonia mydas) in a beach of the north of Veracruz, Mexico. *Revista Mexicana de Biodiversidad*, 84(3), 927–937. https://doi.org/10.7550/rmb.31913

Zuur, A., Ieno, E. N., Walker, N. J., Saveliev, A. A., & Smith, G. (2009). *Mixed Effects Models and Extensions in Ecology with R*. Springer New York. Retrieved from https://link.springer.com/content/pdf/10.1007%2F978-0-387-87458-6.pdf

APPENDICES

A. Lidar Bias Calculations

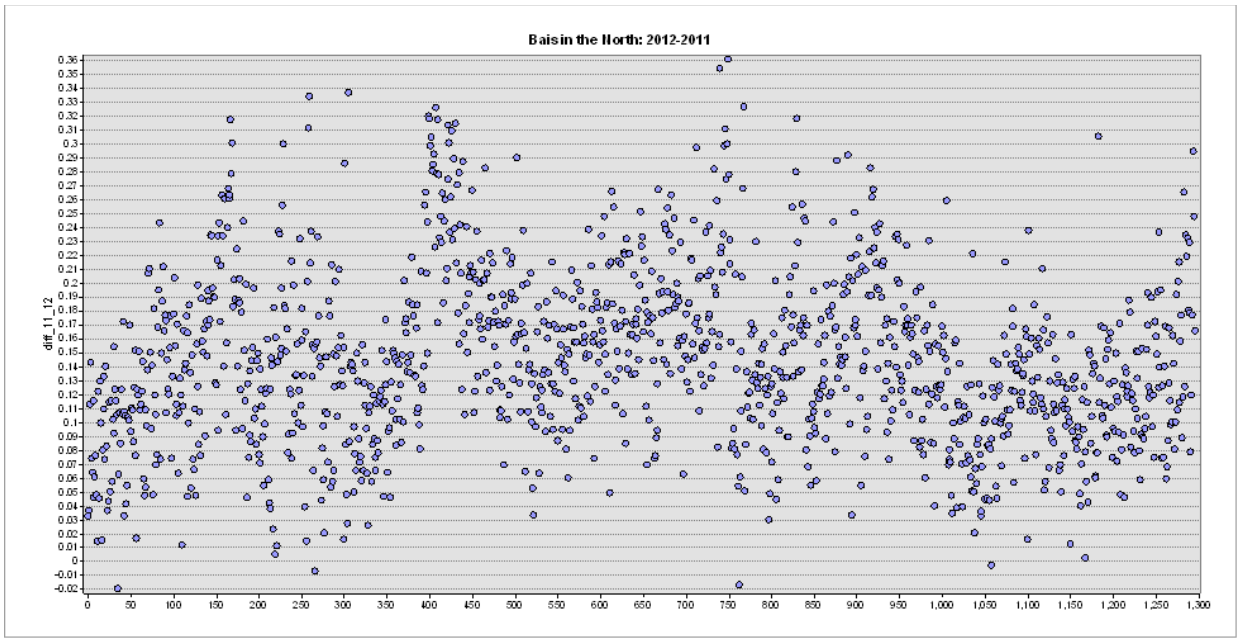

Figure A1: Difference in elevation along the roads of the 2012 and 2011 lidar data in the North.

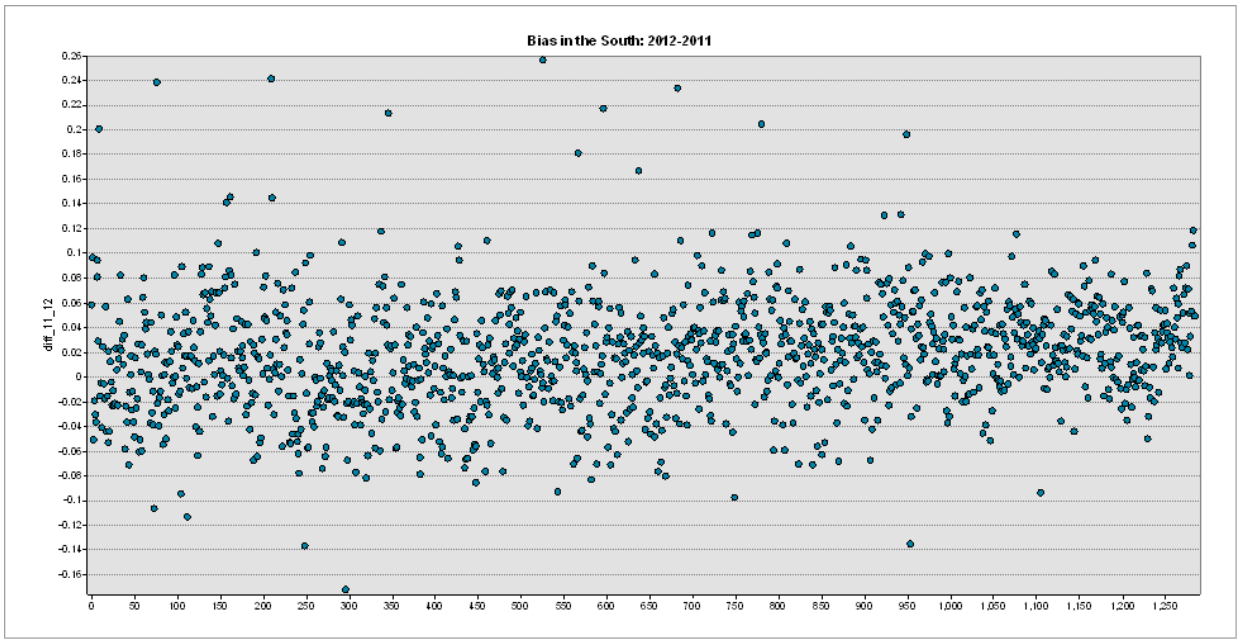

Figure A2: Difference in elevation along the roads of the 2012 and 2011 lidar data in the South.

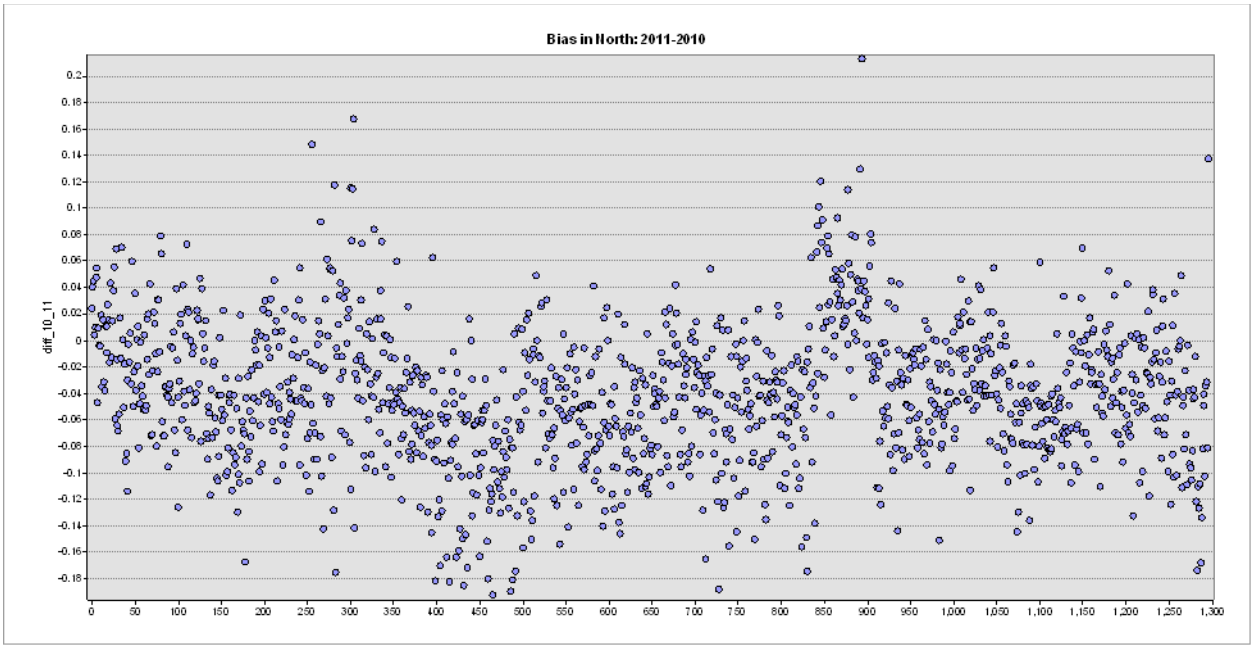

Figure A3: Difference in elevation along the roads of the 2011 and 2010 lidar data in the North.

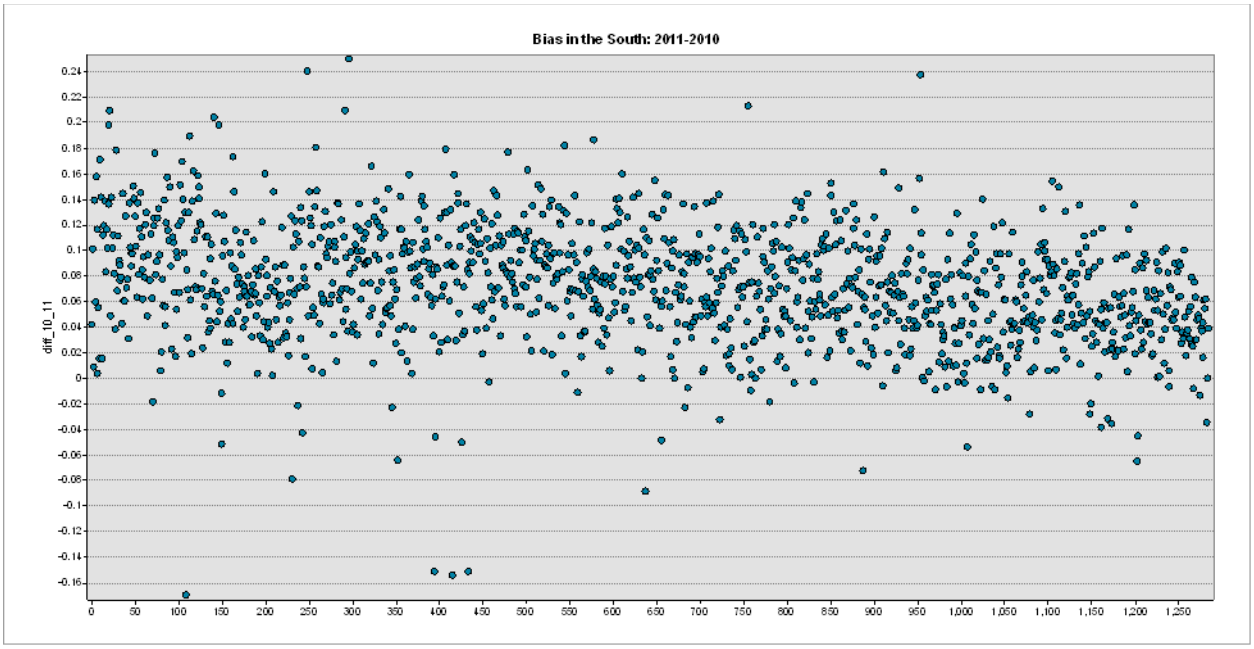

Figure A4: Difference in elevation along the roads of the 2011 and 2010 lidar data in the South.

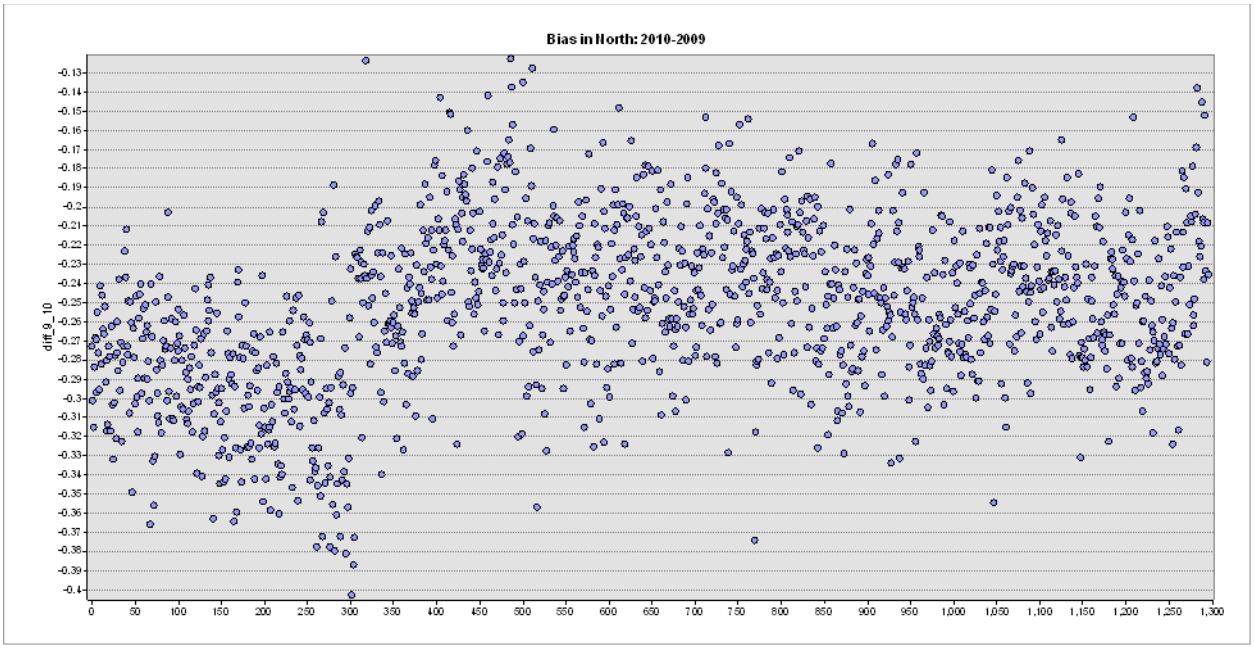

Figure A5: Difference in elevation along the roads of the 2010 and 2009 lidar data in the North.

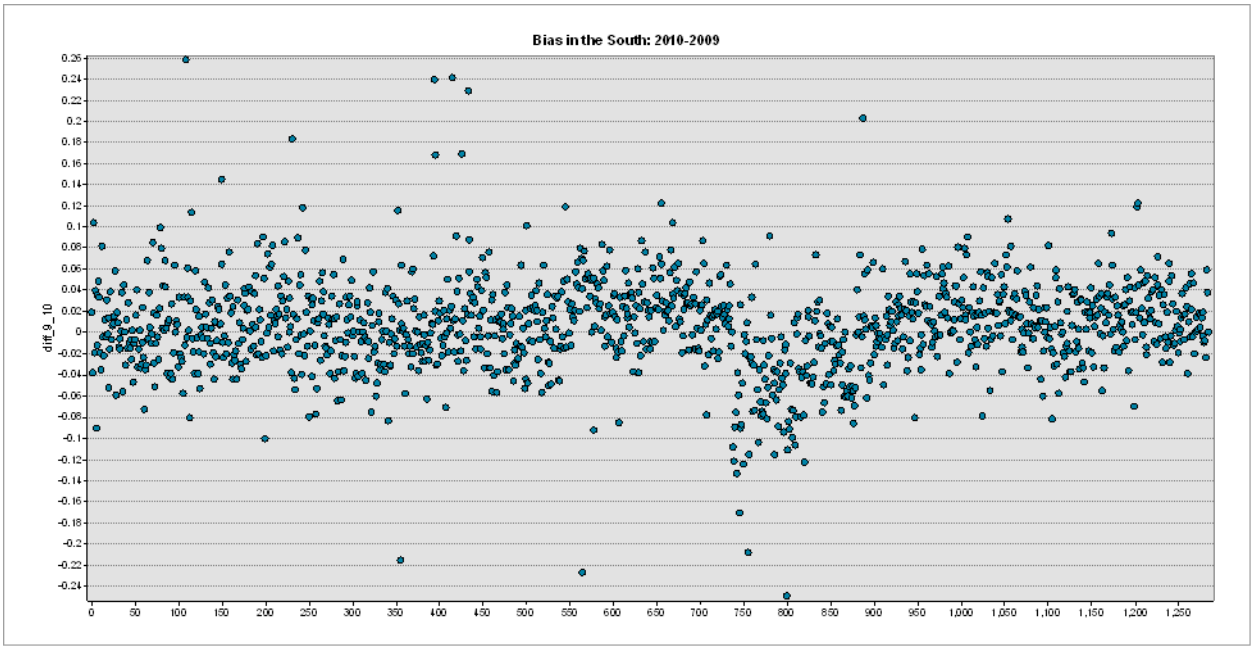

Figure A6: Difference in elevation along the roads of the 2010 and 2009 lidar data in the South.

B. Landward Foredune Boundary Mapping Criteria

I. Identify main foredune complex

1. Relief
- Visually locate dunes
- Find the main foredune complex, it is usually prominent and readily identifiable

2. Elevation and Aspect
- Identify features with an elevation greater than 2m.
- Use aspect as a visual aid to identify the continuous foredune ridge.

II. To determine if neighboring dunes are part of the foredune complex, use the following:

1. Proximity, connectedness, clustering
- Identify groups of dunes that are close to the main foredune feature/ridge.
- Assess if dunes are connected resembling a continuous chain and are clustered together.
- There may be gaps within the foredune complex.

2. Orientation- parallel to the coast
- Neighboring dunes are part of the main foredune complex if the group is oriented parallel to the coast

3. Function
- Dune chains or groups are considered part of the foredune complex if they could potentially act as storm washover protection features given their elevation, orientation to the shoreline, and proximity to the main complex.

III. Other criteria to consider:

1. Excluding man-made structures that disrupt foredune function

2. Consider dune dynamics and vegetation cover if:
    - The foredune ridge is fragmented.
    - The dune environment is highly dynamic.
    - If the area in question is a part of the active aeolian exchange with the beach or foredune.

The Coastal and Marine Geospatial Lab at Harte Research Institute and the Bureau of Economic Geology developed this process, the outputs of which are described in Paine *et al*. (2013).

C. Preliminary Statistical Analysis: Nest Habitat

Table C1: Statistical measures of each geomorphology characteristic for the nest coordinates of all of the years of data combined.

All Years	Aspect	Elevation (m)	Rugosity	Avg Beach Slope (degrees)	Beach Width (m)	Dune Height (m)	Dune Width (m)	Max Dune Slope (degrees)	Avg Dune Slope (degrees)	Distance from Shoreline (m)
Average	113.64	1.20	2.75	2.96	17.46	6.44	250.18	29.03	7.79	19.47
Standard Deviation	71.92	0.77	3.80	0.93	9.25	1.88	75.93	7.72	2.59	61.72
1st Quartile	72.01	0.75	1.22	2.27	11.02	5.38	87.93	24.01	6.07	2.71
Median	92.63	1.11	1.78	2.78	15.53	6.22	123.91	29.17	7.54	12.79
3rd Quartile	120.58	1.47	2.63	3.43	21.05	7.37	189.76	33.92	9.34	23.01

Table C2: Statistical measures of each geomorphology characteristic for the nest coordinates of 2012.

2012	Aspect	Elevation (m)	Rugosity	Avg Beach Slope (degrees)	Beach Width (m)	Dune Height (m)	Dune Width (m)	Max Dune Slope (degrees)	Avg Dune Slope (degrees)	Distance from Shoreline (m)
Average	108.74	1.06	2.36	3.05	14.46	6.48	325.17	28.06	7.88	13.29
Standard Deviation	73.03	0.63	1.57	0.77	6.09	1.84	1378.56	7.14	2.24	41.78
1st Quartile	69.22	0.62	1.49	2.43	10.02	5.52	91.84	23.56	6.36	-0.71
Median	85.37	1.05	1.82	2.88	13.02	6.31	123.34	28.70	7.65	7.97
3rd Quartile	117.39	1.38	2.51	3.59	18.02	7.31	177.58	33.10	9.34	15.66

Table C3: Statistical measures of each geomorphology characteristic for the nest coordinates of 2011.

2011	Aspect	Elevation (m)	Rugosity	Avg Beach Slope (degrees)	Beach Width (m)	Dune Height (m)	Dune Width (m)	Max Dune Slope (degrees)	Avg Dune Slope (degrees)	Distance from Shoreline (m)
Average	131.08	1.14	2.49	2.82	23.42	6.60	354.81	30.07	7.66	18.42
Standard Deviation	86.48	0.52	2.18	0.79	11.14	1.82	1417.28	8.08	2.40	24.70

1st Quartile	70.40	0.89	1.46	2.23	17.02	5.61	101.44	24.75	6.03	6.60
Median	99.61	1.06	1.99	2.65	21.04	6.50	138.54	30.08	7.42	17.46
3rd Quartile	177.91	1.33	2.68	3.23	27.05	7.69	194.48	36.12	9.22	24.81

Table C4: Statistical measures of each geomorphology characteristic for the nest coordinates of 2010.

2010	**Aspect**	**Elevation (m)**	**Rugosity**	**Avg Beach Slope (degrees)**	**Beach Width (m)**	**Dune Height (m)**	**Dune Width (m)**	**Max Dune Slope (degrees)**	**Avg Dune Slope (degrees)**	**Distance from Shoreline (m)**
Average	120.17	1.35	4.39	2.93	19.99	5.79	80.00	29.85	9.25	24.46
Standard Deviation	74.60	1.01	5.42	0.97	7.80	1.51	47.12	7.37	3.17	70.57
1st Quartile	74.40	0.69	1.62	2.13	13.54	4.72	47.62	24.06	7.10	2.23
Median	99.83	1.10	2.21	2.84	20.02	5.68	69.79	29.35	9.17	15.97
3rd Quartile	128.00	1.64	3.89	3.40	25.53	6.51	98.66	34.31	10.73	26.79

Table C5: Statistical measures of each geomorphology characteristic for the nest coordinates of 2009.

2009	**Aspect**	**Elevation (m)**	**Rugosity**	**Avg Beach Slope (degrees)**	**Beach Width (m)**	**Dune Height (m)**	**Dune Width (m)**	**Max Dune Slope (degrees)**	**Avg Dune Slope (degrees)**	**Distance from Shoreline (m)**
Average	96.83	1.31	2.35	3.02	12.94	6.67	178.24	28.49	6.85	23.78
Standard Deviation	41.00	0.88	4.93	1.15	6.97	2.09	81.91	7.89	2.19	91.62
1st Quartile	75.31	0.79	0.58	2.22	9.02	5.42	117.50	23.99	5.57	2.84
Median	88.70	1.31	0.74	2.76	12.01	6.26	156.51	28.65	6.77	13.46
3rd Quartile	103.13	1.69	1.39	3.67	15.01	7.67	232.35	33.57	8.28	23.56

D. Confusion Matrices for GLMs of Varying Ratios of Background to Presence Points

Table D1: Confusion matrix results for Model 1 in Table 5, which was generated using an equal ratio of background to presence points.

Accuracy	0.842
Kappa	0.684
P-value	2.2e-16
Sensitivity	0.892
Specificity	0.793
Positive Prediction Value	0.811
Negative Prediction Value	0.880
Prevalence	0.500
Detection Rate	0.446
Balanced Accuracy	0.842

Table D2: Confusion matrix results for Model 4 in Table 5, which was generated using a 2:1 ratio of background to presence points.

Accuracy	0.834
Kappa	0.638
P-value	< 2e-16
Sensitivity	0.775
Specificity	0.869
Positive Prediction Value	0.747
Negative Prediction Value	0.885
Prevalence	0.333
Detection Rate	0.258
Balanced Accuracy	0.822

Table D3: Confusion matrix results for Model 5 in Table 5, which was generated using a 5:1 ratio of background to presence points.

Accuracy	0.896
Kappa	0.593
P-value	3.29e-16
Sensitivity	0.589
Specificity	0.957
Positive Prediction Value	0.735
Negative Prediction Value	0.921
Prevalence	0.167
Detection Rate	0.0981
Balanced Accuracy	0.773

Table D4: Confusion matrix results for Model 6 in Table 5, which was generated using a 10:1 ratio of background to presence points.

Accuracy	0.930
Kappa	0.436
P-value	3.59e-16
Sensitivity	0.340
Specificity	0.989
Positive Prediction Value	0.747
Negative Prediction Value	0.938
Prevalence	0.090
Detection Rate	0.0307
Balanced Accuracy	0.665

E. Alongshore Habitat Variability Analysis

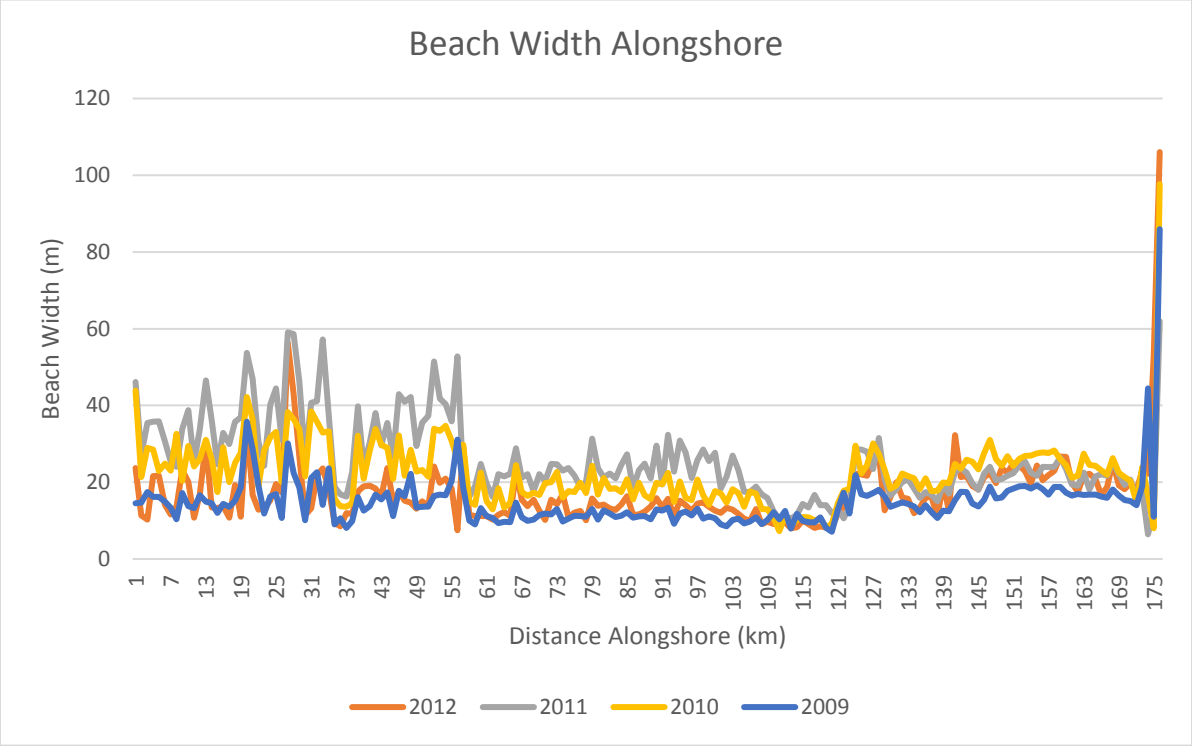

Figure E1: Beach width south to north alongshore the study area.

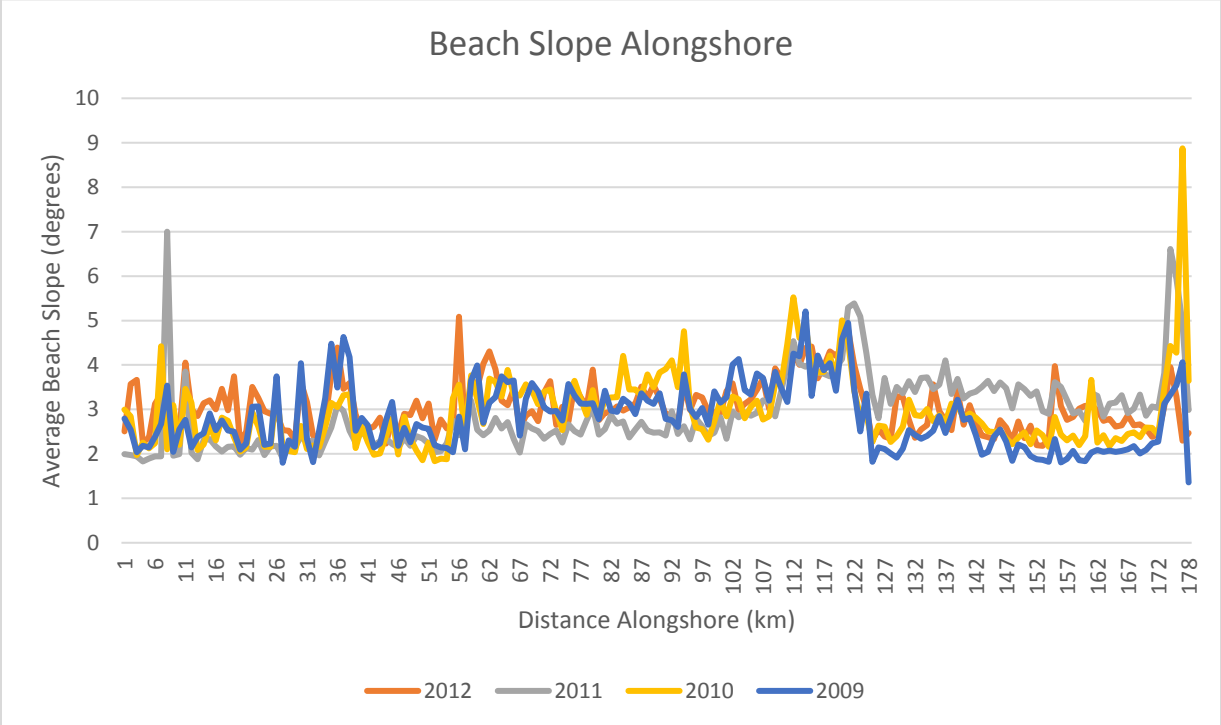

Figure E2: Beach slope south to north alongshore the study area.

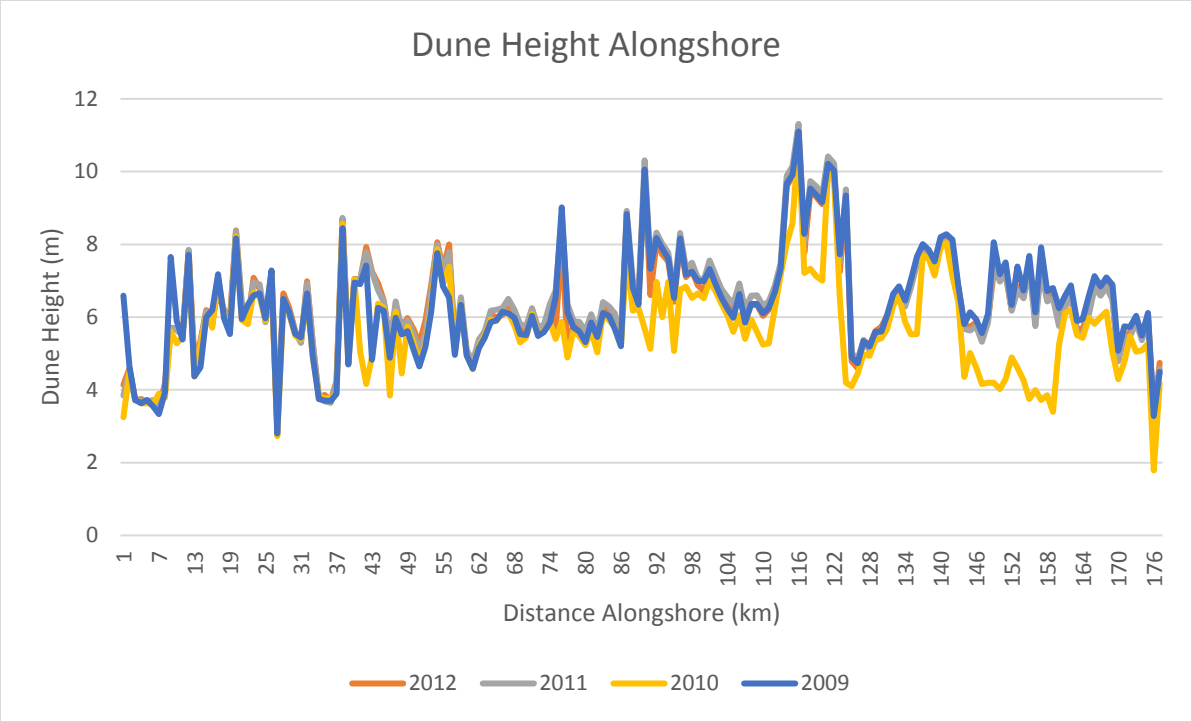

Figure E3: Dune height south to north alongshore the study area.

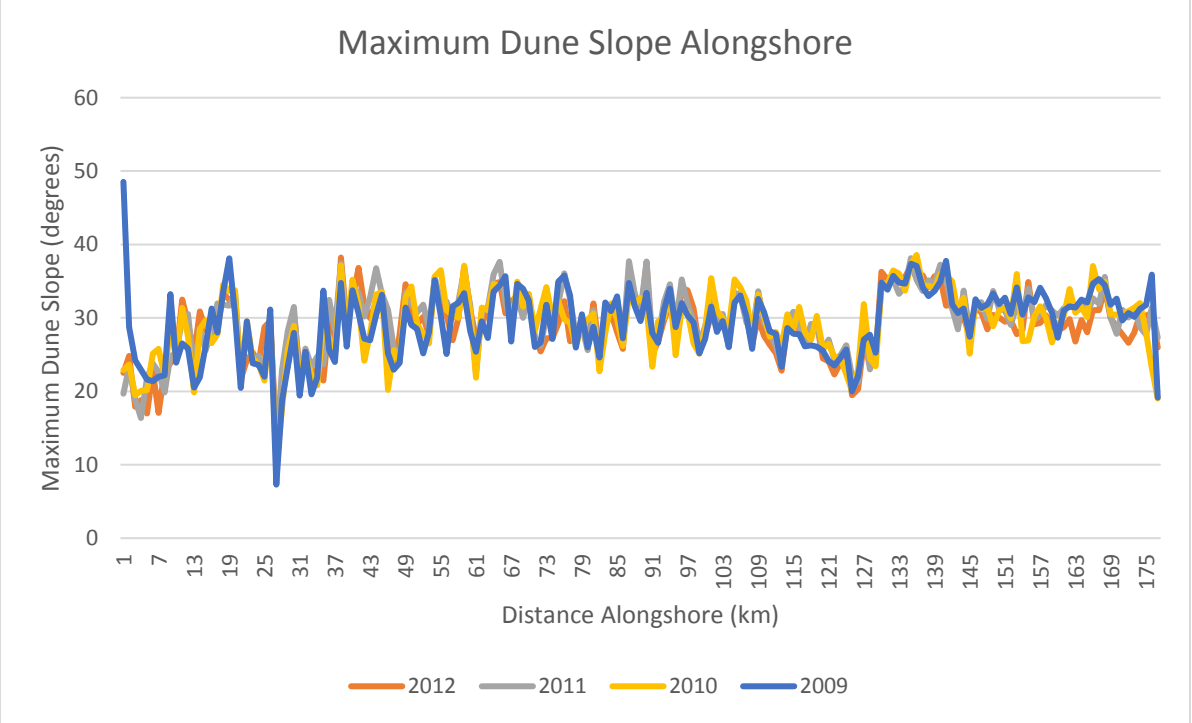

Figure E4: Maximum dune slope south to north alongshore the study area.

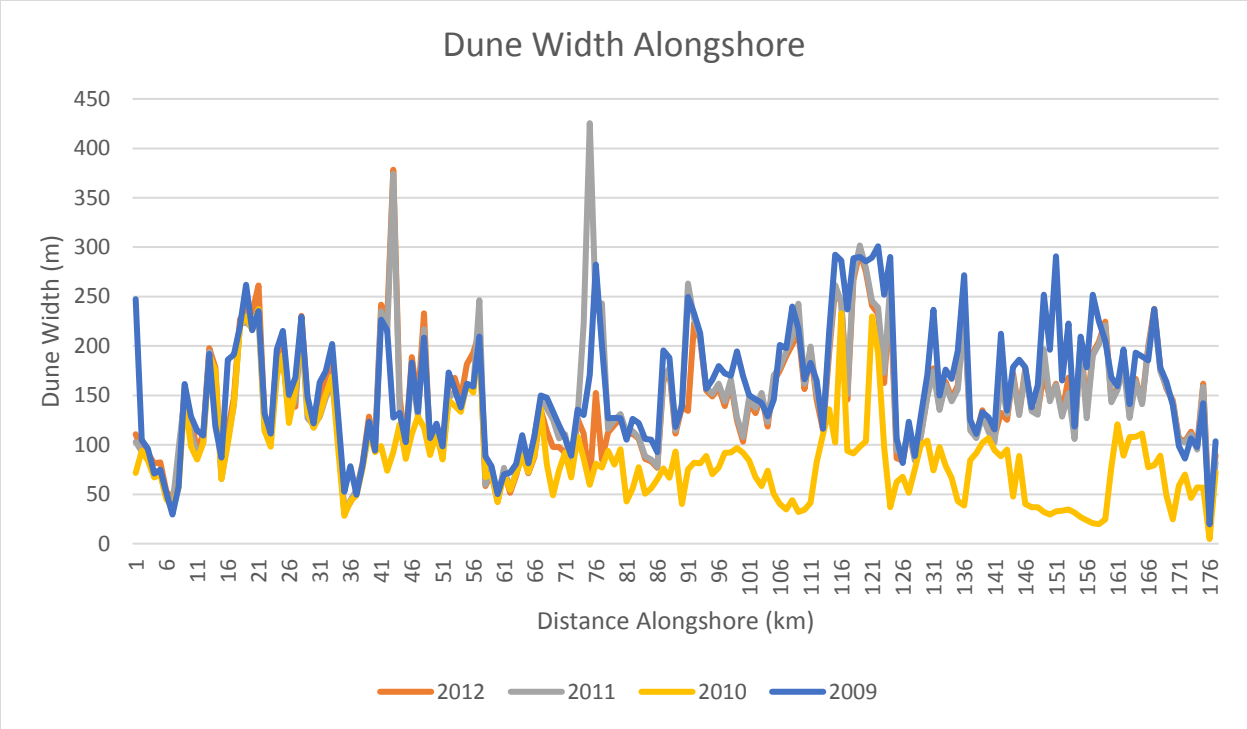

Figure E5: Dune width south to north alongshore the study area.